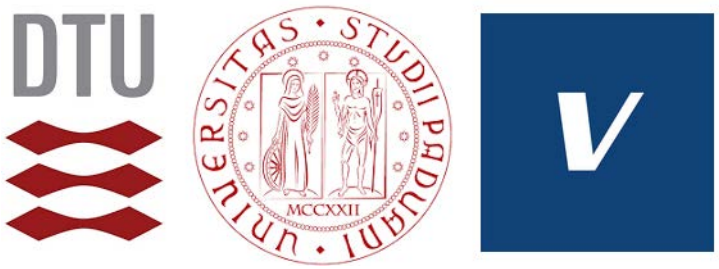

UNIVERSITÁ DEGLI STUDI DI PADOVA

Dipartimento di Ingegneria Industriale DII

Corso di Laurea Magistrale in Ingegneria dell'Energia Elettrica

Design of a hybrid wind-electric vehicles power plant model – fleet model for ancillary services provision in Bornholm

Supervisors: Mattia Marinelli
Roberto Turri
Co-supervisors: Tatiana Gabderakhmanova
Jan Martin Zepter
Lisa Calearo
Michel Rezkalla

Student: Mirko Ledro, 1179267

Academic year 2019/2020

Mirko Ledro, 1179267

Design of a hybrid wind-electric vehicles power plant model – fleet model for ancillary services provision in Bornholm

Design af et hybrid-kraftvaerk, vindmøller og elbiler – flådemodel til levering af systemydelser i Bornholm

Design di un impianto eolico ibrido con ausilio di veicoli elettrici per la fornitura di servizi ancillari nell'isola di Bornholm

Master Thesis, July 2020

DTU Electrical Engineering
Department of Electrical Engineering

DIPARTIMENTO DI
INGEGNERIA INDUSTRIALE

Vestas

Design of a hybrid wind-electric vehicles power plant model – fleet model for ancillary services provision in Bornholm

Author:
Mirko Ledro, 1179267

Supervisors:
Mattia Marinelli, Associate Professor at Technical University of Denmark
Tatiana Gabderakhmanova, PostDoc at Technical University of Denmark
Jan Martin Zepter, PhD student at Technical University of Denmark
Lisa Calearo, PhD student at Technical University of Denmark
Roberto Turri, Associate Professor at University of Padua
Michel Rezkalla, Electrical Plant Design Specialist at Vestas

Department of Electrical Engineering
Centre for Electric Power and Energy (CEE)
Technical University of Denmark
Elektrovej, Building 325
DK-2800 Kgs. Lyngby
Denmark

www.elektro.dtu.dk/cee
Tel: (+45) 45 25 35 00
Fax: (+45) 45 88 61 11
E-mail: cee@elektro.dtu.dk

Release date: 12th July 2020

Class: 1 (public)

Edition: 1. edition

Comments: This report is a part of the requirements to achieve the M.Sc. degree in Sustainable Energy at Technical University of Denmark and the M.Sc. degree in Electrical Energy Engineering at University of Padua. The report counts for 32.5 ECTS for the M.Sc. in Sustainable Energy and 21 ECTS for the M.Sc. in Electrical Energy Engineering.

To the best father, Livio, and my mother, guardian angel, Franca
Al miglior padre, Livio, e mia madre, angelo custode, Franca

PREFACE

This master thesis is prepared at the Department of Electrical Engineering of the Technical University of Denmark in fulfilment of the requirements for acquiring both a Master of Science in Sustainable Energy, study line in Wind Energy, at the Technical University of Denmark (DTU) and a Master of Science in Electrical Energy Engineering at the University of Padua (UNIPD), in accordance with the double degree program T.I.M.E. (Top Industrial Managers of Europe).

Under the supervision of Mattia Marinelli and Roberto Turri (Associate Professors at DTU and UNIPD, respectively), Tatiana Gabderakhmanova (Postdoctoral researcher at DTU), Jan Martin Zepter and Lisa Calearo (PhD students at DTU), and Michel Rezkalla (Electrical Plant Design Specialist at Vestas), the work has been carried out between January and July 2020 at the Department of Electrical Engineering (DTU Elektro) at DTU.

The master thesis counts for 32.5 ECTS for the Master of Science in Sustainable Energy and 21 ECTS for the Master of Science in Electrical Energy Engineering.

AKNOWLEDGEMENT

The last three years have been of great personal growth, a long period rich of satisfactions, conquests, but also many obstacles to overcome. I owe a sense of gratitude and I want to appreciate all who have contributed to help me to be the person I am.

I am grateful to my thesis supervisors Mattia, Tatiana, Jan Martin, Lisa, Roberto and Michel for helping me through my MSc thesis. Particularly, Mattia, for his education, Tatiana and Jan Martin, for their dedication, and Lisa, my mentor since my first steps in Denmark.

I want to thank my Italian friends. Daniele, extraordinarily precious. Alessandro, always willing to help. Anthony, my long-standing friend. Marco, hard worker and reliable man. Lisa, always ready to listen and advise myself. Jessica, my desk-mate in UNIPD. Francesco, my personal mental coach and first believer of this foreign experience, I owe to him my access to Denmark. Federico, omnipresent and bighearted friend, for all the time spent together in Copenhagen.

Through this experience, I met people who helped me to grow as a man. Irene, who took care of me since the first day in DTU. Alina, who taught me how to react to hard life experiences. Luca, a cheerful and very bright friend. I am very appreciative to my flatmates, Mirko and Vittorio, my friend Panos and my girlfriend Mercedes, who transform the Danish lock-down period in a family time. Particularly, Mercedes, my right-hand woman, who has been constantly present and supportive through difficulties.

I want to be grateful to Don Carlo, a 'big brother' more than my high school director, who concretely believes in Christian values, Erik, who hosted myself as soon as I arrived in Denmark, Elio and Giuliana, who educated me professionally in the work environment.

Finally, my family. The family. This my goal is dedicated to every single sacrifice you made. I want to express all my love for my sisters, Sara and Giorgia, my brother, Mattia, my father, Livio, and my grandparents, Bruna, Rosa and Sergio. We know perfectly how life was harsh and is still very complicated, but all together we can go beyond any difficulties. I miss you. I love you.

Heartfelt thanks.

Mirko

ABSTRACT

Environmental concerns are increasingly driving the evolution of the energy sector. A high share of renewable energy sources (RES) in the power system will potentially support the reduction of CO_2 emissions. However, this presents considerable challenges for operating and maintaining the power system in secure state, since thermal generators have been always the ones providing ancillary services (AS). The transition towards a high share of RES replacing conventional plants entails an upsurge in providing AS from the RES, too. In the last years, the concept of hybrid power plant (HPP) grew substantially, which indicates an aggregation of generating units with at least one RES. Simultaneously, the vehicle-grid integration presents an opportunity to pro-actively benefit the modern power system. As a consequence, controllable electric vehicles (EVs) are valuable assets for enhancing the power system operation since they can provide flexibility.

As part of the ongoing European project "Insulae", this thesis analyses the effects of power regulation in an HPP composed of three wind turbines installed in Kalby and an aggregation of EVs in the testbed of the Danish island of Bornholm. A selected model of the Bornholm power system with a focus on the substation of Åkirkeby is utilized to perform simulations in DIgSILENT's software PowerFactory (PF) environment. Detailed EV fleet model and related controllers need to be designed and implemented in order to analyse pros and cons of using EV fleet instead of a battery energy storage system. Indeed, among the thesis' goals, it is requested to detect the EVs' delay influence on the HPP's power output controllability. Furthermore, the EVs charging pattern in Åkirkeby will be analysed since it plays a key role in defining when the EVs are available to provide ancillary services for the HPP.

The EV fleet is controlled thanks to a plant controller designed in PF's dynamic simulation language (DSL), exploiting potential synergies with the wind farm (WF) itself. Indeed, two plant controllers are designed: a *Power-to-Power controller*, which controls the EVs' power consumption as a function of a power error analysis, and an *Energy-to-Power controller*, which controls the EVs' power consumption as a function of an energy error analysis. The EV fleet is equipped with both an EVs' state-of-charge protection and a substation' protection against overloading condition.

Both controllers give rise to interesting outcomes when EVs are combined with the analysed WF. In particular, the *Energy-to-Power controller* results in a less rigid controller in respect to the *Power-to-Power controller*. Consequently, the *Power-to-Power controller* is more influenced if the investigated EVs' attributes are applied than with the *Energy-to-Power controller*. As an conclusion, even though power and energy errors cannot be eliminated completely, the interaction WF – EVs could enhance the wind production reliability as well as a higher integration of RES in the power system if combined with this hybrid configuration.

SOMMARIO

Le preoccupazioni in materia ambientale stanno guidando sempre più l'evoluzione del settore energetico. Un'alta percentuale di fonti di energia rinnovabile (FER) nel sistema energetico supporterà potenzialmente la riduzione delle emissioni di CO_2. Tuttavia, ciò presenta notevoli sfide per il funzionamento e il mantenimento del sistema elettrico. La sostituzione di impianti convenzionali con impianti a FER comporta richieste piú stringenti per questi ultimi, a tal punto di richiedere loro di fornire direttamente servizi ancillari. Negli ultimi anni, il nuovo concetto di "hybrid power plant" (HPP) è cresciuto considerevolmente, il quale indica l'aggregazione di piú unità di generazione con almeno una FER. Allo stesso tempo, l'integrazione di veicoli elettrici offre una valida opportunità per la moderna rete elettrica, sempre piú instabile a causa della crescente quota di FER. Di conseguenza, i veicoli elettrici sono considerati una preziosa risorsa per migliorare il funzionamento del sistema di alimentazione, poiché potrebbero fornire maggiore flessibilità alla rete elettrica stessa.

Parte del progetto europeo "Insulae", questo studio analizza gli effetti della regolazione della potenza in una HPP composta da tre generatori eolici e dall'aggregazione di veicoli elettrici nell'isola danese di Bornholm. L'analisi é focalizzata sulla sottostazione di Åkirkeby, che é stata riportata in PowerFactory (PF) per eseguire le necessarie simulazioni. Al modello base della presente rete sono stati aggiunti i veicoli elettrici con i corrispettivi controllori. I pro e contro dei veicoli elettrici interconnessi alla rete attraverso le colonnine di ricarica unidirezionali sono presentati, e paragonati ai sistemi di accumulo tradizionali. Infatti, tra gli obiettivi del progetto Insulae c'é l'analisi dell'impatto del ritardo dei veicoli elettrici sulla gestione della potenza erogata dall'HPP. Inoltre, il progetto indaga il comportamento dei veicoli elettrici in Åkirkeby, in particolare il loro utilizzo giornaliero, per definire quando e in quali condizioni questi possono essere disponibili per fornire servizi ancillari.

Il modello rappresentante i veicoli elettrici è abbinato a due controllori. Il primo é un controller in potenza (definito *Power-to-Power controller*), che controlla la potenza di ricarica dei veicoli elettrici in funzione della potenza prodotta dal parco eolico. Il secondo invece é un controller in energia (definito *Energy-to-Power controller*), che controlla la potenza di ricarica dei veicoli elettrici ma questa volta in funzione dell'energia prodotta dall'impianto eolico.

Entrambi i controller danno luogo a interessanti risultati quando i veicoli elettrici sono abbinati al parco eolico. In particolare, l' *Energy-to-Power controller* é un controller meno rigido rispetto al *Power-to-Power controller*. Di conseguenza, applicando i diversi attributi dei veicoli elettrici, il *Power-to-Power controller* é piú influenzato dell' *Energy-to-Power controller*. In conclusione, seppur gli errori in potenza ed energia non possono essere evitati completamente, l'interazione parco eolico – veicoli elettrici accresce l'affidabilitá della potenza prodotta dall'impianto eolico, cosí come potrebbe essere facilitata l'integrazione di altre FER se previste di tale configurazione ibrida.

ACRONYMS

AS	Ancillary services
BESS	Battery energy storage system
BMS	Battery management system
CHP	Combined heat and power
DER	Distributed energy resources
DSL	Dynamic simulation language
DSO	Distributor System Operator
ESS	Energy storage system
EV	Electric vehicle
EVSE	Electric vehicle supply equipment
GHG	Greenhouse gases
HPP	Hybrid power plant
HV	High voltage
LV	Low voltage
MV	Medium voltage
NW	Not windy day
PCC	Point of common coupling
PCOM	Point of communication
PEC	Point of electrical connection
PGC	Point of generator connection
POC	Point of connection
RES	Renewable energy sources
SOC	State of charge
SOS	Security of supply
V2G	Vehicle-to-Grid
VW	Variable windy day
W	Windy day
WF	Wind farm
WTG	Wind turbine generator

TABLE OF CONTENTS

List of Figures

List of Tables

1 Introduction

Nowadays, a safe, secure and affordable energy is worldwide required and ensuring everyone has access to energy is also the ongoing challenge to proceed with the global development. Energy is the life blood of the current society [1].

A brief introduction about global energy consumption, greenhouse gases emissions and the renewable energies boost is collected in the first section. Consequently, the concept of smart grid is connected to the high level of security of supply's requirement for the upcoming years, concluding with a big picture of the Danish island Bornholm where the project is carried out.

1.1 Global renewables development and Danish status

Considering the global energy consumption from the First Industrial Revolution to approximately date, an exponential increase, strongly correlated to economic growth and poverty alleviation, can be clearly observed in Figure 1.1a. Indeed, living standards, productivity, healthcare, education services showed a clear improvement, mainly through the last century. Furthermore, energy is strictly related to environment. Through the whole time scale considered, the energy system is primarily composed by fossil fuels, which produce carbon dioxide (CO_2), nitrous oxide, methane and other gasses better known as greenhouse gases (GHG). Figure 1.1b shows how the total annual CO_2 emissions have risen, passing from 2 billion tonnes to over 35 billion tonnes in the last century [2].

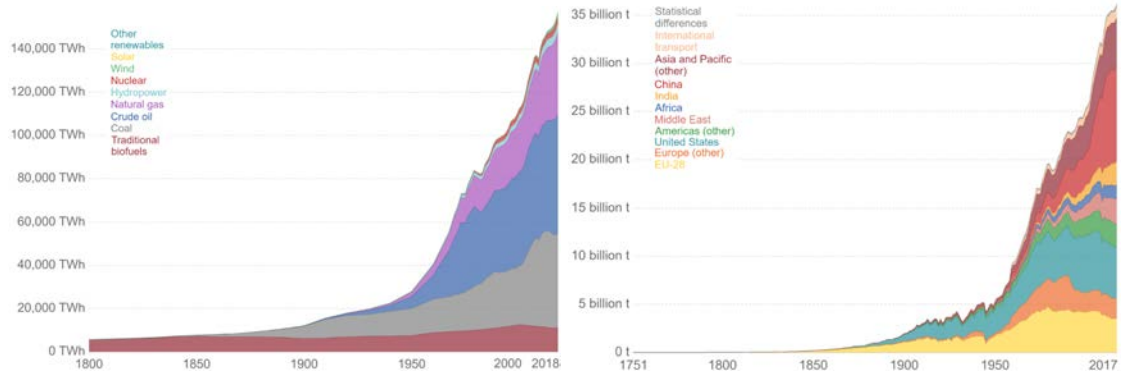

(a) Global Primary Energy Consumption (b) Annual total CO_2 emissions

Figure 1.1: Energy consumption and CO_2 emissions [2]

As a direct consequence, climate change is a well known topic for the current time. From changing weather patterns to increasing the sea levels, GHG' impacts are changing the whole globe drastically and in a unrestrained way.

Since the end of the last millennium, future drawbacks for maintaining the same energy trends were already highlighted, making clear that a radical change needed to be faced. In 1992, the United Nations produced the United Nations Framework Convention on Climate Change (UNFCCC), a first step in considering the climate change problem. Lately, an emissions reduction target has been adopted after that the Kyoto Protocol entered into action in 2008. Then, thanks to the Paris Agreement, new national guidelines have been declared for a sustainable low carbon future. The Agreement's central aim is to keep the global temperature well below 2 °C above pre-industrial levels, trying to limit the temperature to a maximum of 1.5 °C. [3]

Taking into consideration the "old continent", climate and energy packages have been approved from the European Union (EU). In each package, targets regarding GHG emissions, energy produced by renewable sources and energy efficiency have been defined. First, the "2020 climate and energy package" established the goal that must be reached by 2020: a 20 % cut in GHG emissions in respect to 1990, a level of 20 % of EU energy coming from renewables and a 20 % improvement in energy efficiency. Moreover, the EU has already defined the targets that must be hit in the following decade ("2030 climate and energy framework"), where the percentages are 40 %, 32 %, 32.5 %, respectively. All these packages should move all EU countries towards a progressive reduction of GHG emissions, described in the "2050 long-term strategy", making the EU the world's first climate neutral continent by 2050. [4]

Consequently, in Figure 1.2, it is possible to observe how the renewable energy sources (RES) have contributed to the total primary energy consumption in the last decades. Precisely, considering the previous Figure 1.1a, "traditional biofuels" (burning of wood, forestry materials and agricultural waste biomass) are not taken into account, while "other renewables" refers to geothermal, biomass, waste, wave and tidal. Although RES were already increasing steadily, the graph shows a steep improvement from the beginning of the new millennium, making clear how strategies and plans are having their effects on global green energy consumption.

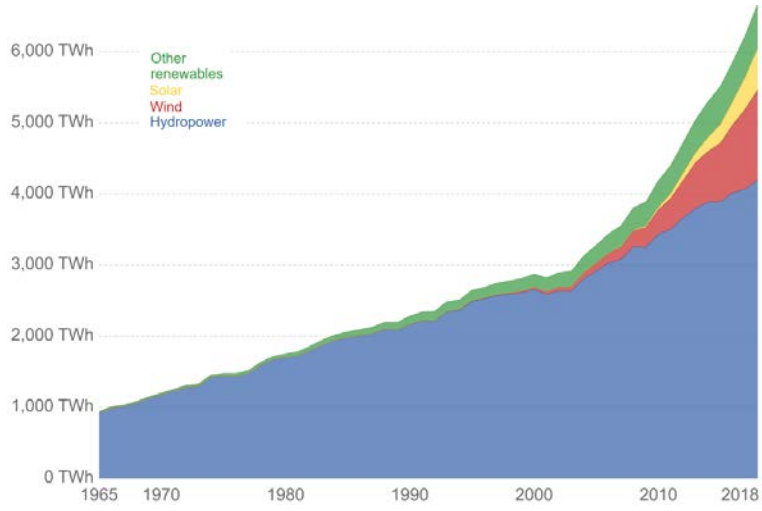

Figure 1.2: Renewable energy consumption [2]

What about Denmark? How is the Danish energy production evolving?

Considering the overall generation's development in the period between 1990 and nowadays, then with a projection towards 2027, it can be seen in Figure 1.3a that Denmark is clearly investing

into renewables. Central power station were dominating the scenario in the 90's, then coal and natural gas-fired central power stations have been gradually decommissioned to firing with more biomass and with a even more investment in green energy. Undoubtedly, wind power have had a marked expansion in the same time-frame, passing from just 2 % to 47 % of the Danish electricity consumption in 2019 and with a expected increase up to 65 % in 2027. Finally, it must be underlined the great increase in photovoltaic power plants in the last few years, with a estimated constant increase toward 2027. The electricity generation from only RES for the last few years and with the relative projection to 2027 is collected in Figure 1.3b. The renewable energy share of electricity generation is expected to increase up to 90 %, basically doubling the level in 2017. The lead will be still taken by wind power although the amount of biomass will continue to rise.

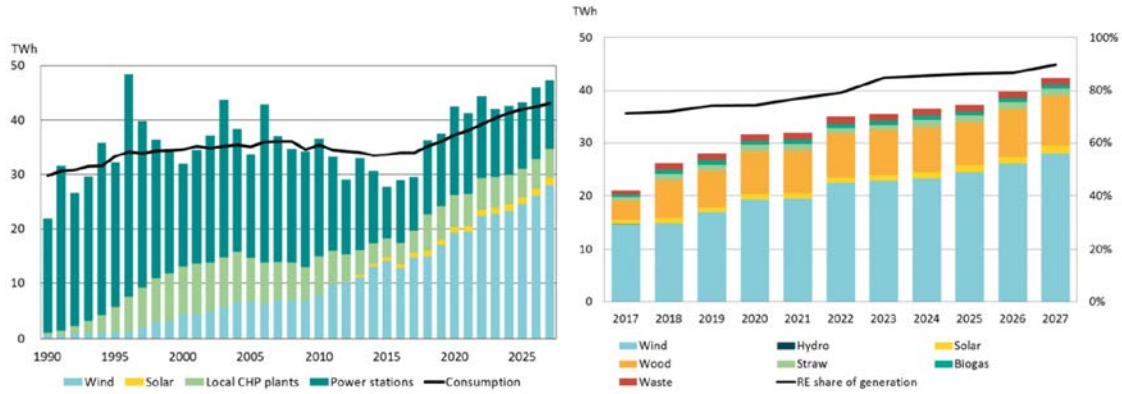

(a) Electricity consumption and generation in DK

(b) Electricity generation from RES in DK

Figure 1.3: Electricity consumption and generation in DK [5]

Due to an expansion of combined heat and power (CHP) plants and the central power plant's renovation, coal, natural gas and oil's consumption has been decreasing, while the biofuels have risen highly. According to the Danish forecast, biofuel's consumption will pass from 35 % in 2017 to 63 % in 2027. The conversion of several power plants to biomass and the combined increase of RES will lead emissions of CO_2 (but also SO_2 and NO_x being part of GHG's family) in Denmark to a trend that is constantly decreasing, as observed in Figure 1.4. [5]

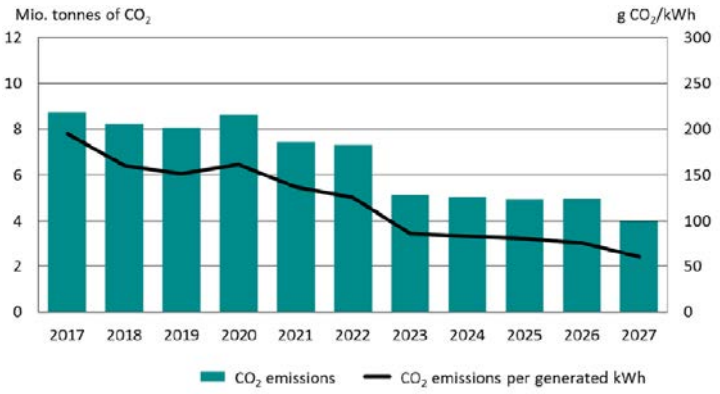

Figure 1.4: CO_2 emissions 2017-2027 [5]

1.2 Smart Grid: the key for a future Danish grid adequacy

The main goal of sustainable electric power systems is to convert energy from one of the naturally available forms (chemical, thermal, mechanical) to the electrical form and then to transport it to the final points of consumption through the transmission network, satisfying a certain quality of the supplied power. The transmission network is divided into three systems: transmission, sub-transmission and distribution, characterized by different voltage levels, distances, interconnected systems and grid operators [6]. Considering just the grid operators, they are defined as:

- TSO is the Transmission System Operator (Energinet in DK), which aims to maintain the high voltage (HV) level (over 100 kV) for long distances within limits and balance the electrical system between production and consumption, meaning stability of the frequency.
- DSO is the Distribution System Operator (Radius, Seas, BEOF... in DK), which aims to maintain the medium and low voltage (MV and LV, respectively) in nodes within limits, guaranteeing voltage quality and continuity of the service, meaning high reliability on security of supply.

Denmark is the only European country divided into two synchronous areas, DK1 and DK2 (respectively Western and Eastern Denmark), connected through the Great Belt Power Link [7]. It means that DK1 follows the ENTSO-E Continental Europe Operation Handbook legislation, while DK2 the Joint Nordic System Operation Agreement. Nonetheless, Energinet is the TSO for both areas since it is an independent public entity underlying the whole country.

The core of Energinet is the so called Energinet's energy trilemma. Its goal is to maintain a high level of security of electricity supply (or simply security of supply, SOS), taking into consideration the national economy as well as assuring the green transition by integrating RES. Currently, the Danish consumers' SOS is one of the highest in Europe, showing just under 22 minutes of outage (in which only 11 seconds in the transmission grid) in 2018, meaning a total SOS of 99.996 %, with no outage minutes owned to generation inadequacy. This result is even more brilliant if combined with the transition from dispatchable to fluctuating solar and wind power generation in the Danish domain. Furthermore, the forecasted increase in power consumption (observable also in Figure 1.3a) plus the grid's ageing contribute clearly to higher probability of grid faults. In order to respond to the challenge of generation adequacy, grid operators and local authorities implemented and will continue to improve automation in the electricity system operation, to react quickly to sudden fluctuations, investing mainly into ancillary services (AS). Energinet defines the AS as "the collective term for the electricity generation and consumption resources used to maintain electricity system balance and stability. [...] AS consist of reserves, regulating power, properties required to maintain power system stability and other system services such as black start services" [8].

Nowadays, due to a continuous increase of variable RES as well as the amount of unpredictable distributed energy resources (DER) in the distributed grid, the interaction and coordination between TSO-DSO is assuming a key point for the grid's integrity. In this context, Energinet is an avantgarde authority to develop a compact Smart Grid in Denmark [9].

The concept of Smart Grid can be used to mobilise and activate flexible electricity consumption from small consumers. The idea is to change DER' mode of operation to fulfil the needs of the power system: the passive consumers, with predictable and regular power consumption patterns, will be converted into interactive consumers by means of automatic and intelligent control system,

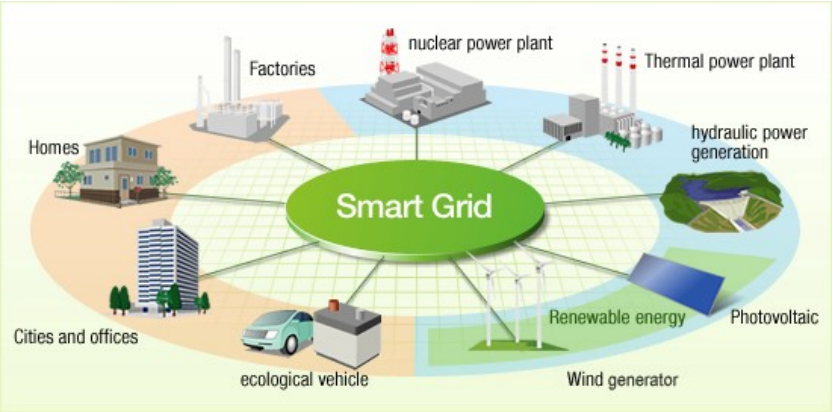

Figure 1.5: Energy system of the future [10]

adjusting their power consumption and realising socio-economic benefits. Two different mechanism can be used for activating flexibility. First, the usage of price signals, giving financial incentives to shift the power consumption to the part of the day when it is more lucrative. Second, having appliances with higher intrinsic flexibility, it is also possible to manage and control their behavior with sudden activation requests by the grid companies and/or Energinet itself [11]. Furthermore, the traditional concept of energy system where the generation is concentrated in just few large and centralized power plants is shifting into a more meshed and distributed medium and small size generators, among which the DER take the lead. The hardly predictable, fluctuating and uncontrollable behavior of wind and solar sources could cause excess in generation during low demand period as well as overproduction in already congested electric grids, weakening the grid's SOS [12]. In this context, the presence of a battery energy storage system (BESS) could bestow a relief to the power system, mitigating these main RES' drawbacks and consequently increase their grid integration.

1.3 Bornholm, the Danish testbed

Bornholm island, small Danish island located just south of Sweden in the Baltic Sea, is the perfect facility to test new Smart Grid technologies.

It is electrically connected through a submarine cable to Sweden, being then part of the Nordic synchronous area (as well as DK2), but it can work (intentionally or due to fault/maintenance conditions) in islanding mode, making it absolutely interesting for different activities, such as flexibility demand and power market, wind power and EV integration in a power grid where RES production take the lead [13]. Moreover, Bornholm's community wants to become a 100 % green and sustainable society by 2035. This goal can be reached merging CO_2 neutral generation with a combination of biomass, wind and solar production, a more flexible electricity consumption side and last - but not least - a smart EVs integration in Bornholm's power system. From the consumers' point of view, several families are in fact making their electrical disposals available (heat pumps, electric radiators) to deeper analysis to obtain higher consumption's flexibility [14]. On the other side, from the producers' point of view, the combination of multiple DER could enable entrances into new markets while improving the overall system power output.

In this new panorama, the concept of hybrid power plant (HPP) comes into view. It is defined

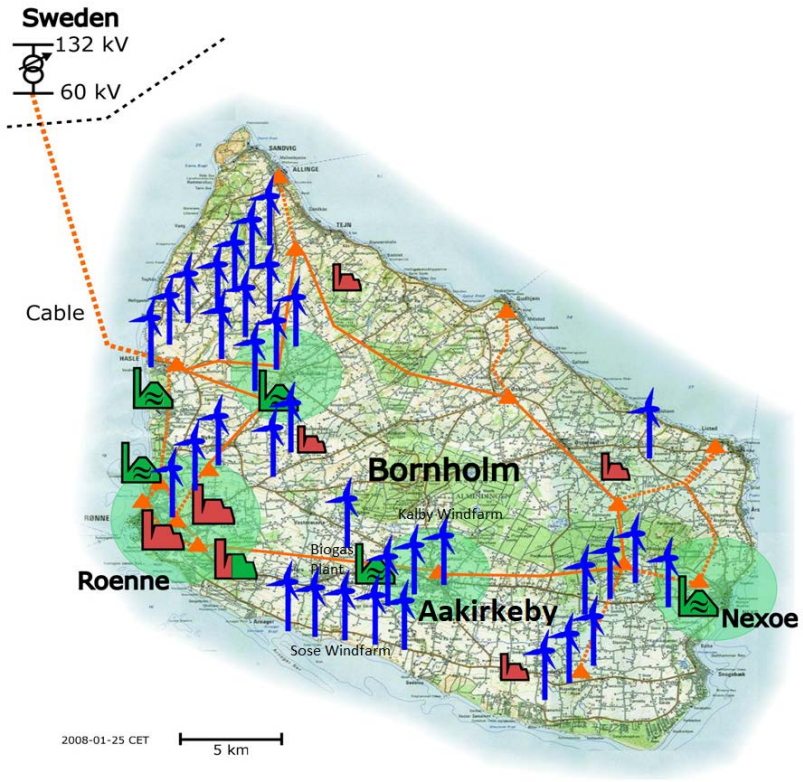

Figure 1.6: Bornholm island, adapted from [13]. The geographical localization of Åkirkeby, Kalby and Sose wind farms is highlighted

as "a power system, using one renewable and one conventional energy source or more than one renewable with or without conventional energy sources" [15]. The main goal of this overview is that, from outside, the HPP should behave similarly to a programmable generating unit (for example a thermal unit), providing all the necessary services required by the grid operator. However, the technological development in energy storage system (ESS) plays a key role in the optimal use of the DER. As a matter of fact, ESSs, in combination with appropriate controls and power electronics, will offer power and energy management in a HPP, providing then at least some of the ancillary services as non-renewable generating units supply nowadays (frequency support, inertial response, reactive power regulations). In this circumstance, the stochastic and variable patterns in wind and solar power generating unit will make the main focus of future HPP the power oscillation control, service know also as power smoothing.

As part of the ongoing European project "Insulae", the challenge is that, having less programmable power plant, new opportunities must be tested to be able to make the island working 100 % renewable power generation in islanding mode. Thus, this thesis analyses the effects of power regulation in a HPP composed by a wind farm and an aggregation of EVs in Åkirkeby's substation. The analysed wind farm is composed of three wind turbines installed in Kalby, while an EVs population is considered as mobile ESS, underlying all pros and cons in respect to install a BESS. Moreover, the main EVs' constraint is due to the chargers' unidirectionality, being possible only the charge and not the discharge of the EVs' battery. The EVs will be paired to the wind farm through a controller, which aim is to mitigate the wind power fluctuations coming from sudden and unpredictable wind speed variations.

1.4 Thesis objective

The thesis concerns about the potential of a HPP connected to the substation of Åkirkeby. This hybrid generation unit is a combination of wind turbines, where the focus will be on its power output at the 10.6 kV voltage level substation, and an aggregated population of EVs able to modulate their charging level. In fact, the set of EVs will be connected at the point of common coupling (PCC) of the substation, adjusting its power consumption to provide ancillary services to the wind farm.

Thus, the thesis' goal is to investigate **how EVs can be coupled with the HPP to mitigate the injection of wind power fluctuations into the power grid**. For this purpose, the main thesis' objectives are collected below:

- **How can EVs manage their output in order to satisfy a desired power or energy profile at the PCC?** Caused by an even higher RES' penetration, the EVs could play a key role in order to contrast unexpected variation of the power profile at the PCC due to wind power fluctuations. The main interest is to design controllers able to detect the wind farm power production to control the charging power consumed by the considered EVs aggregation via unidirectional chargers. A first controller is planned to control the EVs as a function of the wind farm's active power production. Then, a second controller is investigated to control the same EVs population as a function of the wind farm's energy production. The goal is to investigate on the different control logic functions that must be applied to obtain the aforementioned controllers;

- **How much does the EVs' delay influence HPP's power output controllability?** As any physical system, the EVs are characterized by a certain response time to react to a control signal and modify their charging power. As a consequence, this delay could severely affect the capability of controlling the power output of the analysed HPP. In addition, the EVs' time response is not uniquely defined, meaning among the EVs population some of them could react before/later than others. After the delay's representation is developed, it is applied to the different control strategies with the aim to minimize the latency's impact.

- **How can EVs' charging pattern influence the possibility to control the EVs for power regulation?** EVs, in respect to BESSs, are not always grid connected. Thus, it is necessary to consider the EVs battery's characteristics and the average daily driving patterns to detect the EVs' state of charge when plugged in to be charged. Additionally, a feasible charging window when the EVs could be available to provide grid services must be defined. Thus, the resulting influence in the designed controllers is analysed.

1.5 Thesis outline

This thesis is based on the aforementioned objectives organized in seven chapters. Starting with a theoretical background about hybrid power plant, it moves progressively to the description of the wind farm and the EVs that compose the hybrid wind power plant in Åkirkeby. Then, the model implementation and finally the main results are summed up and discussed. A short description of each chapter can be read below:

- **Chapter 2** begins with the definition of hybrid power plant and the benefits that can be obtained with this configuration, focusing on the power smoothing challenge. Then, a broad description of Bornholm's power system and the composition of Åkirkeby's substation is provided.

- **Chapter 3** analyses the first main component of this hybrid configuration: the wind farm installed in Kalby. Starting with a characterization of the requested stages to subtract energy from the wind, the power fluctuations problem is localized in the nominal wind power curve, concluding with the technical data of the three wind turbines installed on site.

- **Chapter 4** contains the second component of this hybrid configuration: the electric vehicles. After a description of the role these vehicles could have for ancillary services, the ongoing technical regulation as well as the electric vehicles attributes to provide flexibility are discussed. The charging pattern's impact is finally connected to Kalby wind farm, underlying shared interests.

- **Chapter 5** described the model implementation of Åkirkeby substation and the two studied controllers. The *Power-to-Power controller* and the *Energy-to-Power controller* are discussed firstly, followed by chargers, electric vehicles response and state of charge protection's models.

- **Chapter 6** collects the technical results of the investigated study cases. The *Power-to-Power controller* and the *Energy-to-Power controller*'s results are displayed following the same structure, thus being able to compare how the EVs' attributes influence each controller. As a conclusion, a comparison in between the three and single phase chargers' application to both controllers is developed.

- **Chapter 7** concludes the thesis, answering to the thesis objectives and pointing at future works.

This thesis contains technical information, mainly focused on real Danish data, aiming to create a realistic and feasible scenario as a small scale pilot project for future studies.

2 Hybrid wind power plant: the study case in Åkirkeby

The combination of RES with BESS can arise benefits for both the renewable producers and the electrical grid itself. Starting with the characterization of a HPP, the services that could be provided by a HPP are described, referring mainly to power smoothing. Then, an overview of Bornholm power system and the on going "Insulae" project is given. Finally, the topology of the investigated substation located in Åkirkeby is reported and commented.

2.1 The hybrid wind power plant concept

The concept of a HPP can be defined as "a power system, using one renewable and one conventional energy source or more than one renewable with or without conventional energy sources, that works in 'stand-alone' or 'grid-connected' mode" [15]. In the specific case of on-grid HPPs, being integrated with the whole power grid, their aim is to supply energy into grid when requested, providing additional ancillary services if possible.

Considering just the RES and not the combination with traditional power plants, a HPP solution can be diversified depending on the RES available and the eventual combination with a BESS. In this project, a HPP composed by wind power generators and a storage system is investigated.

Depending on how the two HPP's partakers are connected to each other and to the external grid, the following traditional set up can be underlined and observed in Figure 2.1 [16]:

i. Co-Located HPP: system where both wind farm (WF) and BESS are connected to the same substation through two different points of connection (POC), being this substation the intermediate point between the HPP and the external grid. It is required that the HPP controller own abilities to manage the individual power output, to such an extent that the whole system can be seen as a single and aggregated power plant (Figure 2.1a).
ii. Wind Turbine Generator (WTG)-Coupled HPP: this configuration, already provided by some wind turbine producers, is focusing on the existing equipment inside the WTG's hub. Taking into consideration the wind turbine type C (see Section 3.1), this set up would require to interconnect the BESS to the DC link in the rotor-side converter, meaning that there will be a BESS for each WTG installed in the wind farm. From the HPP controller's point of view, the characteristics of the previous configuration are still valid, adding up the more advanced functionality to control each single BESS simultaneously but separately in terms of control signals [17] (not shown in Figure 2.1).
iii. DC-Coupled HPP: the interconnection between the two assets is provided with a DC link at a grid level. Different power converters can be arranged if the grid connection is then realized at a high voltage alternating current (HVAC, see Figure 2.1b) or direct current (HVDC, see Figure 2.1c) level. A choice is generally taken as a function of the WF location (onshore or

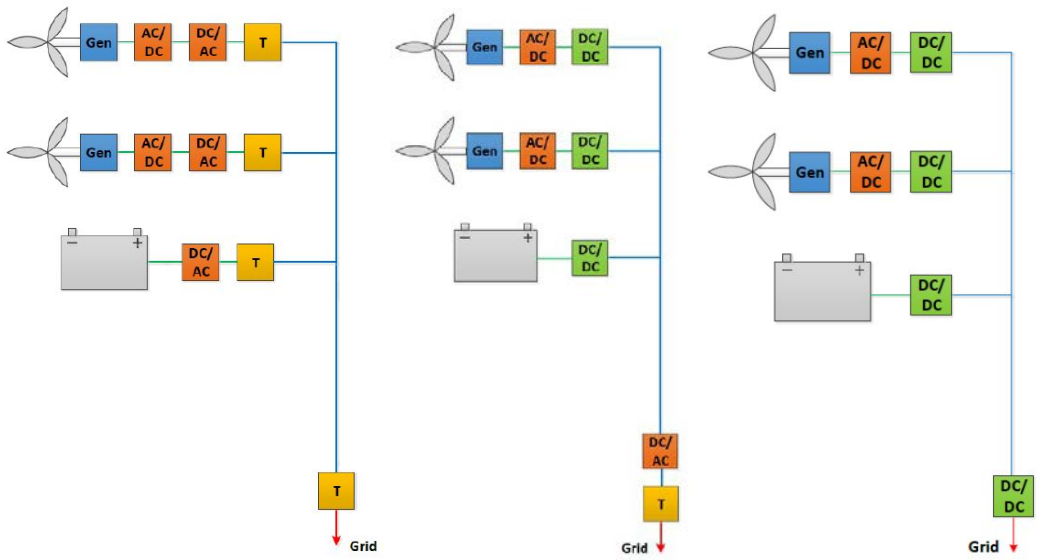

(a) Co-Located HPP (b) DC-Coupled for HVAC (c) DC-Coupled for HVDC

Figure 2.1: HPP's configurations [16]

offshore). From the HPP controller's point of view, its characteristics are closer to the one in a Co-Located HPP.

2.2 Benefits from a hybrid power plant configuration

As a result of several benefits that can arise by combining variable RES and ESS, this new configuration integrating WTGs and BESSs can be compared to a thermal power plant from a perspective of power output controllability, still maintaining the positive traits of sustainable energy generators. In fact, interaction of BESS and WTG will give rise to the increase of the overall power production output and reliability. The main benefits can be summarized as follows:

- **Increase of annual energy production and related capacity factor**. If the HPP output is optimized in respect to the electricity demand, excess energy production can be stored in the BESS, helping to avoid WTG curtailment during high wind speeds, and released by the BESS in case the WTG production level is lower than load demand. It allows to obtain a relatively stable power production and greater total energy production from the grid's point of view [18];
- **Possibility to reduce power output fluctuations coming from each WTG or the overall power output gradient of the HPP itself**. The BESS could be aimed at smoothing power production fluctuations due to stochasticity of the wind speed. Benefits of the "Power smoothing" (or "Power smoothening") method, which is gaining more and more relevance in the past few years, are investigated in this report since this strategy lies behind one of the implemented controllers. It is also possible to find a great number of literature focused on this topic. For example, in [19] a smoothing control method based on the derivative of the produced power is applied to both PV and wind power generation fluctuations, considering an adaptive coordination of the smoothing level to regulate the state-of-charge level of a large-scale BESS. A similar state-of-charge feedback control is investigated also in [20]. In

[21], the adaptive wind power smoothing is realized investigating on the minimum capacity required by the BESS to reach the addressed goals. The concept of introducing the wind power forecast to smooth out the injected power in the grid is analysed in [22], while a closed loop controller using a PI regulator can be found in [23];

- **Increase in HPP power output flexibility**. The control of different technologies through power electronic components can help to fulfil grid code requirements, since the ability of BESS to ramp up and down the active power output with short time response makes the HPP capable of providing AS, such as frequency regulation, synthetic inertia response, and power oscillation damping [24] [25];
- **Possibility for enhancing the energy management**. Deviations between forecasted and actual WF power production could be compensated by a BESS. Its presence leads to a lower dependency on weather forecasts and makes the HPP able to participate into different markets (Day-ahead, Intra-day, Balancing market, as well as AS market) [26]. This concept is realized behind a second controller designed and investigated in this work, that aims to manage the energy production from the considered WF. Particular interest raised behind the control logic of the energy controller implemented in [27].

2.3 Bornholm power system and "Insulae" project

Bornholm is a small Danish island of 588.3 km^2 located south of Sweden in the Baltic Sea. The island is electrically coupled to Sweden through an offshore AC 60 kV cable with a nominal transfer capacity of 60 MVA.

The complete generation set of the island can be summarized as follows [13][28]:

- 16 MW biomass CHP, steam turbine with possibility to be boosted to 24 MW or 36 MW if run with oil or coal;
- 3 MW biogas CHP, composed of two gas turbines;
- 23 MW photovoltaic (PV) panels, divided between 8 MW on rooftops at 0.4 kV and 15 MW among PV parks connected at 10 kV voltage;
- 37 MW wind turbines, obtained by a total of 42 turbines (24 micro turbines under 100 kW, 1 turbine in between 100 kW and 1 MW and the remaining 17 machines over 1 MW).

Moreover, the island can be disconnected from the mainland, running additionally 58 MW of power reserve for islanded operation (25 MW of oil steam turbine and 33 MW of diesel engines). In this regard, different activities have been carried out, testing capability of the Bornholm power grid to operate in islanded mode. For instance, in 2017, the cable had to be de-energized due to technical maintenance through the second half of September. All the undispatchable generation was disconnected while the wind turbines were limited, letting the power reserve to maintain power system parameters into the appropriate ranges. It has been observed that the total generation capacity of the system could support the insular energy demand while taking frequency and voltages into proper admitted values.

In addition, Bornholm is continuously used for research activities to reach the goal of 100% renewable energy generation, being also one of the lighthouse islands for "Insulae H2020" project [29]. The main goal of the project is to promote innovative solutions aiming at EU islands' decarbonization [28]. In fact, usually islands are isolated energy systems, characterised by:

- 3 to 4 times more expensive energy cost than on the mainland;
- 2 to 3 times higher average carbon intensity than pollution level on the mainland;
- up to 10 times higher losses than EU-28 average;
- high dependency on the fossil fuel import.

Scaling up renewables, energy storages, and clean transportation, and improving overall efficiency of the power system can lead to a higher level of energy self-sufficiency and SOS on the island, while fighting against the climate change. Several activities must be carried out to reach these results, dealing with an even more flexible power market. Islanding operations [30], AS provision [13], supplementing uncontrollable generation [31], demand side management, voltage and frequency regulation [32], wind power and PV integration [28], and EVs incorporation into the power system are just few of the ongoing research.

2.4 The topology of Åkirkeby substation

Åkirkeby is the third largest town in Bornholm, with an area of circa 1.71 km^2. It is located between Rønne and Nexø in the southern half of Bornholm. The thesis focuses on Åkirkeby 60/10.6 kV power substation, of which the layout is reported in Figure 2.2.

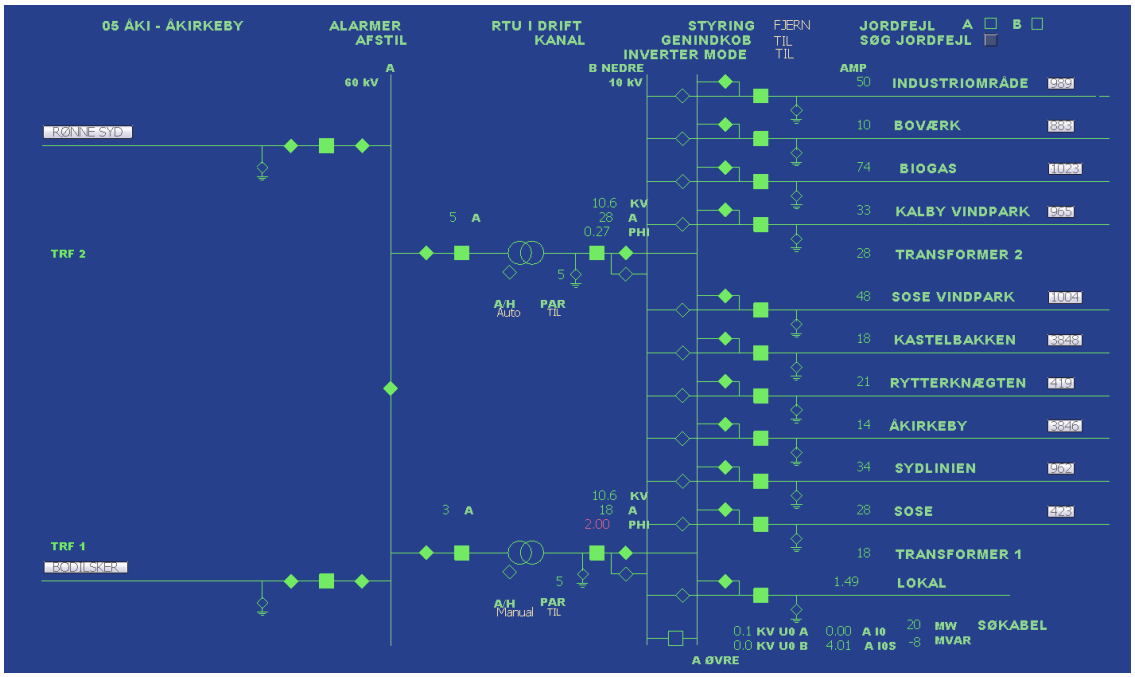

Figure 2.2: Layout of Åkirkeby grid

The substation interconnects Rønne and Bodilsker (4 km West Nexø) via a 60 kV voltage line. In Åkirkeby, the voltage is reduced to 10.6 kV with two 63/11 kV transformers of 16 MVA and 10 MVA (tap-changer positions are adjusted to maintain a voltage of 10.6 kV on the LV side). From the transformers, the grid is split into eleven under-ground cables to connect the users, here specified with their identification number (id.) placed in the white frame on the right side of Figure 2.2. Among these feeders, a substantial distinction can be given by dividing the feeders into consumption and production users.

On the consumption side, the following feeders can be highlighted:

- Industriområde (id. 989);
- Boværk (id. 883);
- Kastelbakken (id. 3848);
- Rytterknægten (id. 419);
- Åkirkeby town (id. 3846);
- Sydlinien (id. 962);
- Sose (id. 423).

For the sake of simplicity, technical characteristics of the cables connecting the station to the consumers are neglected, going beyond the goal of this project.

On the production side, the remaining feeders are the ones summarized below.

- Biogas (id. 1023, acronym BIO) - biogas power plant composed by two synchronous generators with nominal apparent power of 1.891 MVA each and nominal voltage of 10.6 kV, directly connected to the substation without any trasformer;
- Sose vindpark (id. 1004, acronym SOV) - Sose wind farm composed by five WTGs type A with nominal power of 1.3 MW each and nominal voltage of 690 V. Each WTG has an individual transformer ($11/0.7$ kV, nominal apparent power of 1.6 MVA). The first wind turbine is connected to the substation via a double under-ground connection, while between each two consecutive wind turbines a single under-ground connection is installed;
- Kalby vindpark (id. 965, acronym KAV) - the wind farm main focus of the project. A detailed characterization of the WF is presented in Section 3.3. The WF is composed by three WTGs type C with a nominal power of 2.0 MW each and a nominal voltage of 690 V). Each WTG has a individual transformer ($11/0.7$ kV, nominal apparent power of 2.1 MVA). The under-ground interconnection is done following the same structure as in SOV.

A deeper representation of internal interconnection of the listed above production feeders is given in Figure 2.3.

It must be underlined that on the layout in Figure 2.2 an additional feeder representing the 7.5 MW Bodelyngsvejen PV park and connected to the 10.6 kV side of the Åkirkeby substation is missing. For the inability to represent and gather historical production data for this PV park, the presence of the feeder will be neglected during the whole project.

In Table 2.1, types and technical characteristics of each single under-ground cable (following the structure shown in Figure 2.3) are collected. It is defined if it is a single line or two lines in parallel (*single* or *double*), rated voltage and current (V and I) as well as the placed length (L). Moreover, considering the method of symmetrical components [34], the resistance and reactance for the positive and negative sequences (R' and X') as well as the related values for the zero sequence (R_0 and X_0) are collected.

In Table 2.2, the three-phase transformers with their technical characteristics are collected. *ÅKI T1* and *ÅKI T2* are referred to the two main substation transformers, whereas *SOV T* and *KAV T* refer to individual WTG transformers in SOV and KAV, respectively. For each of them, it is reported the nominal transformer ratio (k), nominal apparent power (Sn), vector group, the short-circuit rated voltage for the positive and negative sequences (v_{cc}), copper losses (P_{cu}) and the short-circuit

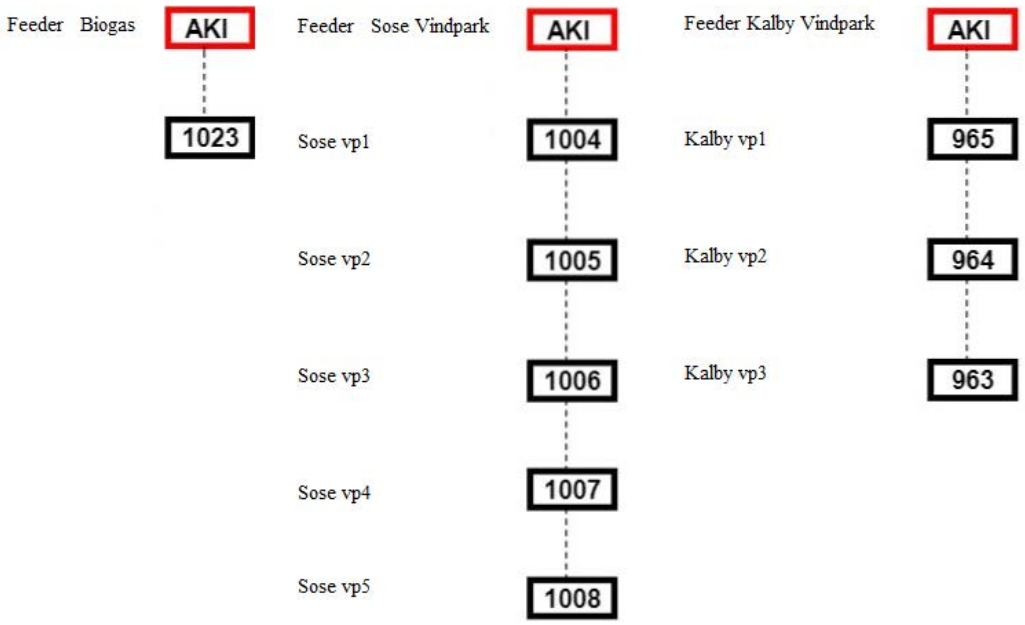

Figure 2.3: Power production feeders' connection, adapted from [33]

Table 2.1: Cable characteristics

Id. section	Cable Type	Lines [#]	V [kV]	I [kA]	L [km]	R' [Ω/km]	X' [Ω/km]	R_0 [Ω/km]	X_0 [Ω/km]
ÅKI - 1023	3 x 95 mm^2 PEX-Al	Single	12	0.307	2.4	0.3207	0.095	0.9621	0.285
ÅKI - 1004	3 x 150 mm^2 PEX-Al	Double	12	0.392	3.24	0.2071	0.09	0.6213	0.27
1004 - 1005	3 x 150 mm^2 PEX-Al	Single	12	0.392	0.3	0.2071	0.09	0.6213	0.27
1005 - 1006	3 x 95 mm^2 PEX-Al	Single	12	0.307	0.3	0.3207	0.095	0.9621	0.285
1006 - 1007	3 x 95 mm^2 PEX-Al	Single	12	0.307	0.3	0.3207	0.095	0.9621	0.285
1007 - 1008	3 x 50 mm^2 PEX-Al	Single	12	0.21	0.3	0.6413	0.106	1.9239	0.318
AKI - 965	3 x 150 mm^2 PEX-Al	Double	12	0.392	0.508	0.2071	0.09	0.6213	0.27
965 - 964	3 x 150 mm^2 PEX-Al	Single	12	0.392	0.282	0.2071	0.09	0.6213	0.27
964 - 963	3 x 95 mm^2 PEX-Al	Single	12	0.307	0.287	0.3207	0.095	0.9621	0.285

rated voltage for the zero sequence (v_{cc0}). For the gathered data, it can be concluded that the two parallel connected transformers in the substation are found to be in the so-called perfect parallel condition. As a consequence, the total power transferred will be equally divided in between them, in a proportional relation in respect to their nominal apparent power: talking in absolute terms, the active and reactive power passing through the transformer *ÅKI T1* will always be greater than the one passing through *ÅKI T2*, being the nominal apparent power of *ÅKI T1* 60% higher than *ÅKI T2*.

Table 2.2: Transformer characteristics

Name	k [kV/kV]	Sn [MVA]	Vector Group	v_{cc} [%]	P_{cu} [kW]	v_{cc0} [%]
ÅKI T1	63/11	16	YNd11	8.87	18	7.51
ÅKI T2	63/11	10	YNd11	8.87	18	7.51
SOV T	11/0.7	1.6	Dy11	8	16	7.5
KAV T	11/0.7	2.1	Dyn5	7.3	10.5	6

For this project, the data gathering has been conducted with the SCADA system, which is a control system architecture for process supervisory management to interface with the electrical grid and

power plants. For each production and consumption feeder previously described and shown in Figure 2.2, the data related to active power and reactive power consumption at the 10.6 kV bus have been collected. It is underlined that the used convention is the one to consider each feeder as a consumption feeder. It means that the power values have a positive sign if the power flows from the 10.6 kV bus to the feeder itself, while a negative sign if the power flows in opposite direction since the feeder is effectively injecting power in the 10.6 kV line.

2.5 Summary

In this section, the concept of hybrid wind power plant is exposed, detailing the main configuration that can be found nowadays. Among all the underlined services a storage system could provide to in a HPP, particular attention has been devoted to the "Power smoothing" cause.

A big picture of Bornholm power system is given, within which a brief introduction about "Insulae H2020" project is proposed, being Bornholm island included in this European project. Finally, the topology of Åkirkeby substation is detailed, main focus of the project, in which all the technical data about the substation, installed transformers and underground cables are collected.

The installed HPP in Åkirkeby is composed of two main components: the Kalby WF and the EVs, which are deeply described in Chapter 3 and 4, respectively.

3 Wind power integration: Kalby wind farm

Wind power represents the most growing RES, nowadays already widely installed all around the globe. Since its penetration level increased significantly, the related impact on the modern power system's operations sparked more and more interest. As a consequence, power electronics and advanced control techniques have been investigated to increase the production's manageability of this uncontrollable RES [35].

In order to understand the impact that a WF can have on the connected power system, it is necessary to understand how the power is converted from mechanical into electrical form, as function of the wind speed magnitude. Then, a description about the wind farm installed in Kalby is reported, including an example of power fluctuations later applied to the designed model.

3.1 Wind power conversion stages

Figure 3.1 provides the stages the wind energy has to pass through in order to be transformed from natural to mechanical and finally electrical energy form.

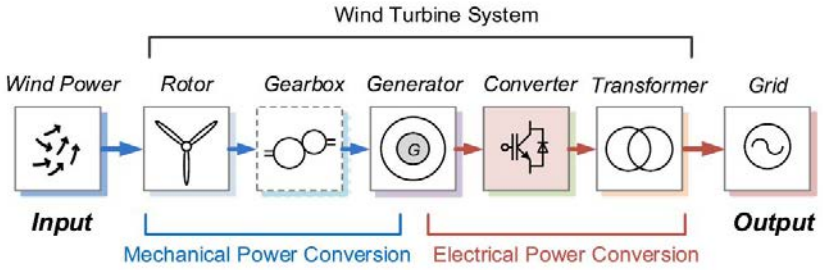

Figure 3.1: Wind power conversion stages [35]

The conversion system can be divided into two main part. First, the power coming from the wind energy itself must be converted into the shaft's rotation of the electrical generator by means of the rotor and (eventually) a gearbox. Consequently, from the terminals of this component, the produced electricity can be controlled via a power converter, when present, and the transformer, to adjust the electrical parameters to the required values of the connected power grid. There are several different possibilities to categorized a WTG, however the most common practise is to consider speed controllability and types of electrical generators, features that define which components illustrated in Figure 3.1 need to be installed, as it can be easily seen in Figure 3.2:

A) Fixed speed asynchronous generator: WTG Type A is the pioneer generator as well as the cheapest configuration. On the mechanical side, the generator is connected to the rotor through a gearbox. On the electrical side, the squirrel cage induction generator (SCIG) is

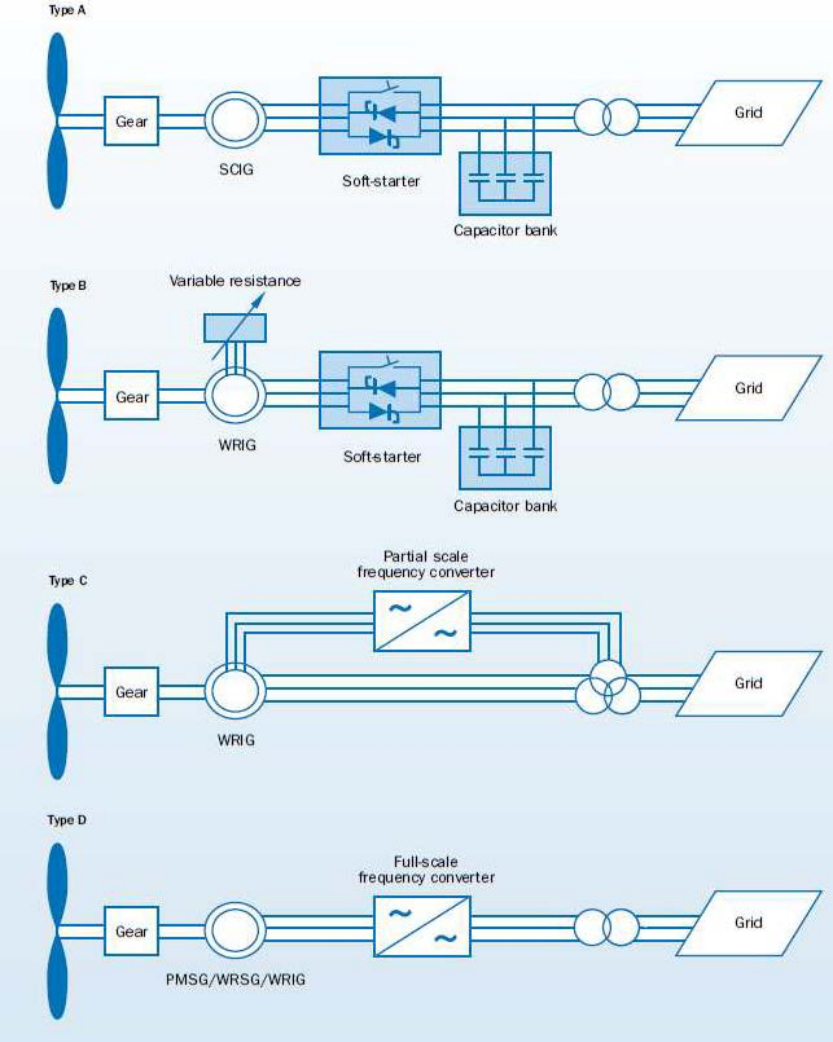

Figure 3.2: Wind turbines typologies [36]

directly connected to the grid, eventually through thyristors to decrease the initial starting current. The capacitor bank is installed to decrease the required reactive power consumption, typical of SCIGs. Being the nature of the SCIG at fixed speed, the wind fluctuations are directly converted into mechanical and then electrical fluctuations. It was the most popular installed WTG due to the cheap and simple SCIG, before the advent of stringent grid code requirements due to which the drawbacks of this typology have to be considered in the first place;

B) Small variable speed asynchronous generator: WTG Type B has a wound rotor induction generator (WRIG), which allows the access to the rotor's electrical terminals to connect an additional variable resistance. Thanks to this additional component, the stiff mechanical curve of the SCIG can be slightly adjusted to improve the fixed speed of the previous configuration. The typical allowed variation is around 0% to 10% above the synchronous speed and the power fluctuations injected into the grid are lightly reduced;

C) Variable speed doubly-fed asynchronous generator: WTG Type C used still a WRIG, however the electrical connections differ from the previous two families. Whilst the stator is directly connected to the grid's transformer, not allowing any apparent speed controllability,

the rotor's terminals are connected through a back-to-back power converter to a tertiary winding of the grid's transformer. This configuration, better known as doubly-fed induction generator (DFIG) is by far the most installed in the wind energy market, mainly for on-shore installations. This scaled power converted, generally installed with a nominal power around 30% in respect to the WTG, admits to a speed variability into the range -30% to +30% in respect to the synchronous rotational speed, making this WTG able to operate in both over and under synchronous area, achieving the maximum aerodynamic efficiency over a wide range of shaft rotational speed. Moreover, thanks to the rotor converter used to balance the active power output, the wind power fluctuations are decreased;

D) Variable speed full converter generator: WTG Type D shows an electrical generator fully decoupled from the grid with a power converter, sized for the whole nominal power. Thanks to this more expensive configuration, the complete freedom in terms of mechanical rotational speed in respect to the electrical frequency is finally achieved, increasing the range in which the maximum aerodynamic efficiency is reached as well as reducing the overall injection of power fluctuations into the grid.

Additionally, the aforementioned WTG typologies are reported in Figure 3.3, where a comparison among power electronic development, rotational speed and WTs' size is shown. The grey area into the swept area of the turbines evidences the percentage by which the power production can be controlled through the electronic converter.

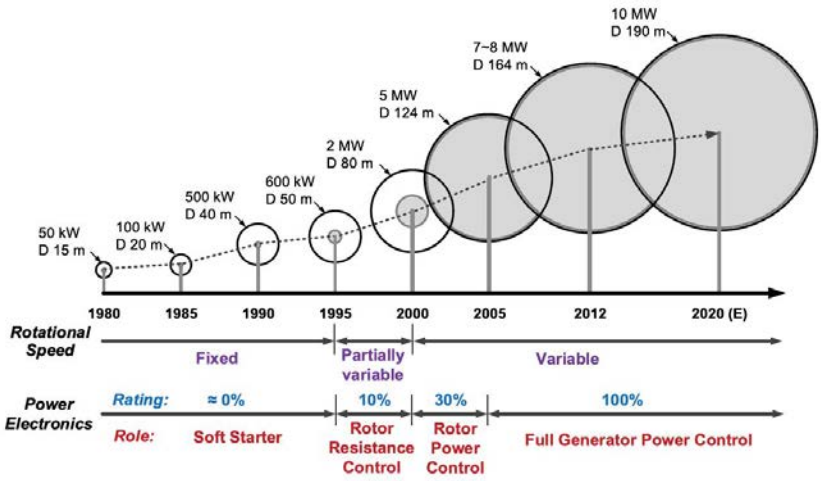

Figure 3.3: Wind turbines development [35]

In conclusion, passing from WTGs with fixed rotational speed (Type A and Type B) to WTGs with variable rotational speed (Type C and D), the advantages/disadvantages are trading their places. In fact, on one side the main advantages for WTGs Type A or B are the robustness, mechanical structure and control system's simplicity and overall low capital cost, while one the other side WTGs Type C and mainly Type D are characterized with an increase in energy capture as well as power quality and a reduction in the mechanical stress, even though leading to higher control system's intricacy and a consequent increase in capital expenditure.

3.2 Power curve and power fluctuations localization

The production of energy from wind can be obtained if the wind is blowing within a specific and defined speed range, generally expressed in $[m/s]$. This intrinsic characteristic, known as "Wind power curve", is a function of the installed WTG typology. A general representation is the one in Figure 3.4, where the main points are highlighted [37].

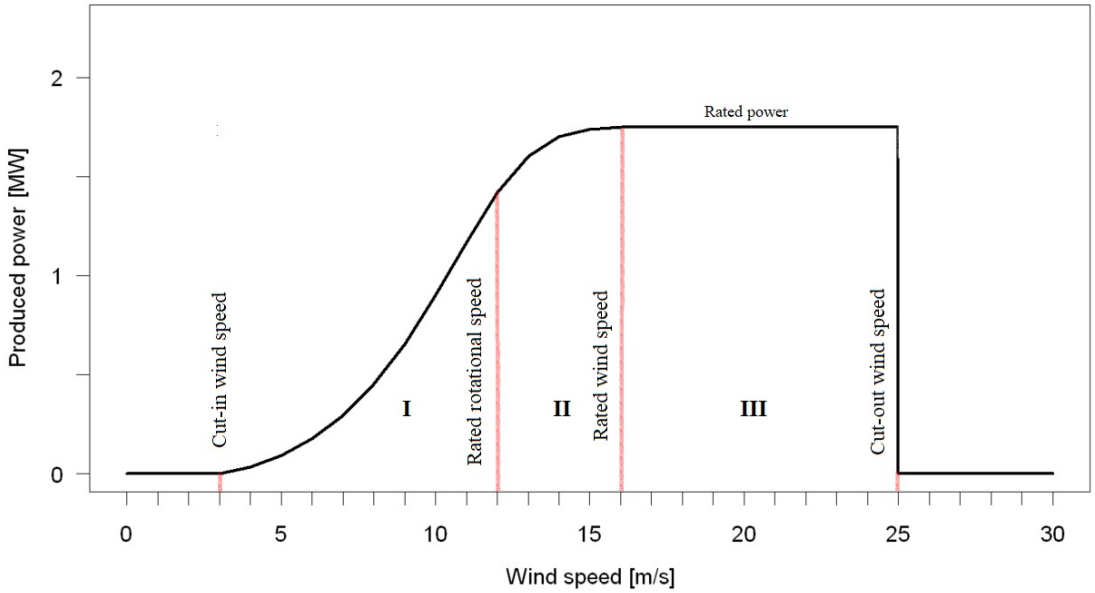

Figure 3.4: Nominal wind power curve

When the wind has a speed higher than the cut-in wind speed (generally in the order 3 m/s – 5 m/s), the production will start to increase, following a cubical function.

In section I of Figure 3.4, the aim is to maximize the production gaining as much as possible from the available wind energy passing through the rotor area, thus the possibility to vary the rotor speed (if available) will clearly help the wind turbine to maximize the aerodynamic efficiency over this whole range.

However, when entering into section II, the aerodynamic efficiency starts to decrease. Indeed, the generator's nominal rotational speed is generally encountered before the nominal power is achieved. Due to this downside, but willing to increase even more the produced power, the blades can be designed to be properly regulated, pointing the blade's profile into the wind direction to gain more power.

When the wind hits the rated speed (function of the WF's location and consequently of the installed WTG, generally around $10 - 15$ m/s), the blade's mechanism is used as a limiter for the power production, being necessary to decrease the gained power, thus escaping eventual excessive mechanical stresses in the generator. The rotor efficiency through the adjustment of the blades' position can be regulated with three mechanism: passive stall, pitch control and active stall regulation.

Finally, when the wind speed is blowing over the cut-out wind speed (quite high wind speed in the order of 25 m/s), it is necessary to decrease drastically the efficiency to zero because of the too

high stresses applied to the blades themselves. The control mechanism is done breaking first the WTG and applying the mechanical lock afterwards.

The wind power curve profile can be used for a better understanding of the related power fluctuations coming from unpredictable variations in wind speed. It is quickly grasped that the cubic dependence of the power curve in the section I in Figure 3.4 implies that even a small variation in wind speed can carry large power output swings, caused by the pronounced steepness of this curve.

A way to compensate these fluctuations is obtained by connecting several WTGs in the considered WF, allowing to a kind of natural mutual compensation. Indeed, the wind variations and gusts are not hitting all the installed wind turbines at the same time, but with time delays among them and with different magnitudes. Considering the same amount of WTGs, the wider the installation's area, the smoother the total power injection in the grid through the point of connection.

However, it is very difficult to reduce these fluctuations. This challenge has been analysed by different authors, some of these studies reported in Section 2.2, then a power controller is also investigated in this thesis, showing the main drawbacks and difficulties behind the not wished oscillating power output. Nonetheless, it could be worthier to consider the wind production as an energy source instead to a power source. With this simple mindset's change, looking at the WF from another perspective, the total energy output in a defined time frame is of a simpler and more accurate forecasting, becoming more a function of the overall weather forecast than the single and instantaneous wind speed prediction.

3.3 The wind farm in Kalby: characteristics and power production

As already mentioned in Section 2.1, the primary interest for this thesis is to analyse the HPP composed by the combination of a wind farm and a storage system. For this analysis, the wind farm installed in Kalby is the chosen one.

The three *V80-2.0 MW*, the technical name of these wind turbines, entered into work in 2006. They are WTGs Type C with a total nominal power of 6 MW, each of them characterized with the main parameters collected in Table 3.1:

Table 3.1: *V80-2.0 MW* data [38]

Rated power	2,000 kW	*Operational interval*	10.8 – 19.1 rpm	*Rotor diameter*	80.0 m
Cut-in wind	4.0 m/s	*Nominal revolutions*	16.7 rpm	*Blade length*	39.0 m
Rated wind	16.0 m/s	*Power regulation*	Pitch regulated	*Blade chord max.*	3.5 m
Cut-out wind	25.0 m/s	*Tower type*	Tubular steel tower	*Nacelle length*	10.4 m
Generator	4 pole, DFIG	*Hub height*	60.0 m	*Nacelle width*	3.4 m
Gearbox	two planetary stage, one helical stage	*Hub diameter*	3.3 m	*Nacelle height*	5.4 m

The rated power as well as the operational wind range can be noticed also in Figure 3.5, showing the nominal power curve of the selected *V80-2.0 MW*. When the wind is blowing at a speed higher than 4 m/s, the WTG starts to produce power. The production will rise with a cubic relation of the wind speed itself until the constraints due to the rotational speed as well as the pitch regulated mechanism are limiting the power at the nominal power of 2 MW, reached at wind speed of 16 m/s. The plateau will be maintained until when the wind will blow with speed of 25 m/s, condition that will turn on breaking mechanism to stop the wind turbine for safety reasons.

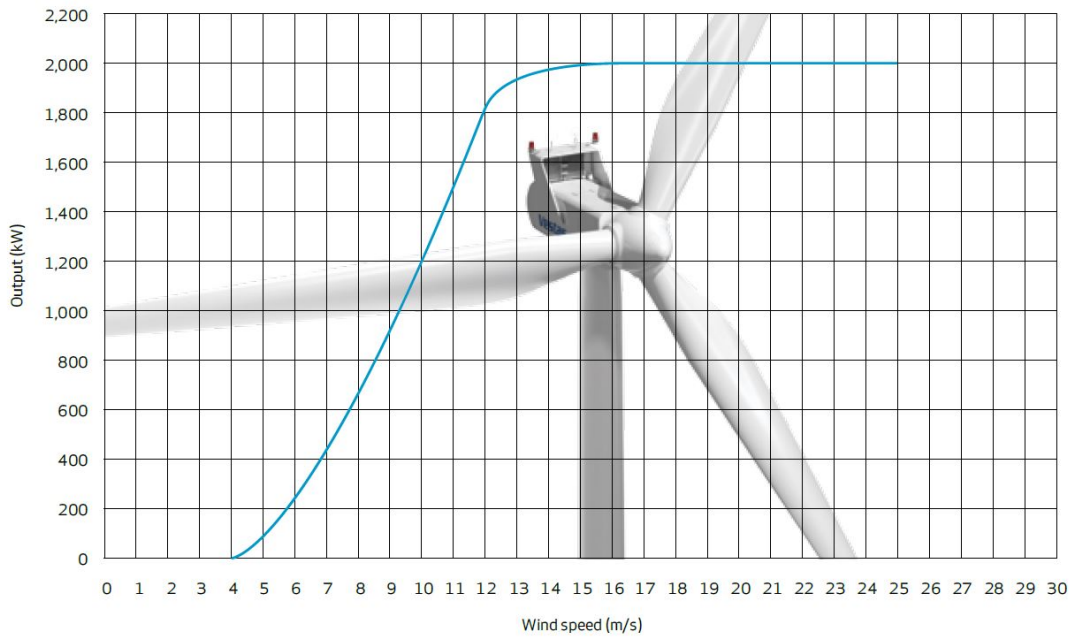

Figure 3.5: *V80-2.0 MW* nominal power curve [38]

The steepness of the power curve highlighted in Section 3.2 is now shown in a practical example, carrying the related production's drawbacks due to unpredictable wind speed oscillations. As a first step, it has been decided to investigate three different scenarios in terms of wind intensity in Bornholm, identified in the following days (additional data can be found in Appendix A) [39]:

- *Windy day*: with an average wind speed of 8.9 m/s, substantially constant high wind speed through the whole day with gusts up to 20.1 m/s, the 3^{rd} January 2020 is identified as a windy day, from now on marked with *W*.
- *Not windy day*: with an average wind speed of 5.5 m/s, substantially constant low wind speed through the whole day with gusts up to 12.8 m/s, the 27^{th} January 2020 is identified as a not windy day, from now on marked with *NW*.
- *Variable windy day*: although with an average wind speed 6.4 m/s, the 22^{nd} January 2020 was characterized by a constant decrease in the wind speed intensity, passing from an average wind speed of 10.6 m/s between midnight – 6 *am* to an average wind speed of 3.15 m/s between 6 *pm* – midnight. For this reason, this day is identified as variable windy day, from now on marked with *VW*.

For each of the selected days, the total injected active and reactive power coming from this WF has been considered, as the summation of the contribution of each wind turbine. The data gathering has been conducted with SCADA system. It is underlined that the used convention of the feeder is the load convention. It means that the power values are positive if the power flows from the 10.6 kV bus to the user itself, negative if the power flows in opposite direction, since the user is effectively injecting power in the 10.6 kV line.

The injected active power from Kalby wind farm is plotted in Figure 3.6, where the three selected days are displayed. It can be easily noticed how, throughout the day, the power injection at the 10.6 kV bus in Åkirkeby's substation is highly fluctuating, due to the sudden and uncontrollable

wind speed variations. Furthermore, the wind speed trend of the three scenarios are reflected in terms of active power production.

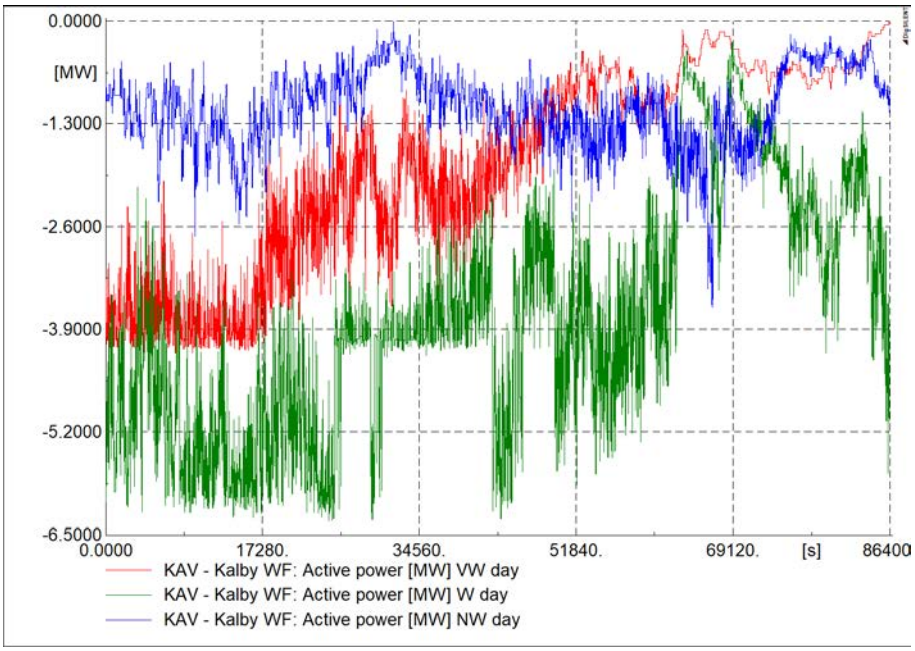

Figure 3.6: Kalby wind farm active power production

Moreover, for each production and consumption feeder previously described and shown in Figure 2.2, the data related to active power and reactive power consumption at the 10.6 *kV* bus have been collected. These data are reported in Appendix B.

3.4 Summary

Among all the RESs, wind power is the one that expanded the most in the last decades. The wind energy market is characterized with several WTG types, based on different components installed in the nacelle. Nowadays, WTGs type C are the most installed worldwide, even though for offshore installation WTGs type D gained more interest in the last years.

The "Wind power curve", describing the technical relation in between wind speed and active power production, is a consequence of the installed WTG type, becoming closer to the ideal power curve if the turbine is pitch regulated and equipped with a variable speed electrical generator. Nonetheless, power fluctuations coming from unpredictable wind speed variations are essentially impossible to be avoided, even though some appreciable reductions can be obtained via WTGs type C and D.

The analysed wind farm, installed in Kalby, is composed of three *V80-2.0 MW* WTGs type C, directly connected through underground cables to the 10.6 *kV* line of Åkirkeby substation. Gaining the power production profiles from SCADA system, it is possible to observe how the wind speed oscillations are translated into active (and reactive) power fluctuations, consequently injected into the power system. The goal of the project is to manage these variations, for a certain extend delivering an AS provision for Kalby wind farm itself, thanks to the EVs aggregation interconnected at the 10.6 *kV* line, which is introduced and described in the following chapter.

4 Electric vehicles in the power system: charging pattern's impact

The electric vehicles are gaining more and more interest in the car industry, becoming day by day more competitive in terms of both performance and cost. After a small background on the existing technologies and their charge modes, the electric vehicles are presented with their added value as ancillary services' providers. Furthermore, being not always grid-connected, the behaviour of the Bornholm inhabitants is investigated to infer the charging pattern of the considered electric vehicles' aggregation, concluding with the shared interests between electric vehicle' owners and Kalby wind farm.

4.1 Electric vehicles characteristics and charger typologies

Considering the Nordic region, electric vehicles' sales have been increased steadily in the last decade, achieving one of the highest ratio of electric vehicles per capita in the world [40]. When talking about electric vehicles, they can be categorized as follows [41]:

- Battery electric vehicles (BEVs) are powered by an electric motor, they have their own on-board battery as energy source which can be charged by plugging the vehicle into the charging station connected to the electrical grid;
- Hybrid electric vehicles (HEVs) are powered by an internal combustion engine as well as by an electric motor, used to complement the conventional engine. However, the electricity is generated internally via a regenerative breaking mechanism, not allowing the battery to be recharged from the power grid;
- Plug-in hybrid electric vehicles (PHEVs) have the same configuration of a HEV but this car can be additionally plugged into the grid to recharge the electrical battery;
- Fuel cell electric vehicles (FCEVs) are finally powered by the electric motor, running thanks to electricity generated from hydrogen or oxygen in fuel cells installed on-board and not through battery.

This thesis deals with the first group described, called from now on simply electric vehicles (EVs).

An EV is generally more expensive than an equivalent conventional car, having almost half of its price due to the battery itself. This drawback makes the complete electrification of the transportation sector even more difficult, connected also to the main concern of not having enough fast chargers. However, cost projections regarding batteries, in particular for Lithium-Ion based batteries, in addition to the very simple structure of the EVs, without many complex motion components, show how batteries and more generally EVs can become more and more competitive in the upcoming market [42] [43]. Throughout the work, the Nissan LEAF 2018 version with a 40 kWh Lithium-Ion battery capacity has been considered.

An EV is composed by an aggregation of several components aiming to control the power from/to the battery, depending on if in discharging or charging mode. In Figure 4.1, 4.2 and 4.3, colors portray components' function. The Battery Management System (BMS), composed of microcomputer based controllers to keep battery operations in safe operating zone, is marked in green. Power electronic components and EV's battery are represented in red and yellow respectively, and finally the external grid and internal safety breakers are shown in grey.

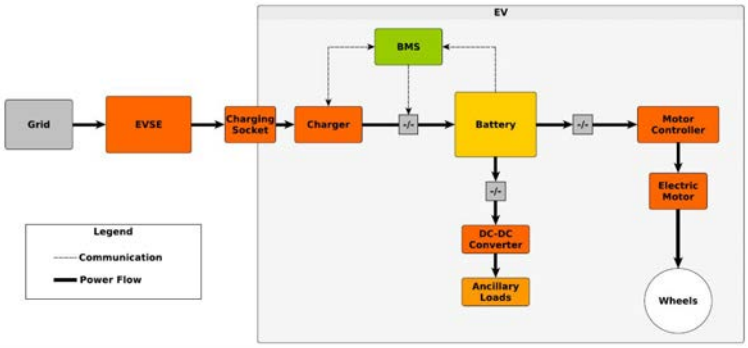

Figure 4.1: EV components architecture [44]

From the smart grid's perspective, EVs can be considered as a mobile DER, with battery and charging mode as main interests among EV's components.

Considering how the EV must be charged, the different Electrical Vehicle Supply Equipment (EVSE) standards and charger types for the Nordic region are collected in [40], described by the International Electrotechnical Commission IEC 62196 and differentiated by the following parameters:

- Current, Alternating Current (AC) and Direct Current (DC);
- Level and power, related to the power output range of the EVSE;
- Mode, describing the communication protocol between vehicle and charger;
- Type, referred to the socket and the connector used.

The chargers typically used for EVs are the on-board AC chargers and the external DC chargers. The most common charger is the AC one, allowing vehicles to be charged anywhere where an electrical socket and the related cable adapter is available. Thanks to the communication link for ensuring safe charging in the cable, the BMS can communicate to the EVSE to close the grid breaker, then AC power flows in the EV and it is converted into DC to charge the battery. On the other hand, EVs can support also a DC charging. In this case, the charging power electronics is placed outside the car, permitting bigger sizes and then supporting higher charging powers (from which it is also called DC fast charger). When the cable adapter is connected, the EVSE converts AC into DC current which is then directly injected into the EV's battery, under supervision of the BMS. These configurations are shown respectively in Figure 4.2 and 4.3.

As a conclusion, it is possible to take into consideration the IEC 61851, electric vehicle conductive charging system documentation [45], which stated that the most common power rates for domestic and public chargers are the ones depicted in Table 4.1.

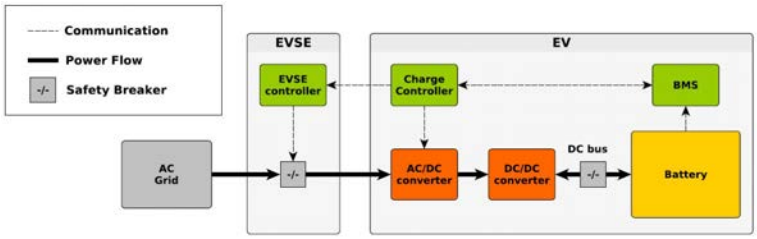

Figure 4.2: AC charging architecture [44]

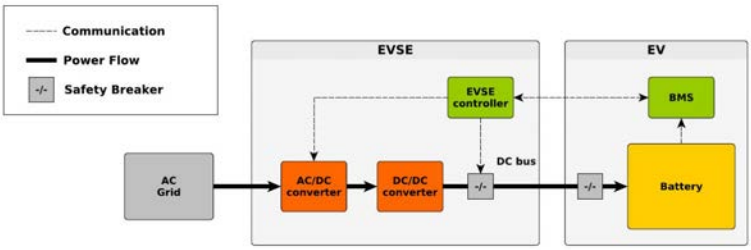

Figure 4.3: DC charging architecture [44]

Table 4.1: Charging power rates

Current [A]	**Voltage** [V]	**Grid Connection**	**Power** [kW]
10	230	1∼	2.3
16	230	1∼	3.7
32	230	1∼	7.4
16	400	3∼	11
32	400	3∼	22

In this project, two of these chargers will be considered: the single phase unidirectional 3.7 kW charger and the three phase unidirectional 11 kW charger, which will be defined from now on as *Ch-1ph* and *Ch-3ph* respectively.

4.2 The role of the electric vehicles as possibility for ancillary services

From the grid operator's point of view the most typical load profile has two power peaks, strictly related to the working hours. In fact, these trends are observed through the morning and the evening. However, considering just the load profile for a common Danish family, it is possible to deduce how these peaks are connected to domestic activities, so dependent upon when families are generally home. In this latter case, power consumption's peaks are found in the early morning (6 am – 8 am) and in the evening (6 pm – 9 pm), with an average energy consumption around $4,000$ $kWh/year$ [46]. The massive penetration of EVs will affect the EV owner's electricity domestic consumption and, looking at the problem from a wider perspective, the national load consumption, both in magnitude and peak shifting. On one hand, in Denmark with an average daily driving distance of 45 km/day [47] and with an average energy consumption of 5 km/kWh, each EV will increase the yearly energy consumption of $3,285$ $kWh/year$, increasing for more than 45% the overall energy

consumption of a Danish family (more details are provided in Section 4.5). On the other hand, EVs are expected to be be charged mainly when users arrive home after work (5 *pm* – 8 *pm*), meaning that the overall grid will be subject to an even higher power consumption.

In the NordPool [48] there are three different main markets [49]: capacity market, energy market and AS market. In order to deal with this expected increase of power consumption and to introduce RESs in the electricity market, the AS market is gaining importance. A RES is highly variable, non-dispatchable and also with limited predictability, making the market operators' job even harder. The solution that can be considered is the flexibility, defined as the "power adjustment sustained from a particular moment for a certain duration at a specific location" [50]. It must be seen as the capability of the system to adapt to variable and unforeseen changes in the power grid. The flexibility can be obtained from different actors, like generation units being able to change their working point fastly (e.g. gas-fires power plants), the power system itself (through interconnections) and from the demand side (through demand response and its integration with storage system in the electricity system).

As mentioned in Section 2.1, the primary interest for this thesis is to analyse the HPP composed by the combination of Kalby wind farm and a storage system. For this analysis, an aggregation of EVs is the storage system considered. In respect to a BESS, constraints coming from the vehicle-grid integration must be considered, defining charging restrictions as well as control strategies.

Indeed, ancillary services provision from EVs could play an important role not only for the analysed wind farm but also for the future power systems around the world. In fact, being characterized from an high degree of flexibility, quick response (seconds range), on-board storage system with eventually bi-directional power flow capability, it would be necessary to develop strategies to reconcile the needs of both drivers and the wind farm to provide power and energy balancing services. The key point behind all these possible strategies is the load behavior of each EV owner, which defines both when an EV is available, meaning connected to the power grid, and the related amount of stored energy. As a direct consequence, if the EV owner is willing to make its EV available, the EV could be used for ancillary services when it is parked, guaranteeing the minimum required state-of-charge (SOC) for the following usage. Without any doubts, controllable devices and related architecture to improve system efficiency, reliability and control algorithms, as well as a thick communication infrastructure to monitor constantly how the EVs aggregation, considered as a smart grid, is changing and varying along the day are cornerstones in a future system where EVs will take an important role for services' provision [51].

4.3 Technical regulation for energy storage systems

Every power plant has to withstand specific requirements set by the TSO, Energinet in DK (see Section 1.2. These regulations govern the connection of electricity-generating facilities to the public electricity supply grid, making sure they are not undermining the Danish SOS. There are dedicated codes for thermal, wind and PV plants, while the EVs have to follow the "Technical Regulation for Electrical Energy Storage Facilities" [52], from which the main definitions and constraints are collected in this section.

An electrical energy storage is defined as a facility or an aggregation of separate units that can absorb/release electrical energy from the public energy supply grid at the point of connection and/or directly from the RES installation. The definition includes both permanently connected systems,

such as BESS, and the temporarily connected facilities, like the EVs, even if the main goal of these on-board batteries is for transport of passengers and goods.

In Figure 4.4, it is possible to observe the different installation's points with the related definitions, summarized as follows:

- Point of common coupling (PCC) is the point in the public grid where consumers are connected and where the power is delivered;
- Point of generator connection (PGC) is the point in which generators' terminals are connected;
- Point of electrical connection (PEC) is the point in which the storage system terminals are electrically connected and the connection is established;
- Point of connection (POC) is the point in the public grid where the energy storage facilities are connected;
- Point of communication (PCOM) is the point from which the communication interface with the facilities is defined.

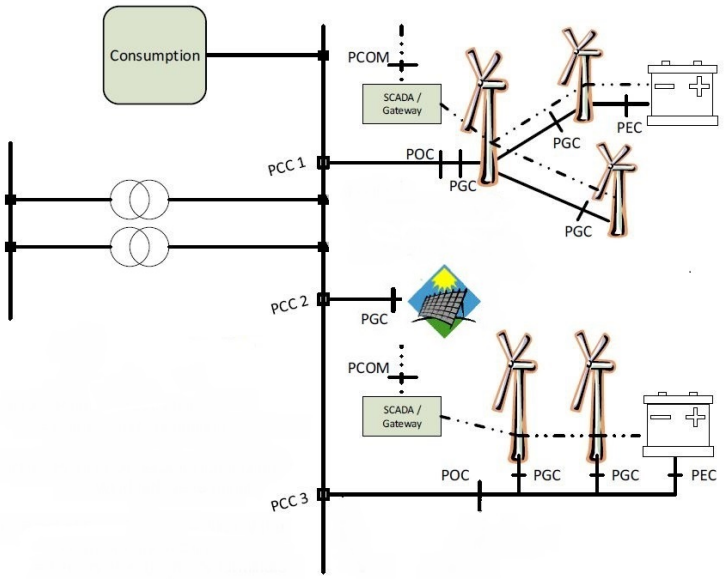

Figure 4.4: Installation points of facilities, figure arranged from [52]

The technical requirements in the regulation are divided into categories, based on the total rated power in the PEC:

A. BESS up to 125 kW;
B. BESS from and including 125 kW and 3 MW;
C. BESS from and including 3 MW up to 25 MW;
D. BESS from and including 25 MW or connected at voltages above 100 kV;
SX. Aggregation of BESSs from categories A and B;
T. Temporarily connected storage facilities.

As underlined in Section 4.1, in this thesis the analysed chargers are unidirectional, which are not technically included in any of these categories since the T group is related to two-way chargers known as Vehicle-to-Grid (V2G). Indeed, the unidirectional charger category has not been studied yet for grid support, as the V2G chargers being more fascinating for their capabilities to discharge

the on-board battery. It is one of the goal of this chapter to underline pros and cons of this one-way charger.

Nonetheless, including unidirectional chargers into category T, the main concern coming from the technical regulation regards the power quality. The leading points are related to DC content, rapid voltage changes and flicker, harmonics contents and measuring method that must be carried out in accordance with the standards stated in the IEC 61000 related to electromagnetic compatibility [53]. For this purpose, charger manufacturer, model number and nominal active power must be provided. For any further information, the reader is referred to the technical regulation itself.

4.4 Electric vehicles' attributes for power system flexibility

In order to investigate the behavior of EVs for AS provision properly, it is necessary to classify the main typical features of their response.

Firstly, it must be pointed out that nowadays, EVs are not capable to provide reactive power services, then no reactive power is exchanged between the EVs and the grid. Thus, the following analysis refers always to active power.

Secondly, the real EVs response cannot be completely ignored. Indeed, the system operator (in case of AS for the grid) or the wind farm itself for this specific project will see the EVs as a "black-box" with predetermined internal characteristics that cannot be easily changed. The stability and reliability of the EVs response can be achieved only by considering how the EVs are replying to a certain requested power output set-point [54].

Hence, the main attributes that characterize an EV flexibility response are [50]:

i. Directionality, related to the power flow's direction, being unidirectional or bidirectional with V2G charger;
ii. Set-point granularity, identifying the linearity of the charging power set-point;
iii. Activation time, time in between receiving the signal and activating the flexibility;
iv. Ramp-up time, period in between activation time and full service provision (upward time)
v. Ramp-down time, period in between activation time and full service provision (downward time)
vi. Accuracy, difference in between requested power and final delivered power;
vii. Precision, oscillations of the delivered power around the set-point value.

In Figure 4.5, the last five attributes are shown, underlying the difference between the requested and delivered power when controlling a flexible EV.

As mentioned at the end of Section 4.1, the two charger analysed in this project are the single phase unidirectional 3.7 kW charger (*Ch-1ph*) and the three phase unidirectional 11 kW charger (*Ch-3ph*), which allow the power to flow one-way from the grid to the on-board battery. Considering the required service for the connected wind farm, an unidirectional charger gives a degree of freedom less than a V2G charger. Indeed, it is only possible to charge the internal battery and the only way to decrease its SOC is by using it for transportation. A befitting analysis is carried out in Section 4.5.

According to the IEC 61851 [45], the EV charging current must be limited between the minimum charging current of 6 A and the EVSE rated current of 16 A for the considered chargers, in discrete

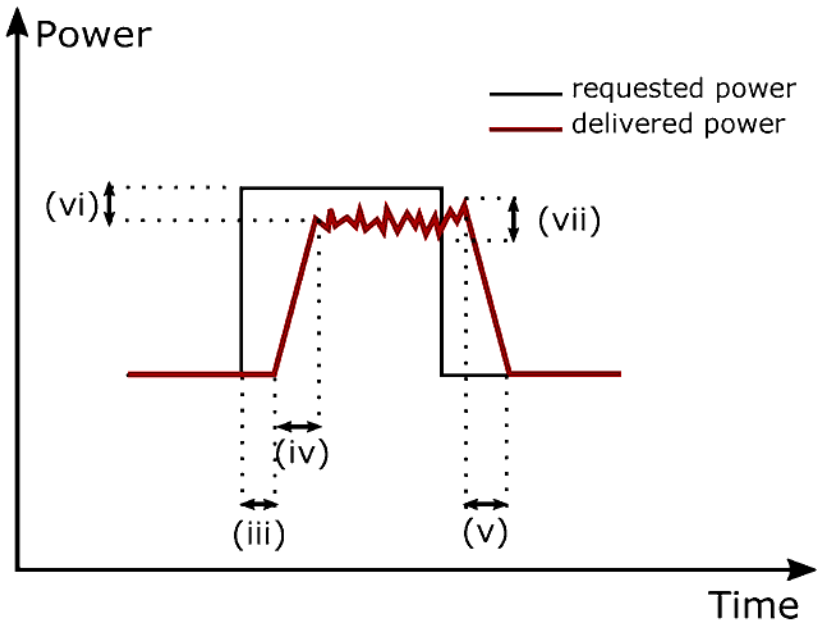

Figure 4.5: EV attributes for flexible demand response [50]

steps of 1 *A* (i.e. 6 *A*, 7 *A*, 8 *A*, ..., 16 *A*). Such capability of limiting the charging current and consequently the charging power is seen as a main step in enabling EVs for grid services. The analysis carried out will consider how this prerequisite can mine the controllers' requirements feasibility [54].

The EVSE installed on each EV receives the set-point signal from a remote position. The planning idea is that an EV aggregator will collect the information from the wind farm under analysis, calculating in a centralized way the appropriate signal that must be send to each EVSE to adapt the charging power output. It is then clear that a total response time, including communication latencies, chargers and EVs delays (considered as activation time), is of fundamental importance to asses the capability of the provision of time-critical services coming from an aggregation of EVs. Particularly, an analysis is performed applying the EVs activation time to investigate how the wind farm's requirements could not be achieved and how much the implemented controllers are depending on the time response.

For the sake of simplicity, it has been decided to consider EVs being able to apply instantaneous ramp-up/ramp-down power operations, making them capable to change the charging current with discrete steps as soon as the control signal is received, after the analysed activation time. Moreover, regarding accuracy and precision, it has been supposed that the EVSE are able to match the requested power with a fairly stable power output.

4.5 Charging pattern

From the power grid's point of view, the energy storage facilities belonging to category T have as main drawback the provisional grid connection, being not able to operate grid services throughout the whole day. It is then necessary to investigate battery characteristics, driving behaviour and charging pattern for the users to obtain a great approximation about daily driven distance, the

expected charging window and the probability that an EV is going to be charged.

A Danish National Travel Survey [55] had been carried out for 11 years (from 2006 and 2017), describing travelling characteristics of around 140,000 Danish inhabitants. In [47], it is investigated on how the aforementioned driving characteristics could influence the charging load as well as the power grid itself in Bornholm, extrapolating data related to Bornholm island and scaled them up for the total number of islanders.

4.5.1 Driving behavior and vehicles availability

Average characteristics for drivers in Denmark, Italy and Norway are collected in Table 4.2. As possible to observe, trends are not differing extremely one to each other. In fact, it is noticeable how the average driving distance per person is around 37 *km* while the average travel time per person is circa 1 *h* and 15 $'$ per day. Considering the average driving distance per person per day, it is an average among the whole week, the results being different for weekdays, Saturdays and Sundays. Taking for example the Danish data, these averages are respectively 45 *km*, 34 *km* and 30 *km*. The similarity in the comparison among different countries and the related extrapolated data ensures that the conducted analysis carried out in Denmark could be scaled for other countries, knowing the travelling data.

Table 4.2: Driving trips characteristics [55] [56] [57], adapted from [47]

Parameter	Denmark	Italy	Norway	Average
Trips per person per day [#]	2.9	2.7	3.26	3
Driving distance per trip [*km*]	14.6	12.2	14.5	13.8
Driving distance per person per day [*km*]	40.1	34.3	35.6	36.7
Total travel time per person per day [*min*]	54.5	89	78	74

Putting the concentration on the investigated island from now on, the averaged reported results in [55] are:

- cars per house (rounded number): 1 car;
- kilometers per car per year: $12,360$ *km* $\longrightarrow$ kilometers per car per day: 33.86 *km*;
- driven hours per car per year: 224 *h* $\longrightarrow$ driven minutes per car per day: 37 $minutes$ $\longrightarrow$ percentage of driven time: 2.56 %;

From these points, it can be underlined that the average distance driven is 34 *km* per day and that the vehicles are parked for more than 97 % of the day, signifying a great potential in terms of grid services if EVs are considered instead to conventional cars. However, it could be pointed out that this available time for the electrical grid is not equally distributed throughout the week. At first, days can be divided into workdays and holidays, easily referred to weekdays and weekends. For the Danish National Travel Survey, it has been deducted that the Danish population does not use the car that often in between 6 *pm* – 7 *am* on weekdays, being in fact the office opening hours usually between 9 *am* – 5 *pm*. Taking into account weekends, it can be deducted from National data that Danish tend to use their car less, leaving their car parked for an higher amount of time.

For the purpose of this thesis, a 100 % EVs penetration scenario on Bornholm is investigated, scaling up the data related to the 1,149 people interviewed on Bornholm to the total population of 39,499 inhabitants in January 2020. The results from this small cross-section give rise to a total of 27,484 inhabitants with a driving licence and a total amount of cars (from now considered just EVs) equals to 19,643. Looking for more detailed data for Åkirkeby, the same proportion has been applied with the population of Åkirkeby itself. The inhabitants in this small town are 2,108 on January 2020, obtaining then a total number of vehicles equal to 1,048 [58].

4.5.2 SOC evaluation

Before proceeding in the charging pattern analysis, battery characteristics related to the SOC must be investigated.

The SOC is defined as the remaining capacity of the battery and it can be evaluated as in Equation 4.1 as a ratio between the stored capacity of the battery at the investigated time *Q(t)* and the nominal capacity *Qn*, obtaining a value expressed in per unit (*pu*):

$$SOC(t) = \frac{Q(t)}{Qn} = 1 - \frac{Qu(t)}{Qn} \tag{4.1}$$

If on the one hand, *Qn* is given by the battery manufacturer, representing the maximum storable energy in the battery pack (as aforementioned in Section 4.1, 40 kWh for the selected Nissan LEAF), on the other hand $Q(t)$ is function of the operating conditions. Indeed, the difference in between *Qn* and $Q(t)$ is the so called used capacity $Qu(t)$, obtained considering the travelled distance after the last time that the EV has been recharged and the time of investigation. Taking as an average range of maximum distance d_{max} of 200 km [47], the ratio between *Qn* and d_{max} can be chosen as average consumption $\overline{c}$ of 0.2 kWh/km (also expressed as 5 km/kWh) for the Nissan LEAF 40 kWh. At this point, thanks to Equation 4.2, it is possible to evaluate the used capacity $Qu(t)$ and finally the $SOC(t)$ can be determined.

$$Qu(t) = km_{driven}(t) \cdot \overline{c} \tag{4.2}$$

4.5.3 Plug-in rate at home and average SOC

As factual data, there is no a clear and predefined charging pattern that can describe the EVs' owner behavior. In fact, equal driven kilometers but different driving style, as well as uncontrollable causes like the outdoor temperature, can cause a different final SOC. Moreover, the anxiety factor can play a fundamental influence on the decision to charge the vehicle, an element that is very difficult to predict. However, considering large groups of EVs, the statistical distribution could allow to erase this latter contribution, observing a more appreciable relation in between the plug-in rate and the SOC.

A Japanese analyses investigated over 10,000 Nissan LEAF 24 kWh [47] and the main results are shown in Figure 4.6. Ten groups of EVs have been considered, which are defined gathering together EVs with similar driven distance per day, as shown in table Table 4.3. Groups G1 - G5 have steps of 10 km while G6 - G10 have steps of 20 km. The SOC is evaluated considering the worst scenario (upper band of the driven distance) and considering an initial SOC unitary. From Figure 4.6 it is

deducible that the plug-in rate increases with a lower SOC while, the SOC being equal, it increases with greater driven distance per day. The last four groups G6 - G10 show approximately the same behaviour, plugging-in their EVs regardless the SOC, while all the groups charge always their EVs if the SOC is lower than 0.55 *pu*.

Table 4.3: EVs groups

Group	Driven distance [*km*]	SOC [*pu*]
G1	$0 < x \leqslant 10$	0.95
G2	$10 < x \leqslant 20$	0.9
G3	$20 < x \leqslant 30$	0.85
G4	$30 < x \leqslant 40$	0.8
G5	$40 < x \leqslant 50$	0.75
G6	$50 < x \leqslant 70$	0.65
G7	$70 < x \leqslant 90$	0.55
G8	$90 < x \leqslant 110$	0.45
G9	$110 < x \leqslant 130$	0.35
G10	$130 < x \leqslant 150$	0.25

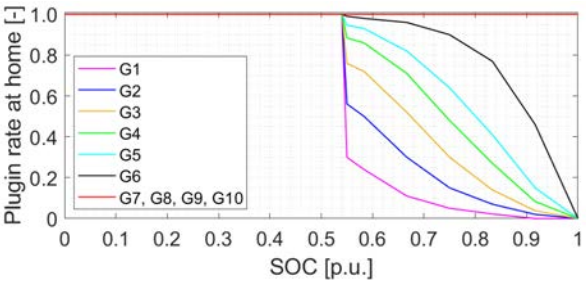

Figure 4.6: SOC - plug-in at home probability [47]

It is clearly deducible that not all the EVs are going to be charged every day when back home, meaning that not all of them could contribute to grid services. It has been found necessary to investigate on how the EVs can be considered in the current project, both in terms of amount of grid-connected EVs as well as their SOC when being plugged-in.

In [47], it has been reported an applied example of Figure 4.6 using 20 EVs, here adapted in table Table 4.4, where only seven groups of EVs are created due to the low amount of vehicles considered. The rows represent the seven groups in which these population of EVs are divided, meaning that EVs located in the same group number will drive the same distance every day (in the defined range). The columns represent the weekly days. For every day, each EV is marked with a combination of a number and a letter:

- the number represents the kilometers accumulated by that vehicle at the end of the day since the last charging. In fact, this number can go from 1 to 10 like the group number. On the one hand, the group number takes into account just the daily driven distance, on the other hand this number is considering the total accumulated kilometers. As a consequence, the written number to mark an EV day by day can never be lower than the group number itself;
- the letter indicates if that EV is charging *Y* or not *N*.

As evident, the daily number-letter combination is marked in black if the vehicle is not charged, while in red in the opposite case, situation in which it is also written the related SOC value from Table 4.3. The weekly analysis and consequently average data can arise, collected in Table 4.5, where the total average $\overline{SOC}$ is obtained with a weighted average, following Equation 4.3:

$$\overline{SOC} = \frac{\overline{SOC}_{Mon} \cdot EV_{Mon} + \overline{SOC}_{Tue} \cdot EV_{Tue} + ... + \overline{SOC}_{Sun} \cdot EV_{Sun}}{TotEV} \tag{4.3}$$

in which the amount of EV on charge on Monday, Tuesday, ..., Sunday (EV_{Mon}, EV_{Tue}, ... , EV_{Sun}), and their summation ($TotEV$) are respectively considered. Clearly, this weighted average is done to

Table 4.4: Example of plug-in model output, adapted from [47]

		Day						
	EV	**Monday**	**Tuesday**	**Wednesday**	**Thursday**	**Friday**	**Saturday**	**Sunday**
G1	1	7Y - 0.55	1N	2N	3N	4N	5N	6N
	2	1N	2N	3N	4N	5N	6N	7N
G2	3	6N	6Y - 0.65	2N	3N	5N	6N	6Y - 0.65
	4	4N	6N	7N	7Y - 0.55	2N	4N	6N
	5	6N	7N	7Y - 0.55	2N	4N	6N	7N
	6	7Y - 0.55	2N	4N	6N	7N	7Y - 0.55	2N
	7	7N	7Y - 0.55	2N	4N	6N	7N	7Y - 0.55
G3	8	3N	5N	7N	7Y - 0.55	3N	5N	7N
	9	5N	7N	7Y - 0.55	3N	5N	7N	7Y - 0.55
	10	6N	6Y - 0.65	3N	6N	6Y - 0.65	3N	6N
	11	6Y - 0.65	3N	6N	6Y - 0.65	3N	6N	6Y - 0.65
	12	3N	6N	6Y - 0.65	3N	6N	6Y - 0.65	3N
G4	13	7N	7Y - 0.55	4N	7N	7Y - 0.55	4N	7N
	14	7Y - 0.55	4Y - 0.80	7N	7Y - 0.55	4Y - 0.80	7N	7Y - 0.55
	15	7Y - 0.55	4N	7N	7Y - 0.55	4N	7N	7Y - 0.55
G5	16	5Y - 0.75	5Y - 0.75	5Y - 0.75	5Y - 0.75	5Y - 0.75	5Y - 0.75	5Y - 0.75
	17	8Y - 0.45	5Y - 0.75	5N	8Y - 0.45	5Y - 0.75	5N	8Y - 0.45
G6	18	6Y - 0.65	6Y - 0.65	6Y - 0.65	6Y - 0.65	6Y - 0.65	6Y - 0.65	6Y - 0.65
	19	6Y - 0.65	6Y - 0.65	6Y - 0.65	6Y - 0.65	6Y - 0.65	6Y - 0.65	6Y - 0.65
G7	20	7Y - 0.55	7Y - 0.55	7Y - 0.55	7Y - 0.55	7Y - 0.55	7Y - 0.55	7Y - 0.55

consider more the SOC of bigger EVs' population. It results in an average amount of charging EVs of 45 % in respect to the total considered population, which have an initial average $\overline{SOC}$ of 62 %.

Table 4.5: Charging EVs and average SOC

	Monday	**Tuesday**	**Wednesday**	**Thursday**	**Friday**	**Saturday**	**Sunday**	**Total average**
EV on charge	10/20 - 50%	10/20 - 50%	7/20 - 35%	10/20 - 50%	8/20 - 40%	6/20 - 30%	11/20 - 55%	62/140 - 45%
$\overline{SOC}$	0.590	0.655	0.621	0.590	0.669	0.633	0.595	0.619 - 62%

4.5.4 Charging time

With the previous considerations in mind, it is now possible to analyse the charging time required by each EV. For the sake of simplicity, it is considered that the charging can happen only once per day, in a single charging session. Moreover, in the Danish National Travel Survey, it has been deducted that the Danish population does not use the car that often in between 6 *pm* – 7 *am*, being in fact the office opening hours usually between 9 *am* – 5 *pm*. As a consequence, the EV availability for grid services can be assumed satisfactory throughout the night.

Generally, it is assumed that the EVs, in this particular case the Nissan LEAF, are charging at constant nominal power when connected, from plug-in to plug-out when fully charged. This is possible thanks to the BMS of the Nissan Leaf, which allows for a constant energy charging session even if the SOC approaches the unitary value. However, always through the BMS, it is also possible to change the charging set-point of the assigned Nissan LEAF.

Defining with P_{Ch} the power at which the EV will be charged, η the charger efficiency, which can be found to be circa 90 % for a common charger [59] and $Qu(t)$ (which was already defined in

Equation 4.2 as the used capacity and then the required energy to be injected to fully charge the battery), it is possible to evaluate the required charging time of an EV following Equation 4.4:

$$T(t) = \frac{Qu(t)}{P_{Ch} \cdot \eta} \tag{4.4}$$

Considering three different charging currents I of 6 A, 11 A and 16 A, which are the minimum, average and maximum charging current supported by the selected chargers, it is interesting to observe the difference in charging time while considering several current values as well as the charger typology.

For a three phase charger, P_{Ch-3ph} can be defined as in Equation 4.5.

$$P_{Ch-3ph} = \sqrt{3} \cdot V \cdot I \tag{4.5}$$

For a single phase charger, P_{Ch-1ph} can be defined as in Equation 4.6, in which V is the phase-to-phase voltage for both chargers, fixed at 400 V for the whole project.

$$P_{Ch-1ph} = \frac{V \cdot I}{\sqrt{3}} \tag{4.6}$$

Considering a final average $\overline{SOC}$ of 0.62 in a 40 kWh Nissan LEAF, the related used capacity is of 15.2 kWh, evaluated as in Equation 4.7, from which Table 4.6 collects the charging time coming from Equation 4.4 with a charging efficiency η of 0.9 pu.

$$Qu(t) = Qn \cdot (1 - \overline{SOC}). \tag{4.7}$$

Table 4.6: Charging time function of chargers and set-point current

Charger\Current	*6 A*	*11 A*	*16 A*
Ch-3ph	4 *h* 4 $'$	2 *h* 13 $'$	1 *h* 32 $'$
Ch-1ph	12 *h* 12 $'$	6 *h* 39 $'$	4 *h* 35 $'$

4.6 Electric vehicles with unidirectional chargers and Kalby wind farm: shared interest

As mentioned in Section 4.2, the ancillary services provision from EVs for Kalby wind farm can be investigated if concerned of all the constraints coming from this connection mode as well as their own interests.

The main interest for Kalby wind farm is to gain as much flexibility as possible from the associated energy storage system. Indeed, the sudden and uncontrollable wind speed variations, translated into power output fluctuations (Figure 3.6), would require a very quick time response (ideally instantaneous), a wide and feasible power output working range and the possibility to acquire/release ample amount of energy from the EVs aggregation. If on the one hand, the time response is of difficult manageability, being an intrinsic feature of measurement and communication latencies,

chargers and EVs delays (see Section 4.4 for extended analysis), one the other hand the power output working range and the plentiful energy management capability are a matter of the charging current set-point and the number of EVs considered in the aggregated population [54].

From the EVs' point of view, an aggregation of vehicles sharing the same technical characteristics as well as charging patterns is considered. In fact, the assumption is to have a dedicated flexibility platform where an EV aggregator can control and manipulate the whole 40 kWh Nissan LEAF EVs family to such an extent that they can be consider as an unique energy storage system, depicted with an average representative SOC level. Moreover, the EV aggregator is also in charge of forecasting and planning the charging demand, considering both EVs and wind farm's interests.

It is now noteworthy to remember that only unidirectional chargers are considered, allowing the charging process of the on-board battery but not the discharging one. It follows that a suitable forecasted charging current must be chosen to give the EVs the possibility to adapt their power output in both upwards and downwards directions in respect to this forecasted current consumption. It is then straightforward to realize how this prerequisite is achieved selecting the forecasted charging current equal to 11 A for every EV [60]. Moreover, assuming an initial SOC value equal to the previously examined weighted $\overline{SOC}$ of 62 %, the charging time required to fully charge each EV can be obtained from Table 4.6. With a $Ch-3ph$ charger, an EV would require 2 h and 13 $'$ at constant current consumption to store the whole consumed energy, while with a $Ch\ 1ph$ this process would take 6 h and 39 $'$, simply because the single phase charger has a power injection capability three times lower than the three phase one.

Last but not least, the EV aggregator can plan the charging demand to make as much EVs available as possible for Kalby wind farm interest. Given a certain finite amount of EVs and considering the related daily time window in which they can be grid-connected, the equal partition of these EVs through the whole on-grid hours is the most straight choice, being not able to predict at which hour the wind farm could require more EVs for power smoothing service or energy management. It is first established that the charging window is in between 6 pm – 6 am, totally included in the time frame 6 pm – 7 am when the Danish population does not use the car that often, following the Danish National Travel Survey. As a consequence, as a function of the considered charger, the EVs are divided as follows:

- 6 even split groups if charged via $Ch\ 3ph$;
- 2 even split groups if charged via $Ch\ 1ph$.

The choice is made allowing the EVs to give always support to the wind farm if the average consumed current in the charging time frame is lower than 12.19 A for each EV. This result can be verified thanks to a reverse formulation of Equation 4.4, where the charging time T is now fixed at 2 h or 6 h, while the unknown variable is the P_{Ch}, and then used in Equation 4.6 or Equation 4.5 to obtain the current value. In contrast to this craved condition, it is also possible that the aggregated EVs family reaches the unitary SOC before the end of the selected time window. In this scenario, the EV aggregator will disconnect the EVs for the remaining time, not being able anymore to operate any kind of service for the wind farm due to the impossibility to discharge their battery. Finally, the EV aggregator has the duty of disconnecting one group of EVs at the end of its charging session of 2 h or 6 h. then connecting the following defined EVs groups. This groups' succession will last until all the EVs passed through a charging session, so until 6 am.

As a conclusion, the adjustment in the EV' power consumption can arise from a control signal generated by the EV aggregator, following a service' request coming from Kalby wind farm. The EVs are then playing the important role to adjust their charging power in order to balance the unforeseeable power fluctuations or the incorrect hourly energy forecast, meaning that the focus will be on the instantaneous power output or the energy production from Kalby wind farm.

4.7 Summary

The EVs are gaining more and more interest in the car industry, becoming day by day more competitive in terms of both technical performance and economic affordability. As a consequence, the number of studies on how these vehicles could influence the power grid have risen highly in the last decades. Starting from the definition of standards requirements for the internal car's equipment as well as the charging connectors, the main focus shifted on the possible use of EVs to provide ancillary services. Thus, the EVs could be used not only for sustainable transportation, but also as BESS while charging.

The electric attributes while charging the EVs are in compliance with the required flexibility for ancillary services provision: instantaneous ramp-up and ramp-down time, high accuracy and precision with possibility of bidirectional power flow with V2G charger are just few characteristics that make clear how more valuable are these means of transport for the future ancillary provisions.

However, the main difference in between BESS and EVs from the power grid's perspective is coming from the not constant interconnection with the grid itself, indeed being the EVs used to drive. As a consequence, the charging pattern analysis is a necessary step that must be investigated to obtain average charging time windows through the day as well as an average daily energy consumption, later translated into SOC value while plugged in to recharge. Considering the average driving data for Bornholm, an EV penetration of 100 % is considered, linking these data to previous studies that analyse the probability to charge the EVs while back home as a function of the driven kilometers and the SOC remaining. Satisfying data have been obtained for the considered town of Åkirkeby.

Indeed, among the $1,048$ EVs in Åkirkeby if under an 100 % penetration scenario, it can be considered that 45% of them are charged daily, with an overall average SOC evaluated for the approximated 480 EVs under charge around 62 %. As a consequence, considering each EV is connected with initial SOC equal to the average value aforementioned, the required charging time is function of the absorbed current. Thanks to the on-board BMS, the charging current can be fixed at 11 A, being able to provide full up and down regulation in terms of consumed current and then power in respect the forecasted charging current of 11 A detected by the EV aggregator. In fact, the analysed charger are unidirectional, being not able to discharge the battery.

Moreover, knowing that the charging window is roughly in between 6 pm and 6 am, the EVs are equally divided into six groups, while charged with $Ch-3ph$, or two groups, if via $Ch-1ph$, concluding that in both situations the EVs are unable to reach full charge if always at reference charging current. In this way, the EVs are giving the possibility to Kalby wind farm to ask for an additional power and energy consumption if required from the controller, enhancing their ancillary provisions' flexibility.

5 Implementation of hybrid power plant controllers

In this thesis, two controllers have been investigated and designed to adjust the EVs' power consumption as a function of Kalby wind farm power output. The first one, named *Power-to-Power controller*, aims at controlling the EVs' power consumption according to power generation profile of the wind farm and a desired power profile. The second one, named *Energy-to-Power controller*, has the task to control power consumption of EVs according to the wind farm's energy injection into the grid, following a desired energy profile. Considering the benefits described in Section 2.2, the first controller is related to the "Power Smoothing", while the second to the "Energy Management".

After a brief recall of PowerFactory, Section 5.2 describes the Åkirkeby substation layout implemented using this software. Then, in Section 5.3 and Section 5.4 the two designed controllers are shown, the *Power-to-Power controller* and the *Energy-to-Power controller*, respectively. Finally, in Section 5.5, home chargers and EV fleet aggregation are shown, followed by the SOC protection model in Section 5.6.

5.1 DIgSILENT PowerFactory

DIgSilent PowerFactory (PF) is an engineering tool for the analysis of transmission, distribution, and industrial electrical power systems. It has been designed in order to achieve the main objectives of planning and operation optimization, since it can easily execute all power simulation functions, such as load-flow, short-circuit calculation, harmonic analysis, protections coordination, stability calculation, and mode analysis. It has been written by "DIgSILENT", which is the acronym of "DIGital SImuLation of Electrical NeTwork" [61].

In this project two main simulation functions are used: load flow analysis and dynamic RMS modelling (a time-domain simulation for stability analysis). The following sequence of actions were performed in PF. First, the load flow analysis is used at the first step to analyse the steady-state of a power system and determine the initial conditions for all the elements in the grid in order to have all the state variables with initial derivative equal to zero. Then, the analysis is carried out running a multitude of power profiles that represent the feeders at the 10.6 kV side of the Åkirkeby substation for each of the days previously described in Section 3.3. A simulation step size has been set to an automatic adaptation with a maximum step of 0.1 s.

When working with PF, it is of main importance to understand how the grid and each single block is implemented and set up. Indeed, PF is characterized by a strict system modelling approach to follow. The fundamental definitions are summarized as follows [61]:

- the *Composite Frame*, which is the diagram that defines the physical connections between inputs and outputs of various models;

- the *Composite Model*, which is based on the *Composite Frame*, is used to combine different elements to run the power system. These elements can be a *Built-in Dynamic Model*, a standard power system element implemented in the standard library of PF, or a *Common Model*;
- the *Composite Block Definition*, which is a user-defined diagram that determines the physical connection between inputs and outputs of various blocks of a model;
- the *Common Model*, which is based on DSL block definition, is used to set parameters of an associated model.

5.2 Åkirkeby substation layout

The goal is to develop a model to study possible synergies coming from the combination of the Kalby wind farm and an aggregation of EVs. In order to do so, the previously shown Åkirkeby substation in Figure 2.2 was realized in PF. A single-line diagram of the substation is presented in Figure 5.1.

Starting from the upper-left side of the diagram, the two main substation transformers *ÅKI T1* and *ÅKI T2* interconnect 60 *kV* and 10.6 *kV* buses. On the 60 *kV* side, the overall Bornholm power system is represented with an external grid component, able to supply active and reactive power to the Åkirkeby substation in the case of unbalance between production and consumption at the 10.6 *kV* side.

On the 10.6 *kV* side of the substation, all feeders have been implemented using the technical data collected in Section 2.4. All the production feeders (the biogas plant (marked in brown), the PV plant, as well as Kalby (– light blue) and Sose (– green) wind farms) are designed and gathered together on the left side, while all the consumption feeders upside down on the right side. Finally, in this study each power generation plant was represented by a simple load (marked with the same colors as the power plant to which are referred to) with dedicated power profiles based on historical data. As already mentioned, due to the lack of historical production data of the Bodelynsvejen PV park, it is not represented in the substation layout and neglected in the project.

Figure 5.2 shows the first composite frame of the project, created to manage the active and reactive power profiles. This frame is composed of 10 pairs of blocks assigned to 10 substation feeders, without considering the one related to the EVs aggregation. The light green blocks of the composite frame serve for importing active and reactive power profiles for each dedicated feeder, and for unit conversion into *MW* and *MVAr*, respectively, which are the user-defined unit of measurement used to converse with the power grid.

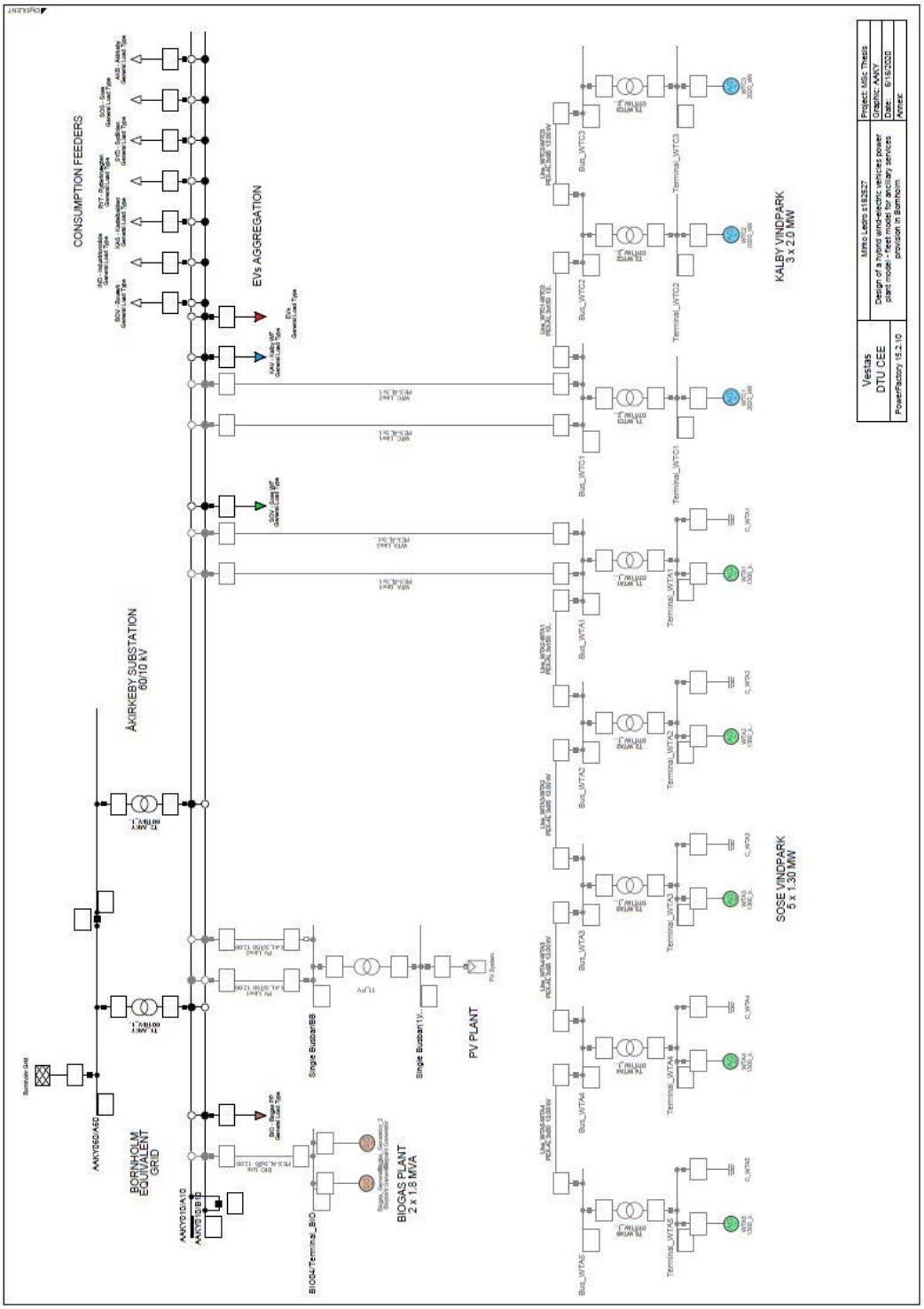

Figure 5.1: Åkirkeby substation designed in PF

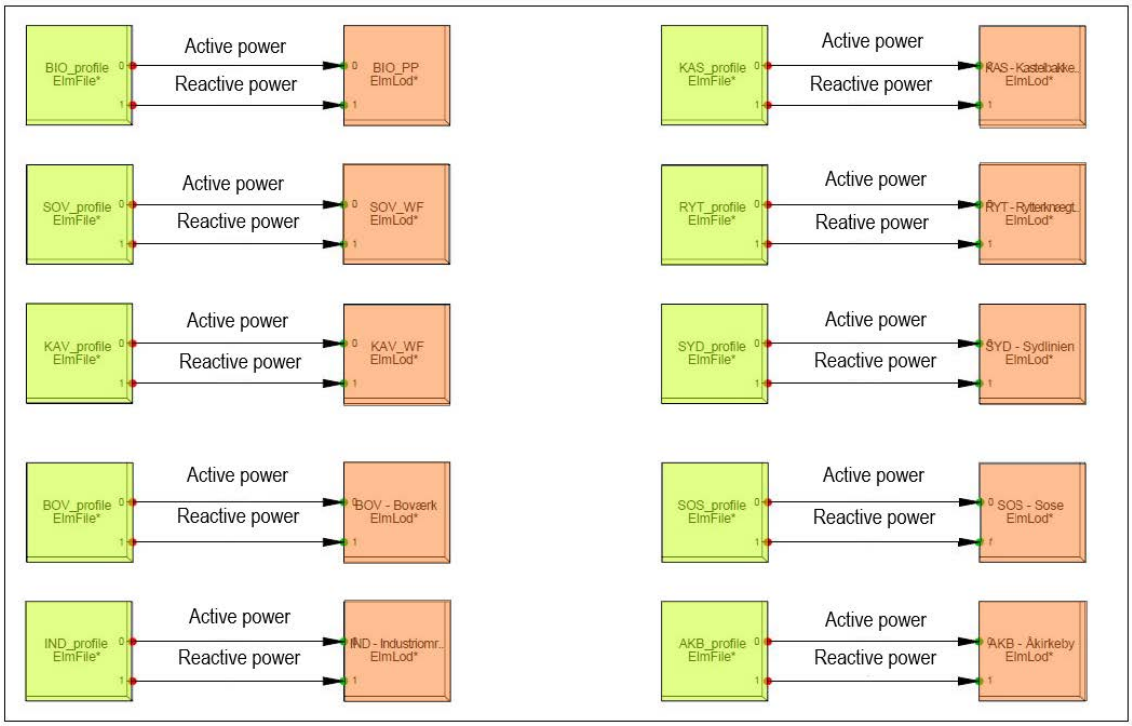

Figure 5.2: Composite Frame *Production Profiles*

As all the feeders are represented by load elements, the following assumption was made: power profiles have a positive sign if power flows from the 10.6 *kV* bus to the feeder, and a negative sign if the power flows in opposite direction (the feeder is injecting power into the grid). The active and reactive power profiles are transferred from light green blocks to dedicated orange blocks, representing load feeder elements of the electrical grid layout.

The EVs aggregation is represented with a load feeder on the right of Figure 5.1 next to the Kalby wind farm feeder.

It should be underlined that in the PF model the 0.4 *kV* EVs feeder is directly connected to the 10.6 *kV* bus without a step-up transformer, due to the high efficiency of transformers nowadays, thus the overall aim is not mined. If a transformer is added instead, losses must be considered to evaluate the power flowing in the EVs feeder. The interconnection of the Kalby WF, the EV fleet, and the 10.6 *kV* is highlighted in Figure 5.3. The acronyms *PGC*, *PEC*, *POC* and *PCC* are defined in Section 4.3. The power output from the WF is marked as *PGC*, while the one from the EVs aggregation as *PEC*. In the designed model, points *POC* and *PCC* are superposed, since no cables/transformers interconnecting *POC* to *PGC* are taken into account. Thus, only the *PCC* is used in this report

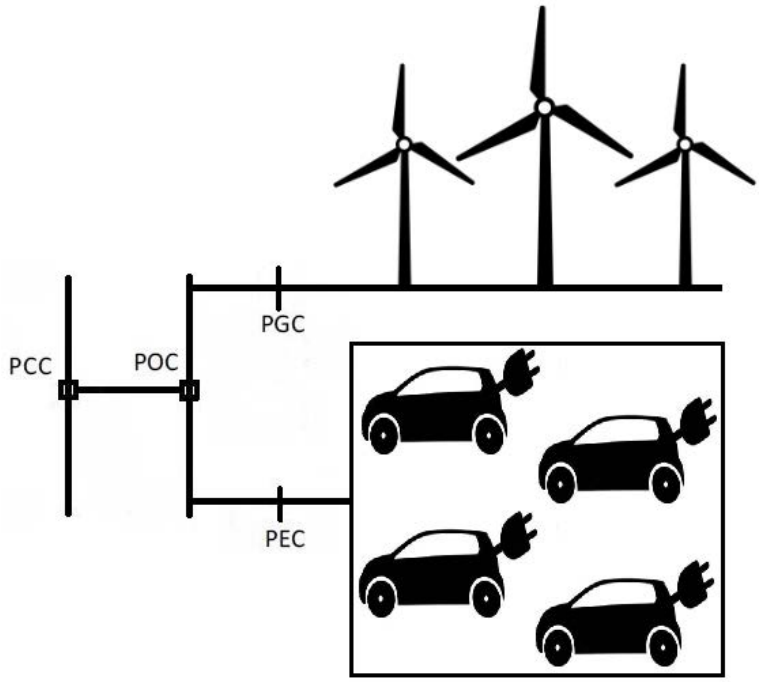

Figure 5.3: A conceptual layout of the wind farm and EV fleet aggregation

5.3 Power-to-Power controller modelling

The description of the *Power-to-Power controller* is divided into two steps: first, a general overview of the model is shown, followed by a more detailed analysis of the main block that characterizes this controller.

5.3.1 Model overview

The task of the *Power-to-Power controller* is to set a reference power to the EVs based on the WF generation profile and a desired power profile at the PCC and ensure that the reference power is fulfilled. In order to implement this controller, a second composite frame is introduced. In Figure 5.4 the composite frame is represented with macro blocks to better illustrate how the composite frame itself has been arranged, while the original layout of the frame realized in PF is shown in Figure 5.5. The leading block is the *Power-to-Power controller implementation* block, marked in light blue, which requires some inputs to operate properly. These inputs as well as the resulting outputs are described in the following paragraphs.

The red blocks serve for collecting and recalculating power measurements at PGC. The *P measurement* block, red block on the left, is defined in PF considering a "generator oriented" convention. It means that the power measured at the PGC will have a positive sign in this composite frame when it is injected from the WF into the grid. Moreover, since the output of this standard PF measurement block is given in $[pu]$ values (normalized to the nominal active power of the WF S_{WF} of 6 MW), besides the measurement block itself there is a second block, a common model user-designed, for recalculating the values back to $[W]$ from the per unit value.

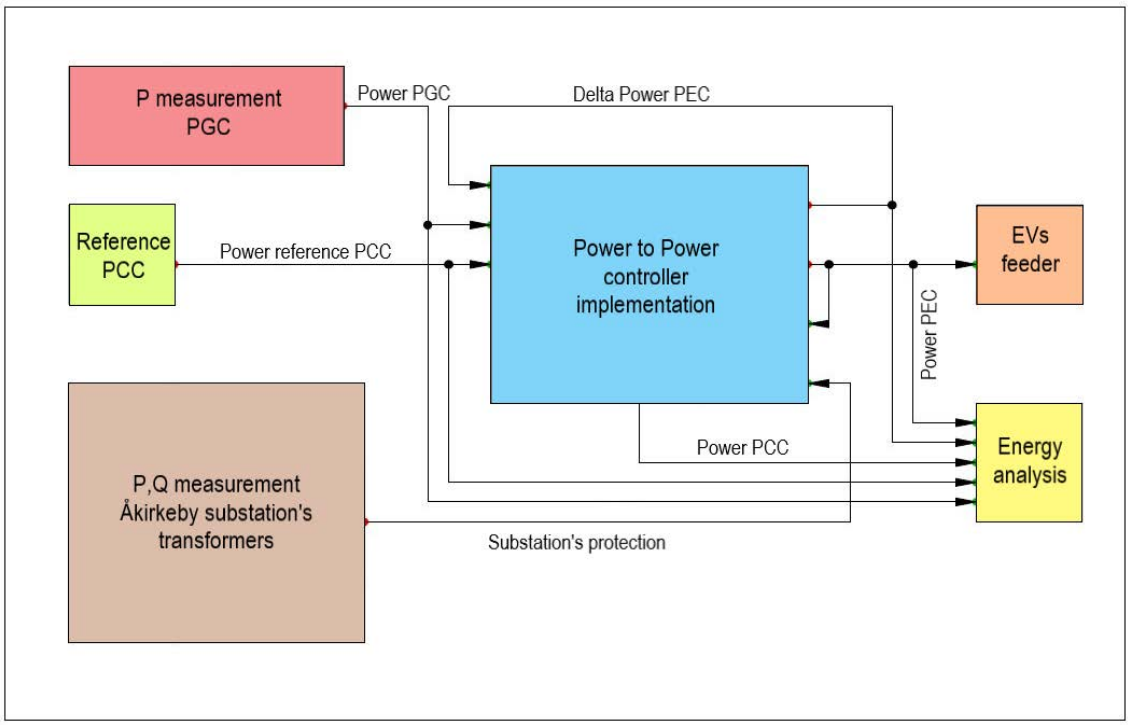

Figure 5.4: Conceptual layout of Composite Fleet Frame with *Power-to-Power controller*

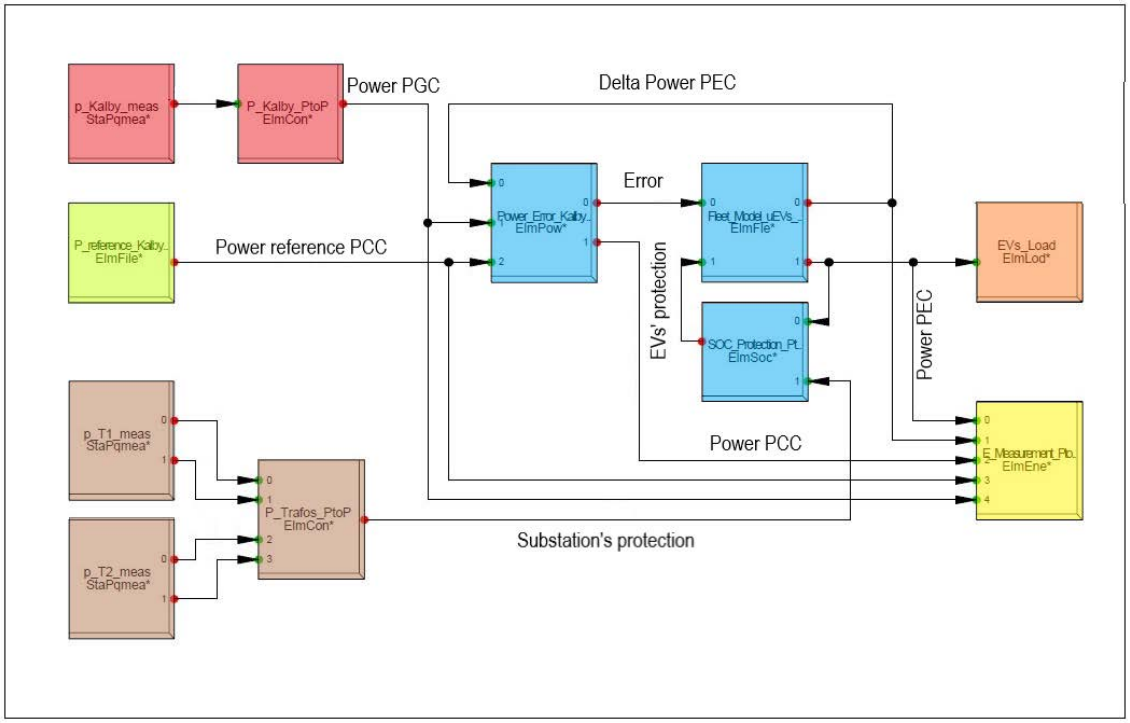

Figure 5.5: Composite Fleet Frame *Power-to-Power controller*

The light green block serves for assigning the active power reference profile at the PCC. The power reference could be the forecasted power each 15 $'$, obtained from wind forecast at the hub height for each WTG, applied then to the nominal power curve of the installed turbines. However, since it

is not of main focus to evaluate the accuracy of wind power forecasting methods, the reference power profile was calculated from the gathered historical active power measurements at the PGC as a set of power values averaged over every 15 $'$. The resulting file is imported as PCC reference power in $[W]$.

The active and reactive power measurements at the two main substation transformers are collected in the brown blocks. The measurements are carried out at the bottom transformers' terminals at the 10.6 *kV* line. As described for the power measurement at the PGC (red blocks), the process is divided into two parts. First, the *PQ measurement* blocks (the two blocks on the left) at the 10.6 *kV* line are defined in PF considering an "orientation of the connected element" convention. It means that the measured power will have a positive sign if the power will pass through the transformers and then be injected into the external grid (local production greater than the consumption), while a negative sign if the power flows in the reverse direction (local production lower than the consumption). As base values for per unit transformation and back to physical units, nominal apparent power values of the transformers were used (S_{T1} of 16 *MVA* and S_{T2} of 10 *MVA* for the upper and lower brown blocks, respectively). Finally, active (p_1, p_2) and reactive (q_1, q_2) power values in $[pu]$ are transferred to the block on the right. This third block is a common model user-defined, for recalculating the values back to $[W]$ from the per unit value. However, this block is mainly used to analyse when the transformers are overloaded, as explained in the next paragraph.

The applied Equation 5.1 is composed of two fractions, each of them with values expressed in $[pu]$ (a value over 1 *pu* means that the considered transformer is overloaded). Since these two transformers work in perfect parallel conditions (Section 2.4), it is possible to consider an unique overall *Loading* variable to aggregate their status. This variable is used to define how much the overall substation is loaded. Furthermore, as this variable is a sum of two per unit values, the factor 0.5 is applied to halve the *Loading*' values range, with the possibility to declare the substation's overloaded condition if *Loading* goes over 1 *pu* (otherwise in the case of full load condition *Loading* variable would be equal to 2 *pu*). Finally, Equation 5.2 shows the equation implemented effectively, with just the active and reactive power measurements in $[pu]$. As a consequence, the user-defined parameter *Limit* in $[pu]$ in the common model is compared to the *Loading* variable. The output variable *Substation's protection* detects the loading level of the substation as well as the power flow direction. If *Loading* is greater than the admitted *Limit* (simply set at 1 *pu* to admit a maximum substation's loading level of 100 %), a signal at level 1 is sent to the controller, otherwise the *Substation's protection* signal is stable at 0. Moreover, this condition is checked only when the external grid supplies power to Åkirkeby substation. On the one hand, if the substation is overloaded because of a very high consumption level, a decrease in the EVs' power consumption could decrease the overall overloading level. On the other hand, if the substation is overloaded because of a very high production level, it is better to not decrease the EVs' power consumption because this manoeuvre would push the substation itself in an even worse working condition. The overloading condition is then detected when the two measured variable p_1 and p_2 have a negative sign.

$$Loading = \frac{1}{2} \cdot \left(\frac{\sqrt{(p_1 * S_{T1})^2 + (q_1 * S_{T1})^2}}{S_{T1}} + \frac{\sqrt{(p_2 * S_{T2})^2 + (q_2 * S_{T2})^2}}{S_{T2}} \right) \tag{5.1}$$

$$= \frac{1}{2} \cdot \left(\sqrt{p_1^2 + q_1^2} + \sqrt{p_2^2 + q_2^2} \right) \tag{5.2}$$

The EVs feeder block presented in orange is used to declare to which feeder a certain power must be assigned to. Indeed, the *Power PEC* is obtained as output from the *Power-to-Power controller implementation* block and it is assigned to the EVs feeder. This feeder is set with a load convention, meaning that the *Power PEC* is positive if it flows from the PCC to the EVs feeder. It can be seen that no reactive power profile is assigned to this feeder, meaning that the reactive power consumption is constantly at zero. In fact, in Section 4.4 it is stated that electric vehicles are not capable to provide reactive power services.

Furthermore, some of the analysed signals are collected in the yellow common block, called *Energy analysis*, conveniently created to evaluate the active power profiles and evaluate the energy exchanged among various elements in the grid.

5.3.2 *Power-to-Power controller implementation* block

Finally, the three blue blocks that compose the core of the *Power-to-Power controller* itself are investigated. The *Power Error* common model (on the left) receives as inputs *Power PGC*, *Power reference PCC* and the variation in power in respect to the forecasted power consumption at the PEC – *Delta Power PEC*. It evaluates the *Error* that must be sent to the regulator, which is designed inside the *Fleet Model of unidirectional EVs* block (to the right) from now on abbreviated with *Fleet Model uEVs*. The two outputs from this latter block are the already mentioned *Delta Power PEC*, used as feedback for the error analysis, and the total power consumption *Power PEC*, which is going to both the EVs feeder as well as the *SOC protection* common model (lower block on the right). The SOC protection block receives also the *Substation's protection* signal from the brown blocks. As observable, the *SOC protection* block generates the *EVs' protection* signal to control charging power of the EV fleet.

Power error composite block definition

In Figure 5.6, the composite block definition related to the *Power Error* common model is shown. The measured *Power PGC*, expressed in $[W]$ is subject to a certain measurement delay in between when the power is gathered at the terminal of the WF and when the signal is ready to be manipulated. In order to simulate this physical lateness, the time parameter M_{del} (in $[s]$) is introduced in the related common model. This value is set and fixed at 1 s for all the following analyses. To obtain a relative error as output of the *Power Error* common model, *Power PGC* is subtracted from *Delta Power PEC* to obtain *Power PCC*, then compared with the imported *Power reference PCC* in the *Error* block, finally normalized with the nominal S_{WF} (user-defined parameter in $[W]$ in the common model). The following scenarios can be found:

- *Power PCC* equal to *Power reference PCC* $\longrightarrow$ null *Error*;
- *Power PCC* greater than *Power reference PCC* $\longrightarrow$ positive *Error*;

- *Power PCC* smaller than *Power reference PCC* $\longrightarrow$ negative *Error*.

If a positive *Error* is detected, meaning that the WF produces more than expected, it is necessary to increase the power consumption of the EVs in respect to their forecasted charging power, meaning that the *Power PEC* increases for the taken convention. On the opposite case, if a negative *Error* is detected, meaning that the WF produces less than expected, it is necessary to decrease the power consumption of the EVs (again, in respect to their forecasted charging power), meaning that the *Power PEC* decrease. However, it must be remembered how PGC, PCC and PEC are characterized with opposite conventions, being PGC and PCC generator orientated while the PEC load oriented. As a consequence, an increase/decrease in *Power PEC*, namely increase/decrease in *Delta Power PEC*, is seen as a decrease/increase in the overall *Power PCC*. Thus, a minus sign was assigned to *Delta Power PEC* at the summation point. Concluding, the applied formula in this common model is reported in Equation 5.3. The two outputs from this common model are the measured *Power PCC*, mathematically observed to detect the results of the EVs' influence, since this point is not physically available in the designed power grid, and the (relative) *Error*.

$$\begin{cases} Power\,PCC\,(t) = Power\,PGC\,(t - M_{del}) - Delta\,Power\,PEC\,(t) \\ Error\,(t) = (Power\,PCC\,(t) - Power\,Reference\,PCC\,(t))/S_{WF} \end{cases} \tag{5.3}$$

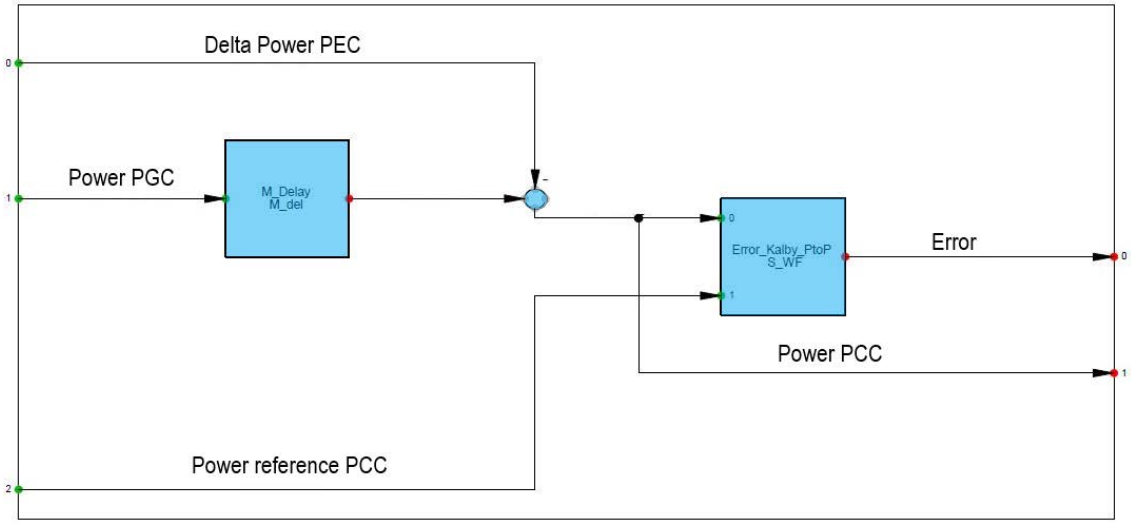

Figure 5.6: Composite Block Definition *Power Error*

It is worthwhile to underline how the *Power PCC* is declared in this project. It is defined as the *Power PGC* subjects to the influence of *Delta Power PEC*. Formally, the power at the PCC is the combination between *Power PGC* and the power consumption of the EVs – *Power PEC*. However, the offset power consumption of the EVs is neglected for power evaluations, considering just the variation with *Delta Power PEC*, while observed when discussing about SOC level.

Fleet model uEVs composite model definition overview and PI regulator

In Figure 5.7, the composite model definition of *Fleet Model uEVs* is represented with macro blocks to illustrate how the composite model has been arranged, successively presented as seen in PF in Figure 5.8. It can be clearly seen how the composite is specular along the horizontal

axis of symmetry. Each side is easily divided into three sections: the regulator is contained in the blue area, the charger – in the light blue area ($Ch-3ph$ in the upper side, $Ch-1ph$ in the lower side), the EV fleet aggregation model – in the aqua green area. Substantially, the two specular sides are differentiating because of the charger model applied to charge the EVs. The white area in the middle, defined as *Power analysis* is created to detect how far the *Power PEC* is in respect to the overall forecasted power consumption at the PEC itself, namely the *Delta Power PEC*. The *Power-to-Power controller* is equipped with a PI regulator and is sensible to the input *Error*. The blue sections of this composite is explained in the following paragraph, while the charger and EV fleet aggregation models are deeply investigated in Section 5.5.

The PID regulator is often used as a control loop feedback controller. The acronym PID stands for proportional (P), integral (I) and derivative (D), which represent the three control settings. The PID regulator controls the system to maintain it at a set point value by mean of the *Error* signal. The three controls settings are time-dependent error signals to the present error, the cumulative past error and the predicted future error, respectively. Through a proper setting of the regulator's gains (proportional gain K_p, integral gain K_i and derivative gain K_d), a quick response with minimal overshoot and oscillations around the set point value can be achieved. However an improper setting, more specifically related to the derivative gain, can cause the circuit to oscillate highly and lead to instability. As a consequence, for the goal of the project, the derivative part is not considered in the implemented regulator, thus a "simple" PI regulator is used. The results of each of the two sections are weighted sum, obtaining a total PI output that will fed the controlled device, in this case the EVs chargers to adjust the EVs' charging set-point.

A manual tuning is utilized for this controller, following the Ziegler-Nichols method [62]. The tuning is carried out for each of the investigated scenarios in the project. The relative gains K_p and K_i are reported in Chapter 6 while discussing about the results.

Finally, the PI output is multiplied by the power base P_{base}, which value is a function of the controlled device, defined as the amount of flexible energy that the EVs can provide. The P_{base}, defined also as flexible power of a EV, differs with the charger model considered. It is defined as the difference in between the maximum and the minimum allowed charging power by using a certain charger. The *phase to phase voltage* of the charger is marked with the user-defined parameter V_{pp} in the common model and fixed at 0.4 kV, representing domestic chargers presented in Table 4.1. The *maximum charging current* and *minimum charging current* of the charger are marked with the user-defined parameters I_{max} and I_{min} in the common model and fixed at 16 A and 6 A, respectively. As a consequence, the flexible P_{base} can be defined as in Equation 5.4 for the $Ch-3ph$, otherwise as in Equation 5.5 for the $Ch-1ph$.

$$P_{base,3ph} = \sqrt{3} \cdot V_{pp} \cdot (I_{max} - I_{min}) \qquad Ch-3ph \tag{5.4}$$

$$P_{base,1ph} = \frac{V_{pp} \cdot (I_{max} - I_{min})}{\sqrt{3}} \qquad Ch-1ph \tag{5.5}$$

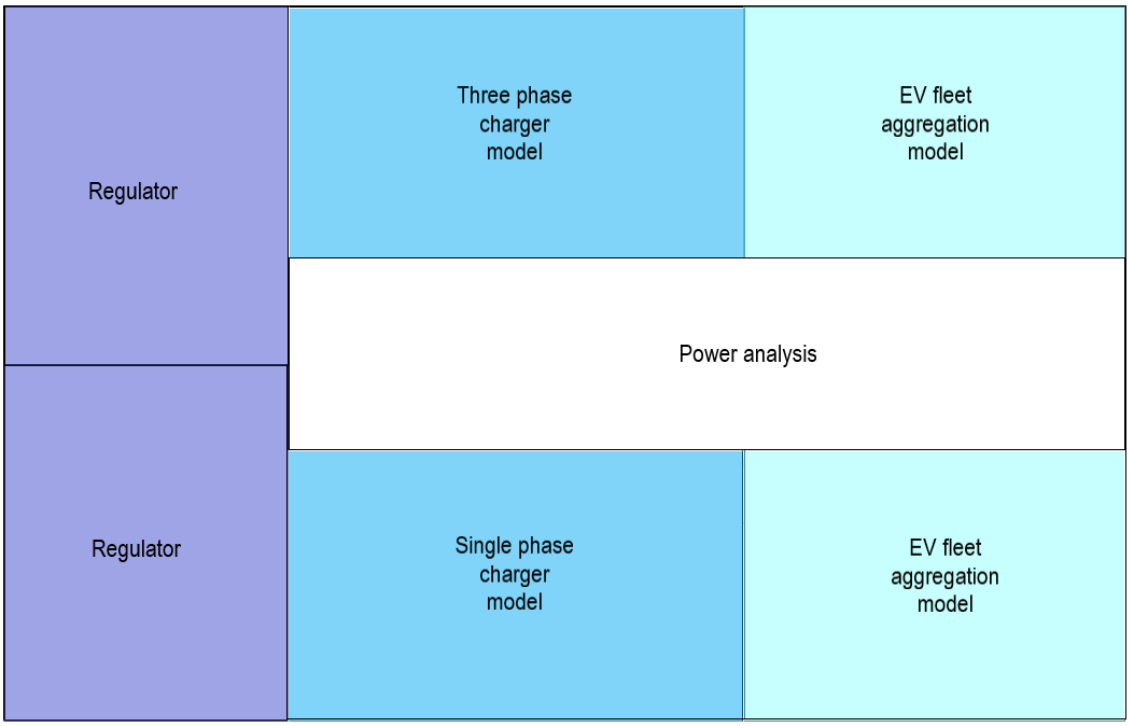

Figure 5.7: Conceptual layout of Composite Block Definition *Fleet Model uEVs*

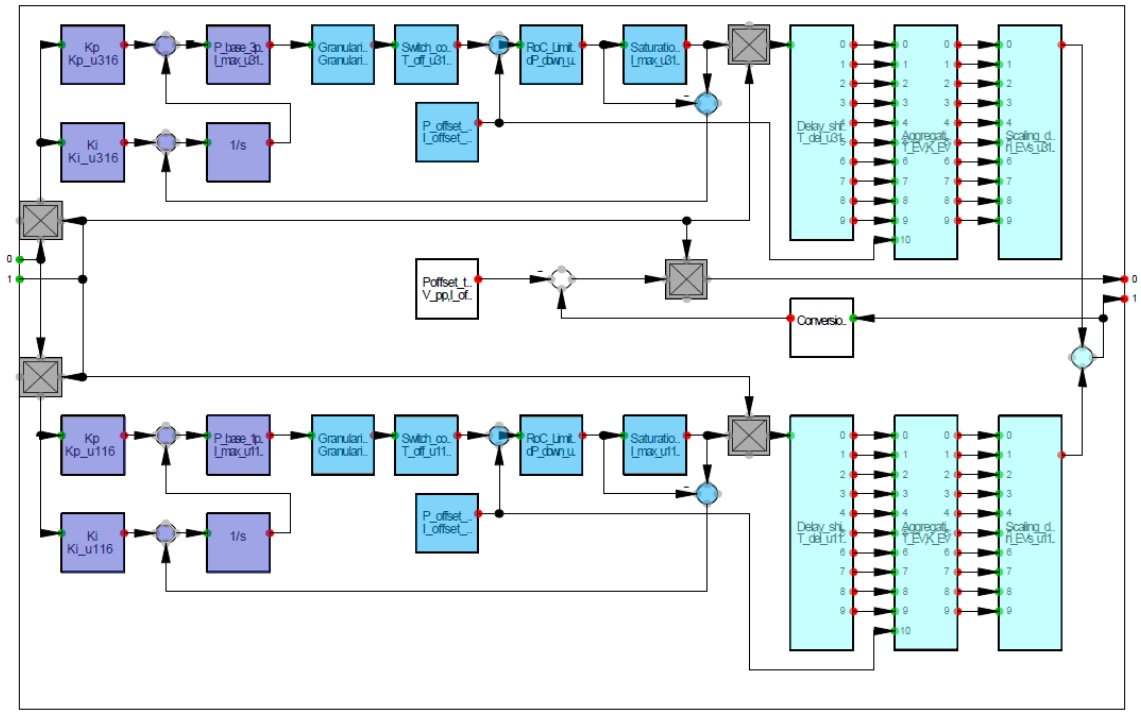

Figure 5.8: Composite Block Definition *Fleet Model uEVs* with PI regulator

5.4 Energy-to-Power controller modelling

The description of the *Energy-to-Power controller* is divided into two steps: first, a general overview of the model is shown, followed by a more detailed analysis of the main block that characterizes this controller.

5.4.1 Model overview

The task of the *Energy-to-Power controller* is to set a reference hourly energy profile at the PCC, desired profile that can be accomplish thanks to a proper PEC power consumption management. In respect to the *Power-to-Power controller*, this controller is more relaxed. Indeed, the control action is not realized to smooth out sudden power fluctuations at the PGC "in real time" but within a longer time frame (in this research it is equal to 15 $'$). The aim of this controller is to apply an energy management at the PCC towards the power coming from the WF by adjusting the EVs' power consumption. Wherein, the WF is considered more as an energy production source that has to inject a planned amount of energy in each specific time window, as suggested in Section 3.2. In order to implement this controller, a third composite frame was designed.

In Figure 5.9 the composite frame is represented with macro blocks to illustrate how the composite frame itself has been arranged, successively presented as seen in PF in Figure 5.10. The leading block is the *Energy-to-Power controller implementation* block, marked in light blue, which requires some inputs to operate properly. These inputs as well as the resulting outputs are described in the following paragraphs.

Some of the displayed blocks have the same configuration as for the *Power-to-Power controller*. For instance, the active power measurement blocks *Power PGC* (red), and the active and reactive power measurement blocks at the lower side of the main two Åkirkeby substation transformers (brown), from which the *Substation's protection* signal is generated. Also, the *Power PEC* is still applied to the EVs feeder through the orange block, whereas the energy evaluations are carried out in the yellow block.

The main difference in respect to the previous controller is seen at the light green block, called *Reference PCC*. In this case, the energy reference profile at the PCC is externally created and then used as an input to the composite frame in $[kWh]$. The reference energy production profile is calculated integrating the hourly wind power production from the historical measurement data from SCADA. Basically, the active power profile at the PGC is run externally in MATLAB, integrated over a time period of an hour, thus 24 energy forecasted levels are calculated for each day. Then, as the energy management in a 15 $'$ time frame of our interest, every hourly energy forecast is equally divided in four groups, obtaining four identical final energy reference values per hour. These values are referred to the energy the wind farm is expected to produce each 15 $'$.

First, an *Energy Ramp Reference PCC* is created to declare the ideal energy ramp the WF should follow to produce the planned energy amount. It starts from zero and reaches the final energy reference value just described for each time window. Then, an *Energy Upper Band PCC* is defined, which starts from +10 % of the final energy reference values and ends at these reference points. Finally, an *Energy Lower Band PCC* is considered as well, which starts from -10 % of the final energy reference values instead, reaching the same final points as the other two bands.

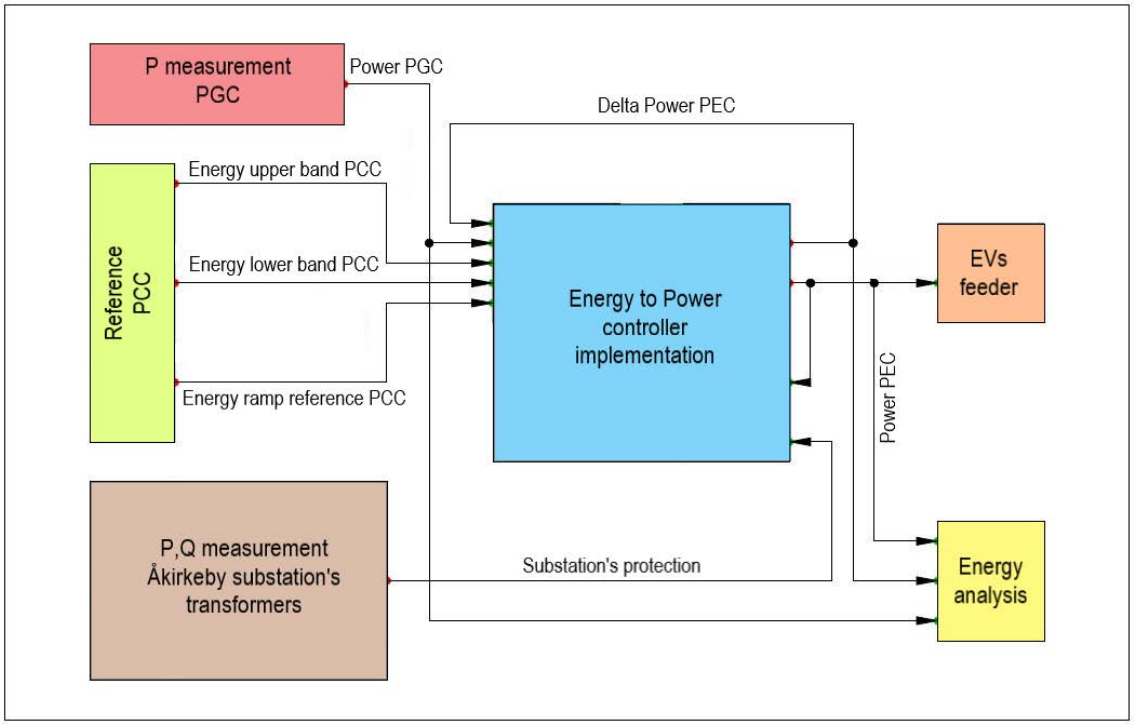

Figure 5.9: Conceptual layout of Composite Fleet Frame with *Energy-to-Power controller*

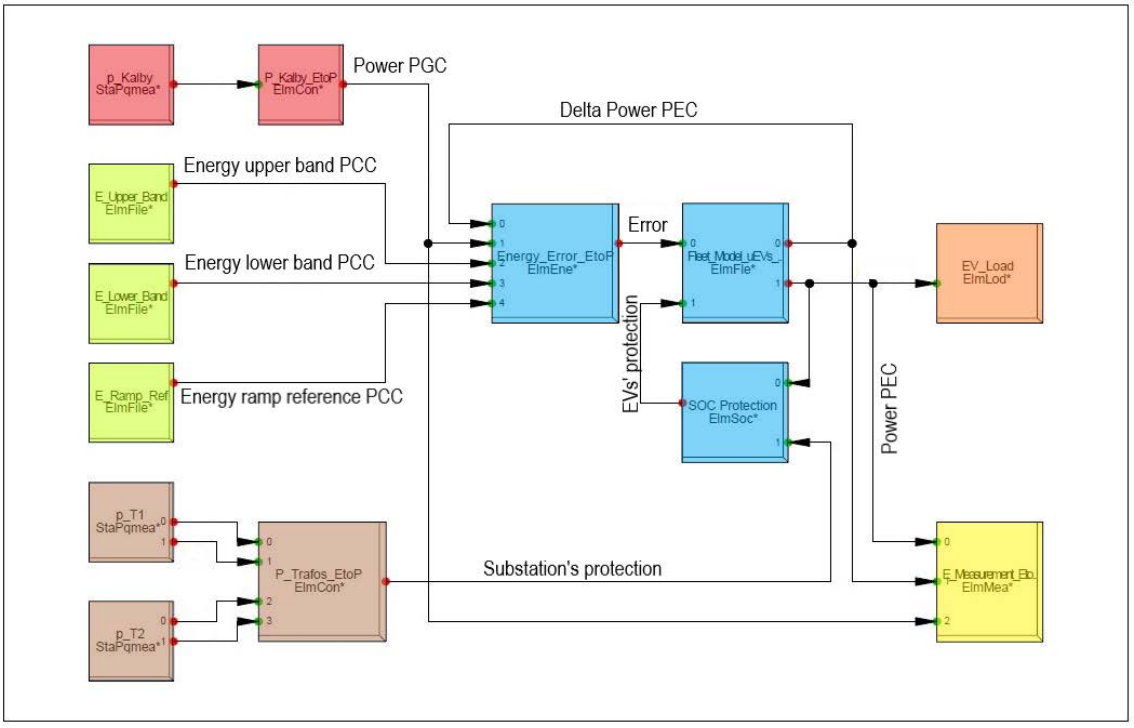

Figure 5.10: Composite Fleet Frame *Energy-to-Power controller*

The shapes obtained are basically 96 narrow energy bands per day (one each 15 $'$), pointed at the calculated energy reference values. Respectively, the upper, lower and ramp reference energy bands used at the PCC are imported from the first, second and third green blocks on the left of this

composite and converge into the *Energy Error* common model. This energy bands analysis is well discussed in [27].

5.4.2 *Energy-to-Power controller implementation* block

Finally, the three blue blocks that compose the core of the *Energy-to-Power controller* itself are investigated.

Energy error composite block definition

In Figure 5.11, the composite block definition related to the *Energy Error* common model is shown. In light blue, blocks to obtain the absolute error for the controller are highlighted and described below. The white blocks are instead used to evaluate the relative errors of *Energy PCC* in respect to the three energy bands. The measured *Power PGC* is subject to a certain measurement delay represented by the user-defined time parameter M_{del} (in $[s]$). This value is set and fixed at 1 s for the whole project, as already mentioned for the previous controller.

In respect to the *Power Error* common model in the *Power-to-Power controller*, in this case the comparison of PGC and PEC must be done in energy and not anymore in power terms. As a consequence, both *Power PGC* and *Delta Power PEC* inputs in $[W]$ are integrated first, then converted from $[Ws]$ to $[kWh]$. Furthermore, the produced *Energy PGC* is subtracted from *Delta Energy PEC* to obtain the *Energy PCC* to be compared with the imported energy bands. As energy bands were created for time windows of 15 $'$ each, the integral action have to be reset at the beginning of a new control band. The 'Integral reset' function designed specifically for this task is described in Appendix C.

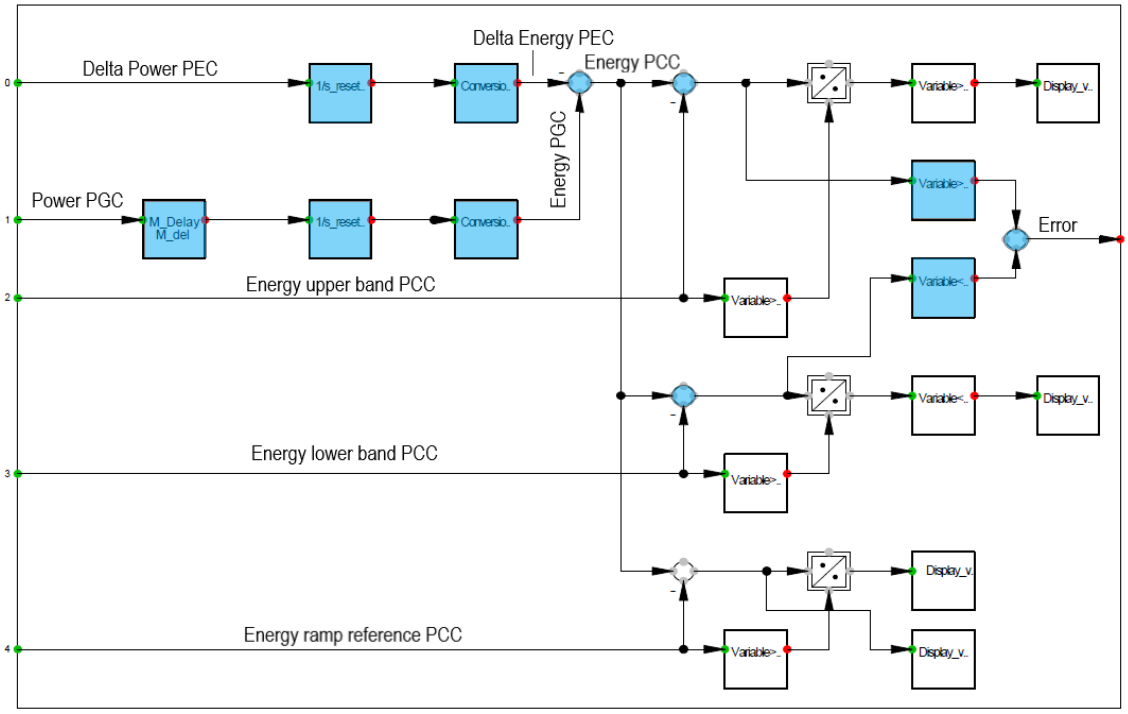

Figure 5.11: Composite Block Definition *Energy Error*

The control logic function to generate the *Error* signal can be resumed as follows:

- *Energy PCC* is between *Energy upper band* and *Energy lower band* $\longrightarrow$ null *Error*;
- *Energy PCC* is greater than the *Energy upper band* $\longrightarrow$ positive *Error*;
- *Energy PCC* is smaller than the *Energy lower band* $\longrightarrow$ negative *Error*.

The control mechanism is similar to the one in *Power Error* common model, although the *Error* can result in zero for a wider data range and not only for a specific reference point. If the difference between *Energy PCC* and *Energy upper band PCC* is positive, meaning that the WF produces more energy than expected, it is necessary to increase the power consumption of the EVs in respect to their forecasted charging set-point, meaning to increase *Power PEC* for the taken convention. Thus PEC will absorb more energy than it was planned.

On the opposite case, if the difference between *Energy PCC* and *Energy lower band PCC* is negative, meaning that the WF produces less energy than expected, it is necessary to decrease the power consumption of the EVs (again, in respect to their forecasted charging set-point), meaning to decrease the *Power PEC*. Thus PEC will absorb less energy than planned.

As defined for *Power PCC* in the *Power-to-Power controller*, also *Energy PCC* considers just *Delta Power PEC* (this time the associated energy) and not the whole *Power PEC*

As a conclusion, if the produced energy is inside the two energy bands, no errors are detected, otherwise the more the distance from the external bands, the greater the error evaluated. Moreover, the more narrowed the energy bands, the more rigid the controller, resulting in the *Power-to-Power controller* if the three energy bands are coincident.

Fleet model uEVs composite model definition overview and droop regulator

In Figure 5.12, the composite model definition of *Fleet Model uEVs* designed in PF is reported. It has the same structure as shown in Figure 5.7. However, in comparison to the *Power-to-Power controller*, the *Energy-to-Power controller* is equipped with a *droop* regulator, which is a fairly simple proportional regulator (highlighted in blue).

As a generic PID, the droop controller is also characterized by a gain called K_{droop}, which value defines the regulator sensibility. In order to make it as pure number, Equation 5.6 is applied, in which both input and output are normalized to base values. Subsequently, the blue blocks are arranged to convert the input energy error ΔE into a variation in power output ΔP, as shown in Equation 5.7.

$$\frac{\Delta E}{E_{base}} = K_{droop} \cdot \frac{\Delta P}{P_{base}} \tag{5.6}$$

$$\Delta P = \frac{\Delta E}{E_{base}} \cdot \frac{1}{K_{droop}} \cdot P_{base} \tag{5.7}$$

The energy base value E_{base} is defined as 1 kWh, while the power base P_{base}, which value is a function of the controlled device, is defined in Equation 5.4 for the $Ch-3ph$, otherwise in Equation 5.5 for the $Ch-1ph$. The accurate choice of this parameter leads to a better understanding on how the *droop* regulator is varying the power output as a function of the energy error in input.

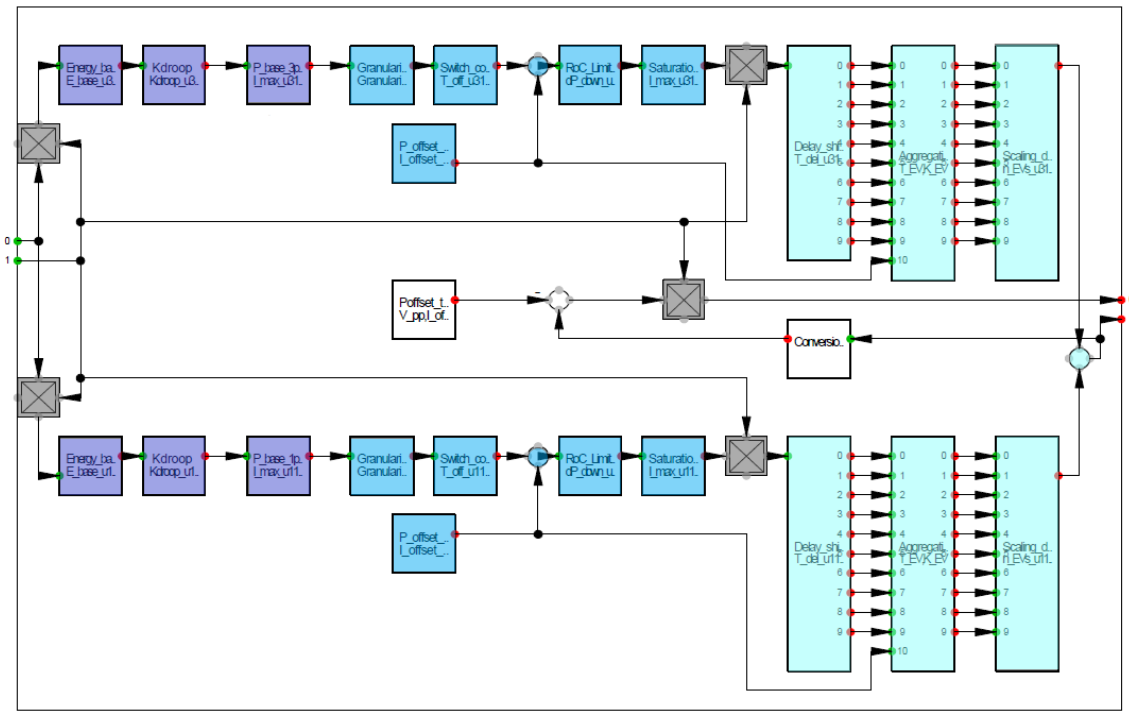

Figure 5.12: Composite Block Definition *Fleet Model uEVs* with *droop* regulator

Indeed, the K_{droop} is defined in such a way that with an energy error of 1 kWh over the upper band or under the lower band the *droop* regulator has to adjust the power output with a variation of +10 % of the flexible P_{base} in the first case or -10 % in the second case. As a consequence, the assigned to the K_{droop} gain value is equal to 10, as evinced from Equation 5.8.

$$K_{droop} = \frac{\Delta E}{E_{base}} \cdot \frac{P_{base}}{\Delta P} = \frac{1\ kWh}{1\ kWh} \cdot \frac{P_{base}}{0.1 \cdot P_{base}} = 10 \tag{5.8}$$

5.5 Modelling of home chargers and electric vehicles response

In Section 5.3 and 5.4, composite block definitions of the *Fleet Model uEVs* are explained from a regulator side, marked in blue. In fact, two different regulators are used as a function of the applied control logic. Instead, the chargers model as well as the EV fleet aggregation model are explained in this section.

As previously announced, the composite block definition *Fleet Model uEVs* (shown in Figure 5.8 and 5.12) is horizontally divided into two parts: the upper side is related to the EVs charging through $Ch-3ph$, while the lower side to the EVs charging through $Ch-1ph$. The overall goal is to represent the EVs attributes for AS provision, considering the main typical features of the chargers as well as the EVs response, investigated in Section 4.4.

5.5.1 Chargers model

The implemented charger model is marked in light blue color. Starting from the PI regulator power output, the signal passes through four blocks in the following order: *Granularity*, *Switch*, *Rate of*

change (ROC) limiter, and *Saturation*. Moreover, after the first two blocks, a summation point can be noticed. The summed signal is created in the *Power offset* block P_{offset}, used to define the forecasted power consumption for each EV (P_{offset}) and related to the offset charging current (I_{offset}) equal to 11 A. This offset power can be calculated with Equation 4.5 for the $Ch-3ph$ and with Equation 4.6 for the $Ch-1ph$. As a consequence, *Granularity* and *Switch* blocks act just on the regulator power output, meaning the variations on the EVs power consumption around P_{offset}, while *ROC limiter* and *Saturation* blocks are applied to the overall power consumption of a single EV.

With the *Granularity* block, the admitted charging current in discrete steps between I_{min} and I_{max} is reproduced, displayed in Figure 5.13 . This granular behavior can be activated manually. In fact, using the user-defined *Granularity switch* parameter, the EVs charging power can have infinite (blue curve) or discrete admitted values in the defined interval (red curve), depending on the investigated scenario. If the *Granularity* block is not active, the input signal is just transferred to the output signal without applying any alteration. It is important to mention how, being the regulator's power output in $[W]$, this granular behaviour is designed in PF in power terms too. In order to do so, the minimum and maximum charging power for an EV (P_{min} and P_{max}, respectively) are evaluated as in Equation 4.5 for the $Ch-3ph$ and in Equation 4.6 for the $Ch-1ph$. Then, the interval is divided into eleven equally spaced discrete steps. Even if related to the same current values, the two implemented function will differ in power terms.

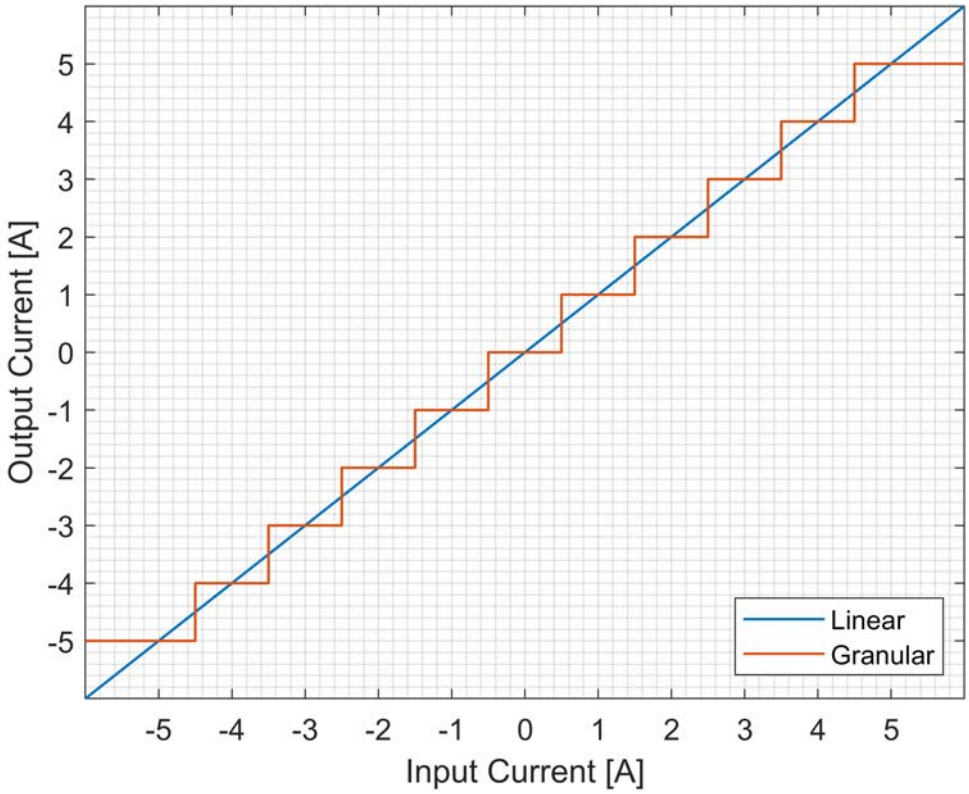

Figure 5.13: *Granularity* block

The second block used in the *Energy-to-Power controller*, called *Switch*, is a time-dependent block.

Indeed, its aim is to prevent the *droop* regulator from acting in the last seconds of each hour, admitting the considered EVs to come back at their P_{offset}. In this way, the EVs are at their P_{offset} and they will not influence the overall *Energy PCC* in the following hour. In fact, considering that EVs are subject to response delay, a regulator control signal sent in the last instants of an hour will influence the EVs action in the following one. Therefore, the user-defined T_{off} (in $[s]$) parameter in the common model is fixed at 10 s, ensuring that the last 10 s of each hour the regulator control actions are prevented.

Afterwards, the *RoC limiter* is implemented and applied to the overall power consumption of an EV, being summed the P_{offset} through the summation point. In this block, the ramp-up/ramp-down time response can be applied, fixing an upper and lower maximum cap to the power consumption's derivative. As stated in Section 4.4, it has been decided to consider EVs being able to apply instantaneous ramp-up/ramp-down power operations, although this block can lead to further analysis. Indeed, the two user-defined parameters dP_{up} and dP_{down} can be freely modified in the common model.

Last but not least, the *Saturation* block is introduced. This is important when the *Granularity* block is not considered. Indeed, in the case in which the *Granularity* block is out of order, the charging power of each EV has still to remain between the minimum and maximum admitted charging power (P_{min} and P_{max}). Moreover, the output and input signals of this block are useful to create the *anti-windup* signal for the PI regulator in the *Power-to-Power controller*. The idea is to prevent the integral to accumulate errors above or below the pre-defined saturation levels. Comparing the two composite block definition *Fleet Model uEVs* with the PI regulator and *droop* controller (Figure 5.8 and Figure 5.12, respectively), this signal is unnecessary in the latter case, being not present an integral side that can accumulate errors.

5.5.2 EV fleet model

The goal of the EV fleet model is to represent the EVs response to a change in the input control signal. As an overall, given a population of n EVs, k_{EV} the EV controller's gain, T_{EV} the first-order time constant of EV batteries and T_{del} the EVs response delay, the transfer function representing the fleet model of a generic population of EVs, all of them acting with the same defined features, is shown in Equation 5.9 [50].

$$H(s) = \frac{n \cdot k_{EV}}{1 + T_{EV} s} \cdot e^{-T_{del} s} \tag{5.9}$$

However, the EVs activation time differs among the EVs that compose the population considered. In fact, after the control signal is sent to the on-board BMS, each EV changes the power output with a certain delay, not uniquely defined. Considering results of real hardware tests, the total average activation time via a centralized remote control setup is found to be in between 6 s to 7 s [50]. Being an average delay, some EVs enter earlier or later than this found value. In order to represent this behaviour, the three aqua green blocks in the composite block definition *Fleet Model uEVs* are defined as follows.

Firstly, the *Delay shift* block contains ten parameters $T_{del,i}$, each of which is indexed with a different i. These user-defined time parameters (set in $[s]$ in the common model) are used to apply different

temporary shifts on the input power signal of this block. If the input power signal is defined as P, the obtained output power signals $P_{del,i}$ are calculated as in Equation 5.10 in Laplace domain.

$$P_{del,i}(s) = P(s) \cdot e^{-T_{del,i}s} \quad i \in \{1,\dots,10\} \tag{5.10}$$

Afterwards, the ten defined delayed signals are transferred to the *Aggregation* block, in which the first-order transfer function is applied. For each of the power signals $P_{del,i}$ in input, the output power signals $P_{agg,i}$ are calculated as in Equation 5.11, where the user-defined parameter T_{EV} is fixed at 0.1 s, while k_{EV} equals to 1, being the EV controller's gain externally applied in the blue section.

$$P_{agg,i}(s) = \frac{k_{EV}}{1 + T_{EV}s} \cdot P_{del,i}(s) \quad i \in \{1,\dots,10\} \tag{5.11}$$

Finally, in the *Scaling* block, all previously calculated power signals $P_{agg,i}$ are collected together to obtain the total EVs' power consumption (*Power PEC*). These signals are not simply summed. Indeed, a discrete Gaussian EVs distribution is applied to the considered population. The idea is to simulate that the further activation time from the mean value, the lower the amount of EVs changing their charging power set-point. In Figure 5.14a, the probability density function and the cumulative distribution function for the standard Gaussian curve are shown ($\mu = 0$, $\sigma = 1$). However, it is necessary in discrete terms, dividing this Gaussian curve into ten steps, having the same similar cumulative distribution function. As a consequence, in Figure 5.14b, the cumulative distribution function is composed with a segmented line, obtained with a linear interpolation of the continuous cumulative curve through eleven points. Afterwards, the probability discrete density function is evaluated, showing how the EVs population could be divided around the mean value to represent a Gaussian partition. Finally, each power signal $P_{agg,i}$ in input is multiplied by the EVs' number n_i that must be associated to a defined time delay, then summed together to obtain the final total EVs' power consumption, as shown in Equation 5.12.

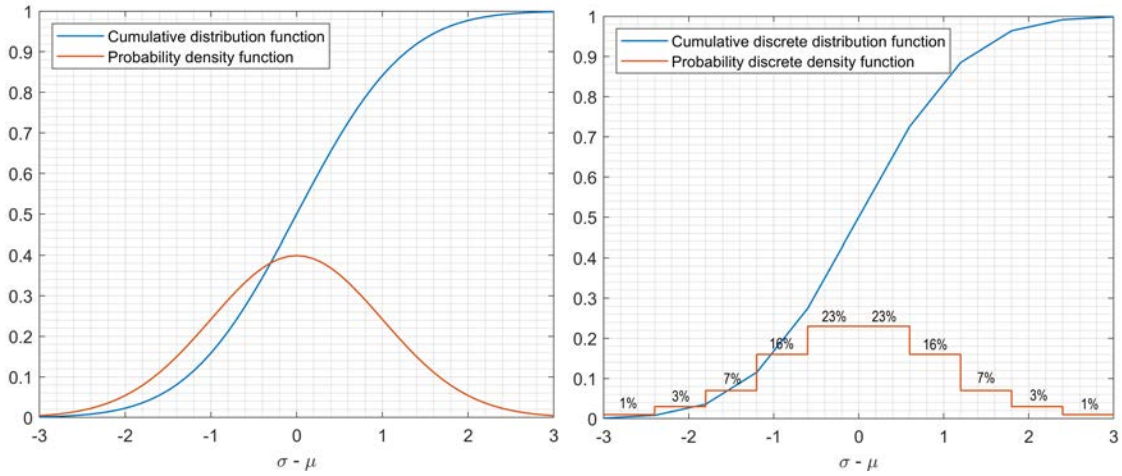

(a) Continuous (b) Discrete

Figure 5.14: Standard Normal Distribution analysis

$$P_{EVs}(s) = \sum_{i=1}^{10} P_{agg,i}(s) \cdot n_i \quad i \in \{1,\dots,10\} \tag{5.12}$$

As discussed in Section 4.7, the EV fleet population is composed of 480 EVs, which are equally divided into six groups if charged with $Ch-3ph$ (80 EVs per group), or into two groups if charged with $Ch-1ph$ (240 EVs per group). Consequently, it is necessary to slightly adapt the percentages that compose the probability discrete density function in order to apply the aforementioned power signals to an integer amount of EVs. Therefore, Table 5.1 reports the adjusted percentages and, for each of them, the relative applied time delay. While the percentages are directly implemented inside the *Scaling* block, the user-defined time delays $T_{del,i}$ can be manually set in the common model (in $[s]$) to compute various scenarios. In this project, time delay values were chosen to be equally spaced between 1 s – 10 s. Thus the mean time delay of the EVs aggregation is of 5.5 s. To obtain the overall delay time of the implemented controller this value was added to the measurement delay M_{del} of 1 s. Finally, in order to obtain the *Power PEC*, the calculated P_{EVs} is converted in $[MW]$ to be addressed to the EVs feeder.

Table 5.1: Discrete Gaussian distribution and applied time delays

Index i	n EVs [%]	Adjusted n EVs [%]	T_{del} [s]	Index i	n EVs [%]	Adjusted n EVs [%]	T_{del} [s]
1	1	1.25	1	6	23	25	6
2	3	2.5	2	7	16	15	7
3	7	6.25	3	8	7	6.25	8
4	16	15	4	9	3	2.5	9
5	23	25	5	10	1	1.25	10

5.5.3 Power analysis

To complete the treatise of the *Fleet Model uEVs*, the *Power analysis* area is described. In this section, the *Power PEC* is first reconverted into $[W]$, then the total offset power consumption $P_{offset,tot}$ of the EVs population is considered to obtain the *Delta Power PEC*. The $P_{offset,tot}$ is easily obtained multiplying the single P_{offset} for the total amount of EVs considered in the simulation (80 EVs per group if charged via $Ch-3ph$, and 240 EVs per group if via $Ch-1ph$). As previously described, if *Delta Power PEC* is positive it means the EVs are charging at higher power than the forecasted one, while negative values refer to the lower charging power than forecasted one. As a consequence, *Power PEC* output is defined in $[MW]$, while *Delta Power PEC* output in $[W]$.

5.6 State of charge protection and vehicle behavior application

The last composite block definition that must be described is related to the *SOC protection* common model. This block is used both to control the overall SOC of the EVs as well as to set different charging modes and EVs behaviour to analyse different operation scenarios. In Figure 5.15, the composite block definition is represented with macro blocks to illustrate how the composite itself has been arranged, successively presented as seen in PF in Figure 5.16.

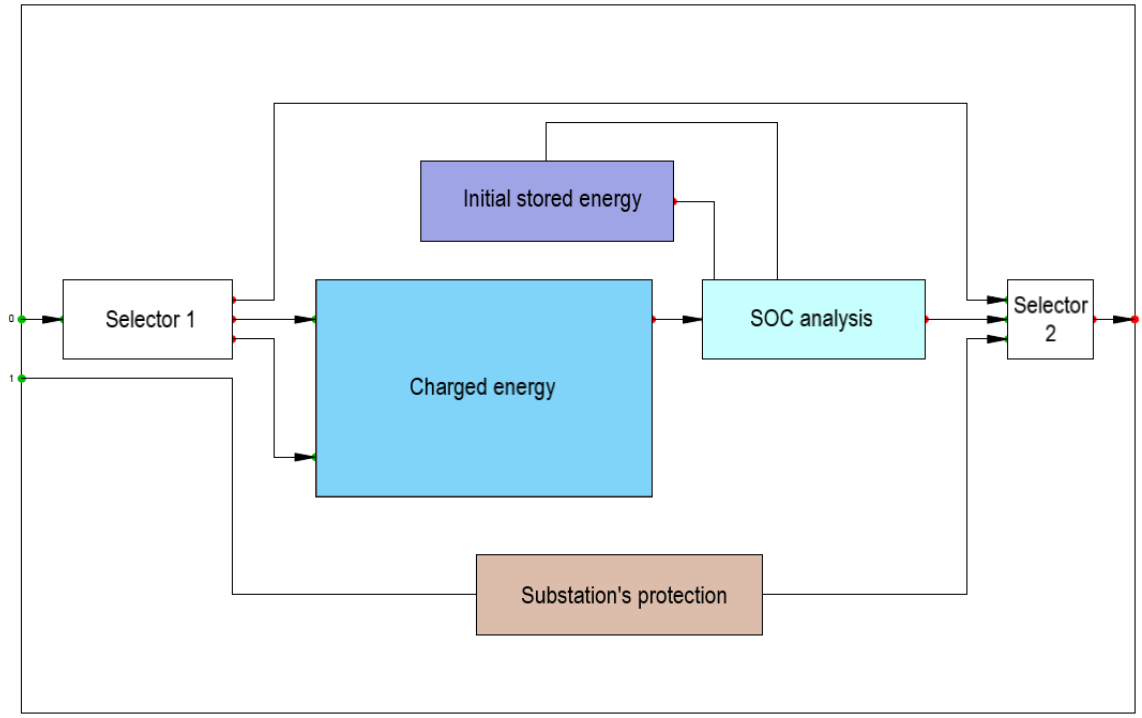

Figure 5.15: Conceptual layout of Composite Block Definition *SOC protection*

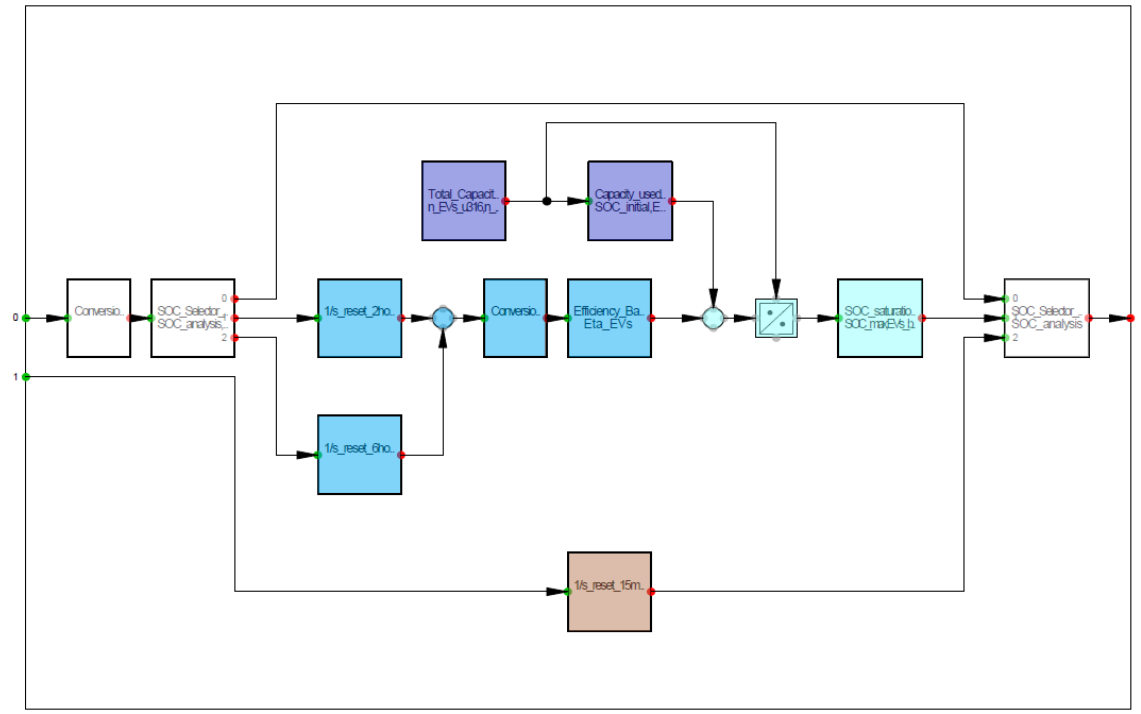

Figure 5.16: Composite Block Definition *SOC protection*

The *Selectors* are presented in white blocks. As a function of the set parameters, the input *Power PEC*, converted into $[W]$, is carried in one of the output signals. With the user-defined *SOC analysis* parameter in the common model, it is possible to decide if the SOC of the EVs is investigated or it is assumed the EVs are able to store as much energy as required from the controller. If the SOC is not of main interest, the first output signal of *Selector 1* is activated, in which a constant unitary signal is carried to *Selector 2* and assigned to the output signal of this common model. On the contrary, if the SOC analysis must be carried out, the second and third output of *Selector 1* are considered.

In the light blue blocks, the *Charged energy* is obtained. The output selection of *Selector 1* is function of the charger considered. Indeed, if $Ch-3ph$ is used to charge the EVs, the *Power PEC* is integrated with the upper integral block, which is reset every 2 h. Instead, if $Ch-1ph$ is used, the lower integral block is considered which is reset every 6 h. This choice is related to what has been explained in Section 4.6, being necessary to change the EVs under charge every 2 *hours* if via $Ch-3ph$ or 6 *hours* via $Ch-1ph$. These reset blocks simulate a switch in the considered EVs connected at the PEC, the EV aggregator being able to charge different groups of EVs throughout the whole day of simulation. The 'Integral reset' function is shown in Appendix C. After integrating the charging power, the obtained energy is converted from $[Ws]$ into $[kWh]$, which is basically the energy absorbed at the PEC (E_{PEC}) in a certain analysed charging time. Finally, the charger's efficiency is applied in the light blue block on the right, within which the user-defined parameter η in the common model is fixed at 0.9 *pu*, as stated in Section 4.5.4, obtaining the real actual charging energy $E_{charged}$ that will be transferred into the EVs battery, after considering the own losses, with Equation 5.13.

$$E_{charged} = E_{PEC} \cdot \eta \tag{5.13}$$

In the blue blocks, the *Initial stored energy* is detected. In the first blue block on the left, the total capacity of the EVs connected at the PEC (Qn_{tot}) is calculated in $[kWh]$. It is obtained by multiplying the number of charged EVs in each charging-time frame (user-defined parameter n equal to 80 EVs for $Ch-3ph$ or 240 EVs for $Ch-1ph$) for the nominal capacity of a single battery (user-defined parameter Qn fixed at 40 kWh in the common model), as introduced in Section 4.5.2 and shown in Equation 5.14.

$$Qn_{tot} = n \cdot Qn \tag{5.14}$$

As demonstrated in Section 4.5.3, the user-defined parameter $SOC_{initial}$ associated to each EV is fixed at 0.62 *pu* in the common model. As a consequence, with the blue block on the right, it is possible to calculate the total initial stored energy $E_{initial}$ in the EVs aggregation, multiplying the total capacity Qn_{tot} for the $SOC_{initial}$, as observable in Equation 5.15.

$$E_{initial} = Qn_{tot} \cdot SOC_{initial} \tag{5.15}$$

Finally, in the aqua green block, the SOC level's increment due to the injection of charging energy $E_{charged}$ is detected. The total stored energy E_{stored} is first obtained at the summation point, adding

$E_{charged}$ to $E_{initial}$, as seen in Equation 5.16. Then, using Qn_{tot}, the actual SOC_{level} in $[pu]$ can be detected with Equation 5.17.

$$E_{stored} = E_{charged} + E_{initial} \tag{5.16}$$

$$SOC_{level} = \frac{E_{stored}}{Qn_{tot}} \tag{5.17}$$

The aqua green block on the right of Figure 5.15 is used to apply the SOC protection. The SOC_{level} is compared with the user-defined parameter SOC_{max}, fixed at 1 *pu* in the common model, representing the maximum admitted SOC level. If the SOC is still under the maximum admitted level, then the output of this block is at unitary level, otherwise it is forced to be at zero. Additionally, it is possible to select if the EVs behavior needs to be analysed or not through the user-defined parameter *EVs behavior* inside this block. If this parameter is active, the EVs will be available at the PEC just in between 6 *pm* – 6 *am*, namely throughout the night, being disconnected and not charged throughout the day. Thus, in between 6 *am* – 6 *pm* the output signal of this block is fixed at zero, while during the night is function of the comparison in between SOC_{level} and SOC_{max}.

The brown block represents the *Substation's protection*. In fact, the second input of this common model is the *Substation's protection* signal, defined while exposing Figure 5.5, which can assume level 1 if the substation's *Loading* level reaches the imposed *Limit*, otherwise it remains at level 0. In this composite block definition, this signal passes through the integral block, which is reset every 15 $'$ of the simulation time. The integral block works as a memory for the built system. Indeed, if *Substation's protection* signal is at level 0, the integral will remain at zero as well, while if at level 1, the output will result in the integrated value and will remain not zero until the reset will occur.

Last but not least, the *Selector 2* in the right white block is considered, which output is the *EVs' protection* binary signal, already defined while describing Figure 5.5. This block is basically working along the *Selector 1* line. Indeed, if *SOC analysis* is deactivated, the first input is selected, then the unitary value will be directly transferred to *EVs' protection* signal for the whole simulation time. Contrarily, the second input port is assigned to the *EVs' protection* signal, which value can be zero or one as a function of the aqua blue block output on the right. Moreover, this block considers also the *Substation's protection* signal, previously integrated in the brown block. If the integrated signal is zero, namely a *Substation's protection* signal equals to 0 for the considered 15 $'$, the protection is not activated and the *EVs' protection* signal is function of the previous two inputs. Otherwise, if the integrated value is detected to be not zero, namely a *Substation's protection* signal not constantly 0 in the considered 15 $'$, the implemented protection logic is of primary level and the *EVs' protection* signal is forced to be 0 until a new 15 $'$ time window will restart.

As a conclusion, it is observed that the *EVs' protection* signal is a vector that can take the value of 0 or 1. The signal is sent to the *Fleet Model uEVs* and imported with the grey blocks, which are multiplier blocks. Their goal is observable in Figure 5.8 and 5.12: if the *EVs' protection* signal is equal to 1, the *Fleet Model uEVs* works unaffected. Instead, if a level 0 of *EVs' protection* signal is detected, it forces to switch off all the EVs.

5.7 Summary

This chapter concerns about the technical implementation of the two analysed controllers in this project. An overview about the Åkirkeby substation layout is treated, with the goal of associating the designed PF model with the real data collected in Section 2.4. Each feeder (both generation and production unit) was represented by a simple load with imported power profiles based on historical data.

The *Power-to-Power controller* and the *Energy-to-Power controller* are presented, showing their related frames. For each of them, it has been first given a general overview about the built frame, then going more specifically into the *controller implementation* block. Inside the *Fleet Model uEVs*, the chargers' model as well as the EV fleet aggregation is described in a detached section, being these frame's sides identical for both controllers. Finally, the *SOC protection* block is analysed. Within this block, the *Substation's protection* signal is integrated and the EVs behavior applied too.

6 TECHNICAL RESULTS

In this chapter, the technical results of the thesis are presented. The investigated scenarios are described in Section 6.1. Then, Section 6.2 contains the results related to the *Power-to-Power controller*, while the *Energy-to-Power controller*'s results are shown in Section 6.3. Finally, the main differences observed while charging the EVs' aggregation via $Ch-3ph$ or $Ch-1ph$ are discussed in Section 6.4.

6.1 Investigated scenarios

In this first section, a main view and explanation on how the technical results are displayed is planned.

The chapter is divided into 3 main sections:

1. *Power-to-Power controller* results (Section 6.2), analysing all the three different windy situation in *VW*, *W* and *NW*;
2. *Energy-to-Power controller* results (Section 6.3), analysing the only *VW*;
3. Comparison between three- and single-phase chargers (Section 6.4) in *VW*.

The first 2 sections presents different scenarios, following the same structure:

- Controller behavior: fixing a high amount of EVs, it is shown how the controller should work ideally (Section 6.2.1 and 6.3.1);
- EVs' charging behavior influence: the EVs' attributes are analysed to detect their consequences on the requested EVs' power flexibility (Section 6.2.2 and 6.3.2). In this scenario, three EVs' features are added one at a time, following this order:
  a. EVs' delay effect;
  b. Gaussian distribution effect;
  c. Granularity effect.
- EVs' behavior in Åkirkeby: the results are shown with all the aforementioned EVs' features applied, in addition to a reduced number of EVs for grid services. Moreover, EVs are not available all day long but only during nocturnal hours (6 *pm* – 6 *am*). The *Power-to-Power controller* is applied in Section 6.2.3, while the *Energy-to-Power controller* is described considering an accurate energy forecast in Section 6.3.3 and an inaccurate energy forecast in Section 6.3.4.

These first 2 sections collect the results when EVs are grid connected via $Ch-3ph$. As a consequence, a comparison in between $Ch-3ph$ and $Ch-1ph$ is carried out in the last section, applying this latter charger to both controllers (Section 6.4.1 and 6.4.2).

6.2 Power-to-Power controller results

This section collects the technical results obtained with the *Power-to-Power controller* and it is divided into three main parts. First, the controller behavior analysis is carried out (Section 6.2.1), observing the outcomes under EVs' ideal conditions. Then, the EVs' charging influences are considered one by one (Section 6.2.2), later applied to the controller as a whole (Section 6.2.3). Since the only $Ch-3ph$ is considered in this section, a selected EVs' group is charged for 2 h, being necessary to replace the EVs under charge when this charging window is expired.

6.2.1 Controller behavior

Firstly, the behavior of the *Power-to-Power controller* is shown. To exhibit its functioning, each group under charge is composed of 800 EVs, resulting on a total of charging EVs of 9600 for each day. Moreover, since the EVs' charging influences are still not considered, the minimum T_{del} of 1 s is applied to the EVs aggregation, delay after which all the EVs could adjust their charging power linearly in between the minimum and maximum allowed power and without any relative delay among EVs. The following results are obtained with the installed PI regulator tuned with K_p of 0.3 and K_i of 0.6 for all the three considered days.

Figure 6.1 reports the produced power by the wind farm (*Power PGC* in red) and the adjusted power output at the PCC (*Power PCC* in blue). The *Power reference PCC* is underlined in black, which was evaluated as the average wind farm power output for each 15 $'$, so the wind fluctuations are not considered. It must be noticed how *Power PCC* is not exactly the power measured at the PCC. As already mentioned in Section 5.3.2, the overall EVs' power consumption is not considered while declaring this variable. Although it is called *Power PCC*, it shows how the applied variations at the EVs' offset power consumption will influence the WF's power output (the application of *Delta Power PEC* to *Power PGC*).

Then, *Power PEC* is collected in the upper plot of Figure 6.2, in which it is clear to see that *Delta Power PEC* is applied to the forecasted and constant EVs' charging power of 6.097 MW with 800 EVs. The lower plot shows how the SOC level evolves in each EVs' groups per charging window. Specifically, each groups composed of 80 EVs is charged for 2 h, increasing the *SOC level*, which starts from the *SOC initial* of 0.62 pu. When this charging session of 2 h expired, the EVs' group is substituted by the EV aggregator. Thus, a new EVs' group will start to increase its *SOC level*. This plot show how the *SOC level* evolves in each charging window.

These figures are combined with Table 6.1, which facilitate for a better understanding. This table provides:

- *PGC* and *PCC power fluctuations*, expressed in [%]: these first two parameters represent the fluctuations' intensity at PGC and PCC, respectively. These values are defined as the average ratio in between the standard deviation and the average power in a 15 $'$ basis, as explicated in Equation 6.1 and 6.2. The *Power-to-Power controller* works positively if a decrease in the *PCC power fluctuations* is obtained in respect to the value at PGC;
- *PGC energy output* [kWh]: total energy generated by the wind farm throughout the day;
- *PCC energy output* [kWh]: total energy injected at the PCC under *Delta Power PEC*'s influence. Again, this value is not considering the EVs' offset power consumption;

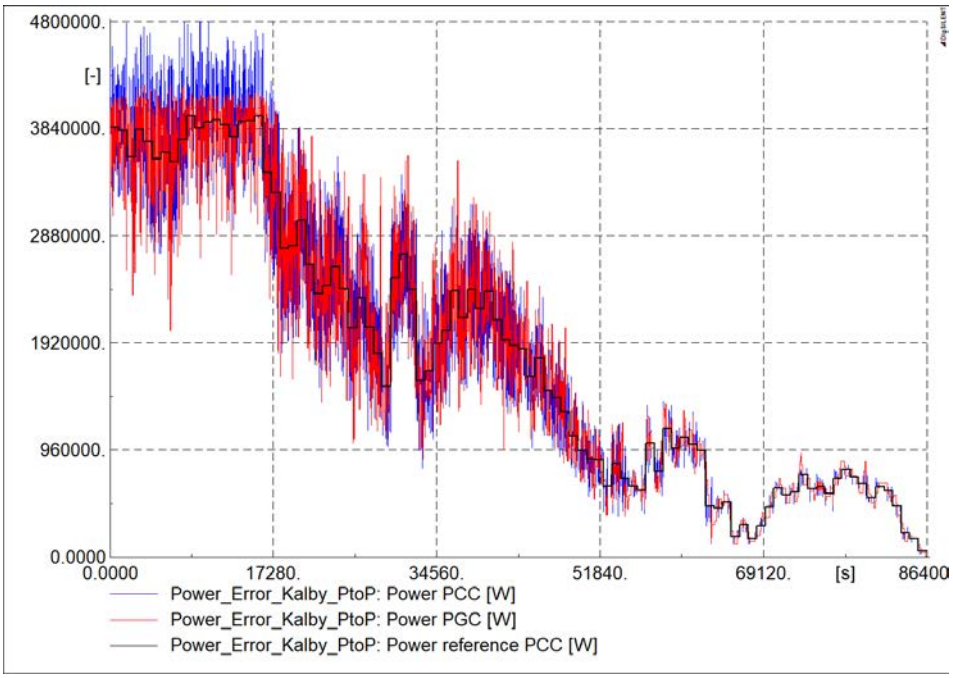

Figure 6.1: PGC, PCC and reference power in *VW* under ideal conditions

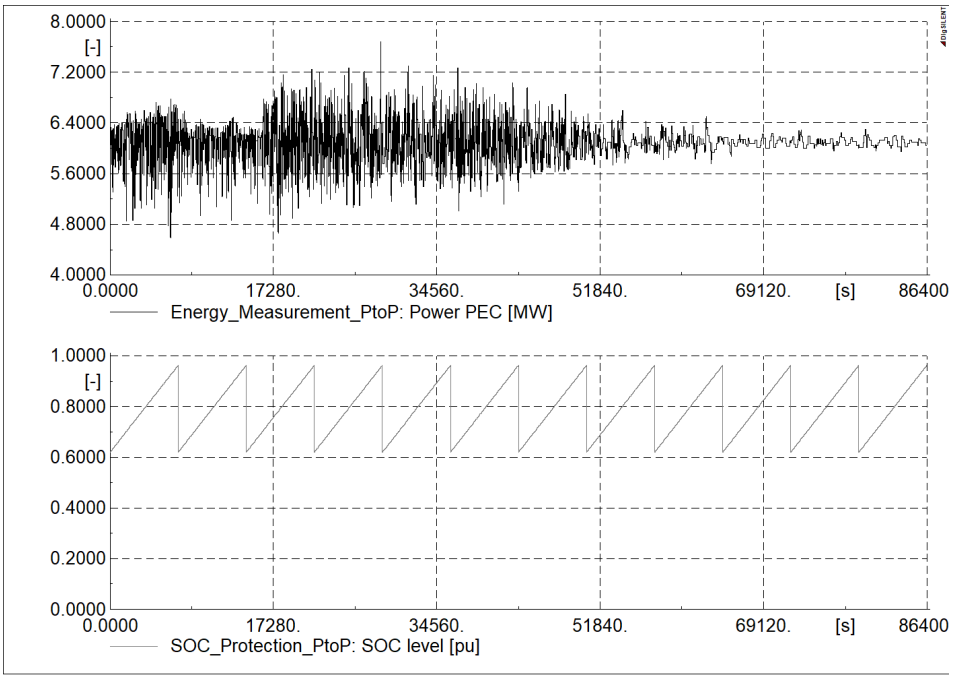

Figure 6.2: Power PEC and SOC level in *VW* under ideal conditions

- *PCC energy reference* [kWh]: energy reference obtained with the *Power reference PCC*. The *Energy-to-Power controller* works positively if *PCC energy output* matches with the requested *PCC energy reference* in each designed energy band;
- *PEC power max/min* [kW]: maximum and minimum detected power consumption at PEC, used to check if the chargers' saturation limits are reached. The EVs' offset power consumption is clearly considered to obtain these values;

- *PEC energy gained, managed, consumed, released* [kWh]: these values show the energy analysis at the PEC. The *PEC energy gained* is the amount of energy that PEC gains at the end of the day in respect to the forecasted energy consumption. If this parameter is null, it means that, even though the EVs changed their charging set-point, they absorbed the same amount of energy as they were working at the forecasted power all day long. The *PEC energy gained* is observable in the difference in between *PGC energy output* and *PCC energy output*. When the EVs absorb more than forecasted, *Delta Power PEC* is integrated to detect the *PEC energy consumed*, while when they absorb less than forecasted, the same variable is integrated to obtain the *PEC energy released*. The sum of these two last parameters gives the overall *PEC energy managed*, while the difference again the *PEC energy gained*.

$$PGC\,power\,fluctuations = average\left(\frac{STD(Power\,PGC)_{15'}}{mean(Power\,PGC)_{15'}}\right) \tag{6.1}$$

$$PCC\,power\,fluctuations = average\left(\frac{STD(Power\,PCC)_{15'}}{mean(Power\,PCC)_{15'}}\right) \tag{6.2}$$

Summing up, all the results in this chapter show the influence of *Delta Power PEC* to *Power PGC*, obtaining than *Power PCC*. Indeed, the idea is to somehow simulate the bidirectional power exchange while under unidirectional chargers. The only parameters that consider also the EVs' offset power consumption are *PEC power max/min* and the SOC analysis.

Table 6.1: Results of *Power-to-Power controller* under ideal conditions

	VW	**W**	**NW**
PGC power fluctuations [%]	15.64	13.47	19.70
PCC power fluctuations [%]	8.66	7.94	8.60
PGC energy output [kWh]	43,599	89,704	26,470
PCC energy output [kWh]	43,596	89,703	26,470
PGC energy reference [kWh]	43,599	89,704	26,470
PEC power max / min [kW]	7,677 / 4,584	8.629 / 3,530	7,799 / 5,086
PEC energy gained [kWh]	3	1	0
PEC energy managed [kWh]	4,557	8,787	4,162
PEC energy consumed [kWh]	2,280	4,394	2,081
PEC energy released [kWh]	2,277	4,393	2,081

As already stated, the aim for the *Power-to-Power controller* is to smooth out the sudden and unpredictable WF's power oscillation observed in *Power PGC*. As a consequence, the controller acts on *Power PEC*, varying the overall injected *Power PCC*. In Figure 6.1, it is clearly observable how *Power PCC* shows greater peaks in respect to *Power PGC*, occurrence better displayed and investigated later while analysing Figure 6.3. Nevertheless, the overall *PCC power fluctuations* show a reduction in all the three analysed days. For the shown *VW* in this section, the *PCC power fluctuations* are almost halved in percents terms in respect to the effective *PGC power fluctuations* produced from the WF, decreasing these power oscillations from 15.64 % to 8.66 %. In the *W* and *NW* (which graphs are collected in Appendix D), these fluctuations passed from being 13.47 % and 19.70 % at the PGC to 7.94 % and 8.60 % at the PCC, respectively. The three days have been analysed to see how the wind fluctuations are translated into power oscillations as a function of the wind intensity. From this table, the overall turbulence's intensity produced by the WF at the PGC in a *NW* is greater than in a *W* while the *VW* lies in between them. However, the final turbulence's

intensity effectively injected at the PCC is approximately levelled out around the same value in percent with the shown ideal controller.

Moreover, in all the three considered days, the chargers' saturation limits are not reached, being of $8,868\ kW$ for the upper level and $3,326\ kW$ for the lower one. In addition, the SOC_{max} level is not reached throughout any of the considered days. Indeed, the *PEC energy gained* should be ideally zero, being the *Power reference PCC* defined as mean power of PGC for each $15\ '$, so *PGC* and *PCC energy output* should be coincident. These small gained energies are a consequence of the delays considered (M_{del} and T_{del}), which are not influencing the overall final SOC level, being approximately constant around $0.963\ pu$ (forecasted final SOC level if at constant charging set-point current of $11\ A$) at the end of each charging window (of 2 hours via $Ch-3ph$). It must be remembered how, *PEC energy gained* is not the value that goes into the EVs' batteries, but just the energy variation in respect to the forecasted consumption at the PEC seen from the grid's perspective. In fact, this energy must be added to the forecasted charging energy and then multiplied by the charger's efficiency η to obtain the effective charging energy to analyse the SOC.

6.2.2 Electric vehicles' charging behavior influence

Step by step, the EVs time delays, their Gaussian distribution response when subject to a change in the control signal as well as the granularity of each EV's power output are introduced. Each variation is set one at a time, validating it before to check the influence of another attribute.

EVs' delay effect

First, the mean T_{del} is shifted from being 1 *s* to 5.5 *s*, where the latter value is the mean delay of the Gaussian distribution applied in the following step. These results show the first 100 *s* of the *VW*, obtained with the installed PI regulator tuned with K_p of 0.4 and K_i of 0.1.

The graphs on the left of Figure 6.3 are just a simple zoom in the first 100 *s* of the previous figures, which can be used to motivate the greater *Power PCC* peaks in respect to *Power PGC* peaks. Since the WF output *Power PGC* is higher than the reference power at the beginning of the simulation, it means that the injected power in the grid should be reduced. As a consequence, *Power PEC* increases to bring *Power PCC* back to the reference values, being then stabilized when this transient ends (always remember the difference in the applied convention). When a new power fluctuation comes, the oscillation is seen at the adjusted *Power PCC* until when the *PI* controller will act to move the *Power PEC* again, in order to balance *Power PCC* to the reference value one more time. The two implemented time delays (M_{del} and T_{del}) are consequently influencing the EVs' response and then the time after which the *Power PEC* will be adjusted, being impossible to avoid completely the fluctuations' injection in the grid.

Applying the new mean T_{del} of 5.5 *s*, the *Power PEC*'s response is shown on the right of Figure 6.3. It can be clearly deduced that the new mean T_{del} has a strong influence in the EVs' power output, making longer the transient period. However, the stability at the *Power reference PCC* is not undermined when all the EVs act together after 5.5 *s*, result accomplished thanks to a less aggressive PI regulator tuning.

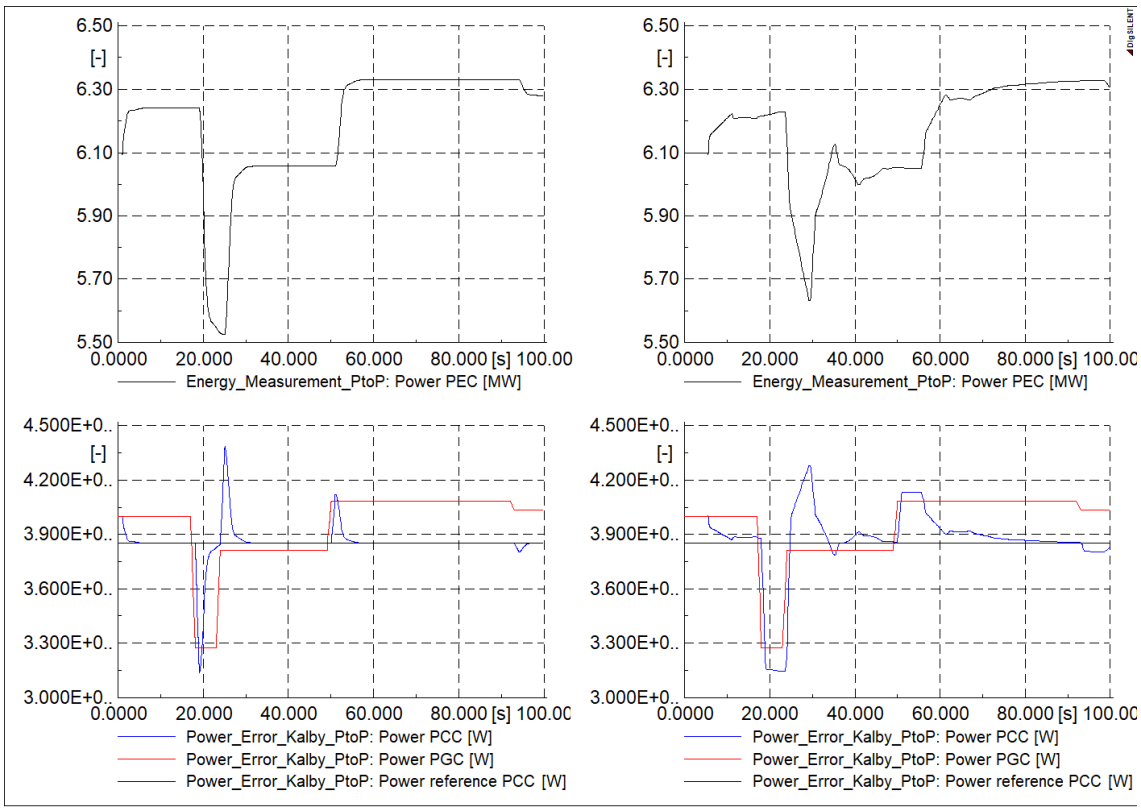

Figure 6.3: Comparison between T_{del} of 1 *s* and 5.5 *s* with *Power-to-Power controller*

Gaussian distribution effect

Second, considering the new mean T_{del} of 5.5 s, the EVs' response represented with a Gaussian distribution is analysed. As described in Section 5.5.2, the EVs aggregation is divided into 10 groups, each of them composed of a certain number of EVs obtained from the normal distribution analysis of Figure 5.14 and subject to different time delays, which are encompassed in between 1 s – 10 s. The considered pairs "T_{del} - n EVs" can be observed in Table 5.1. These results are obtained with the installed PI regulator tuned with K_p of 0.5 and K_i of 0.12.

In Figure 6.4, the consequence of applying the Gaussian distribution is shown on the right. The softener *Power PEC* variations can be detected thanks to a more gradual EVs' response than in the graph on the left when all the EVs act together at the defined T_{del} of 5.5 s. After this new applied effect, it can be seen that the stability at the *Power reference PCC* is not deteriorated, in fact being reached with a slightly less aggressive PI regulator tuning in respect to when all the EVs act at the same time.

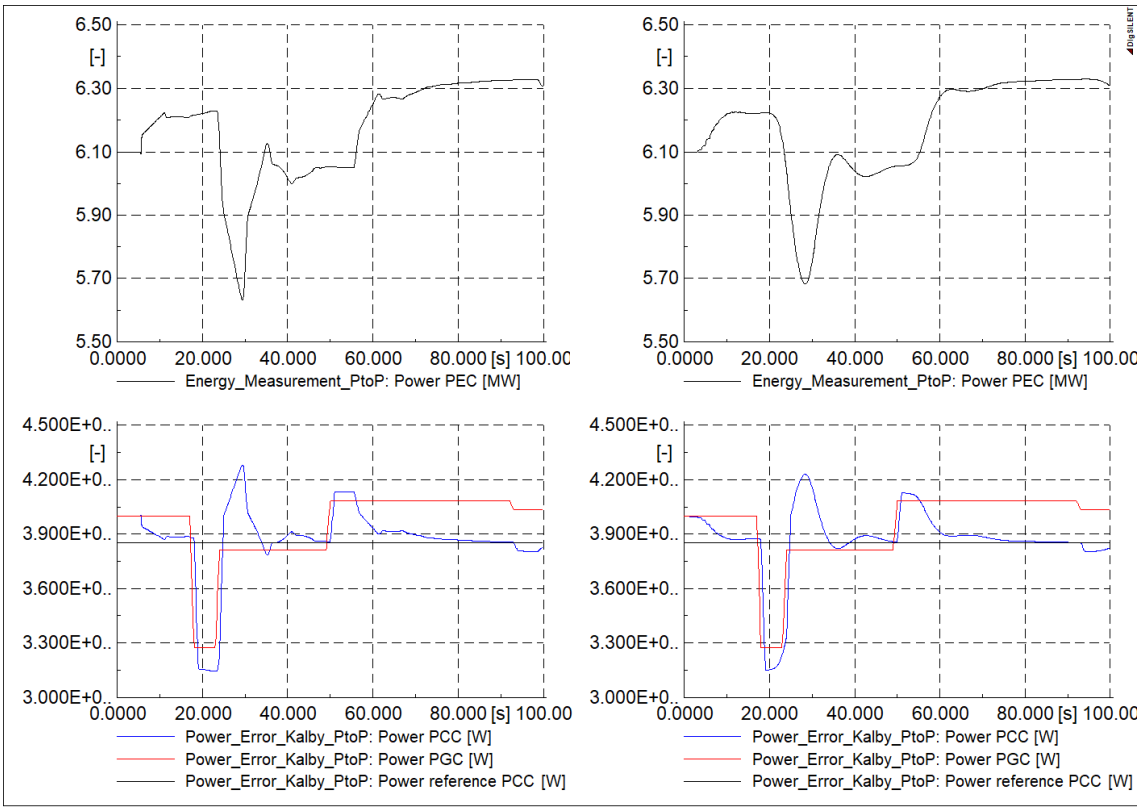

Figure 6.4: Comparison without and with Gaussian distribution effect with *Power-to-Power controller*

Granularity effect: impossibility with the *Power-to-Power controller*

Finally, it is interesting to observe how the *Power-to-Power controller* is influenced if the granularity power output is considered for each EV. In Figure 6.5, it is possible to see how the power output can reach just discrete powers, not all the values as previously seen. Basically, the output will remain stable at the beginning of the simulation even if there is a certain error. The integral part of the PI regulator starts to integrate the error in input until a control signal is sent to all the EVs to change their charging set-point power to the following admitted discrete power output, as shown in Figure 5.13. Consequently, the reference level cannot be reached anymore. Thus, the oscillations cannot be stopped and the *Power-to-Power controller* does not satisfy its goal if the granularity effect is applied. In conclusion, the only Gaussian distribution effect with mean T_{del} of 5.5 s is taken into account to apply the EVs behavior to the *Power-to-Power controller*.

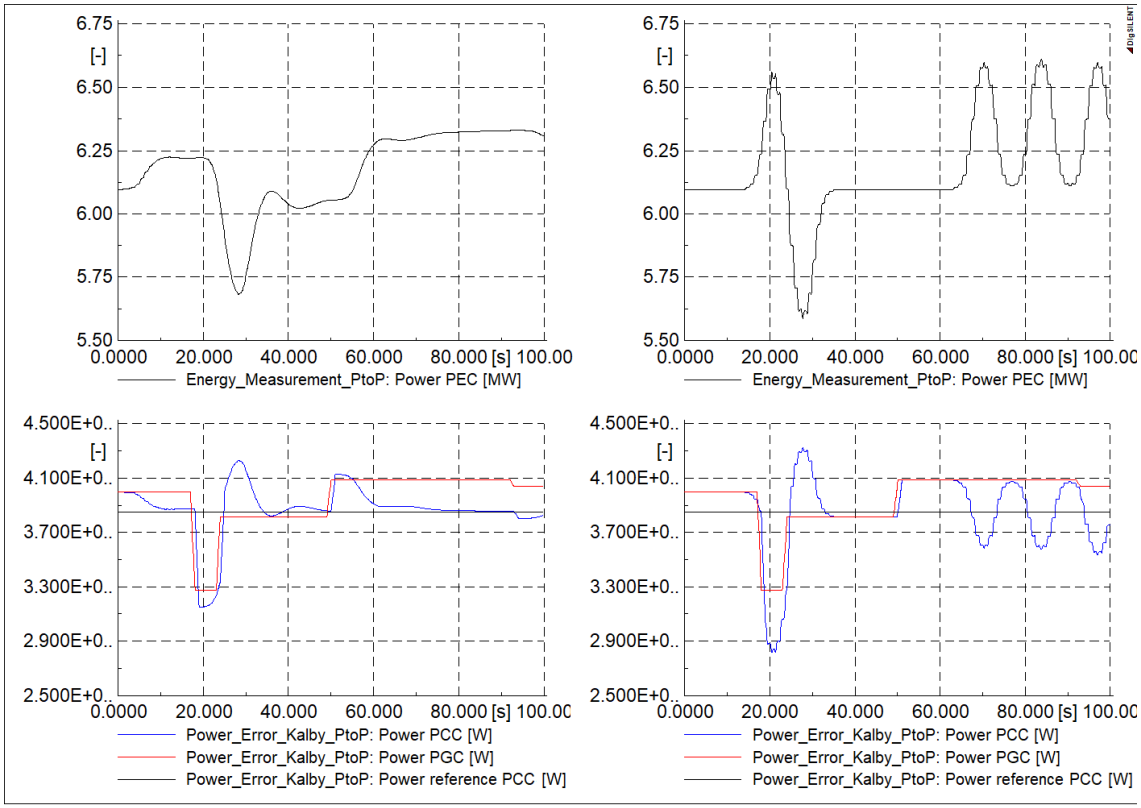

Figure 6.5: Comparison without and with granularity effect with *Power-to-Power controller*

6.2.3 Electric vehicles behavior in Åkirkeby: final results

Considering the only Gaussian effect with mean T_{del} of 5.5 s, the *Power-to-Power controller* is applied to the investigated EVs population in Åkirkeby. In order to define the EVs behavior, in addition to the delays and the Gaussian distribution effect, each group of EVs is considered to be composed of 80 EVs and the availability for grid services is just in between midnight – 6 *am* as well as 6 *pm* – midnight. The following results are obtained with the installed PI regulator tuned with K_p of 5 and K_i of 1.2.

Figure 6.6 and 6.7 represent the previously considered parameters immerse in this real scenario, figures that can be correlated with Table 6.2.

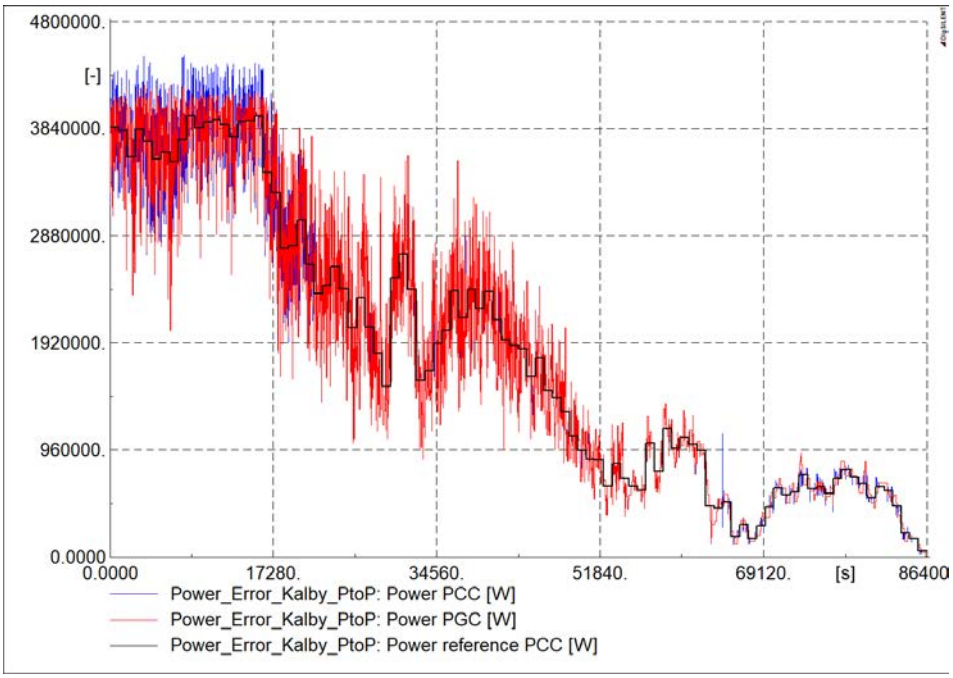

Figure 6.6: PGC, PCC and reference power in *VW* under real conditions

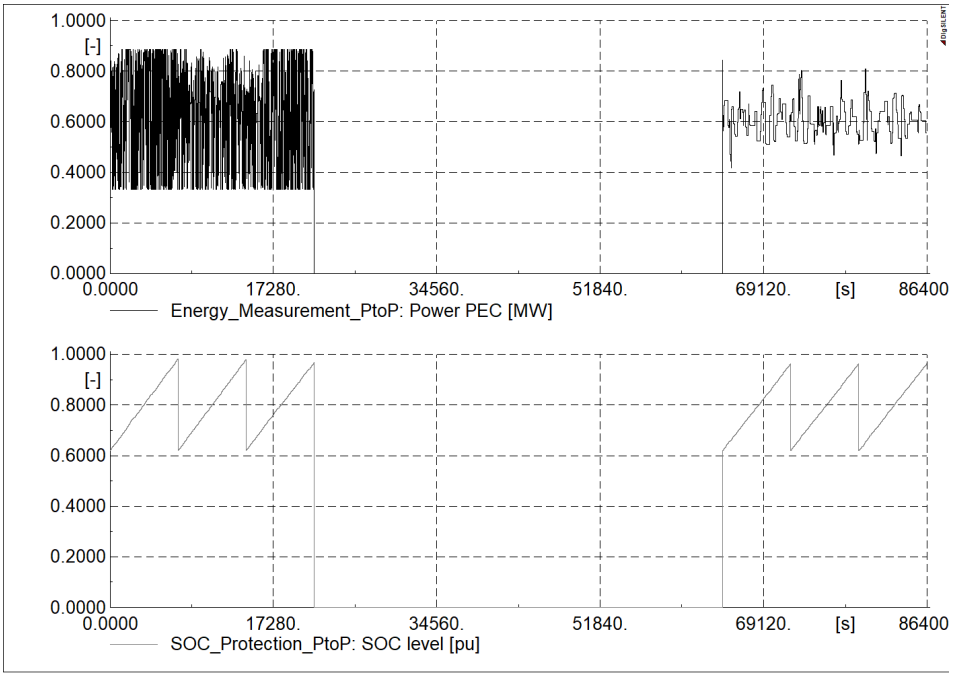

Figure 6.7: Power PEC and SOC level in *VW* under real conditions

At first blush, it is clear how the EVs are not grid connected in between 6 *am* – 6 *pm*, then *Power PEC* and the related *SOC level* are stable at zero. From the grid's perspective, it means that *Power PGC* and *Power PCC* are coincident in that time period, being injected all the WF power fluctuations into the grid. Considering instead when the EVs are plugged in, it is detected how the upper and lower chargers' saturation levels are reached, especially in between midnight – 6 *am*.

Indeed, decreasing the amount of available EVs, the power flexibility that EVs can give for grid services is reduced too. Being now the EVs' offset power consumption of 609.7 *kW* with 80 EVs, the upper and lower chargers' saturation levels are 886.8 *kW* and 332.6 *kW*, respectively, ten times smaller than the previous ideal condition with 800 EVs. This consequence can be observed in Figure 6.8, in which a zoom to see how *Power PCC* is influenced if the chargers' saturation limits are reached is shown. Basically, *Power PCC* cannot satisfy the request to reach *Power reference PCC* all time long, a condition that will increase the overall *PCC power fluctuations*.

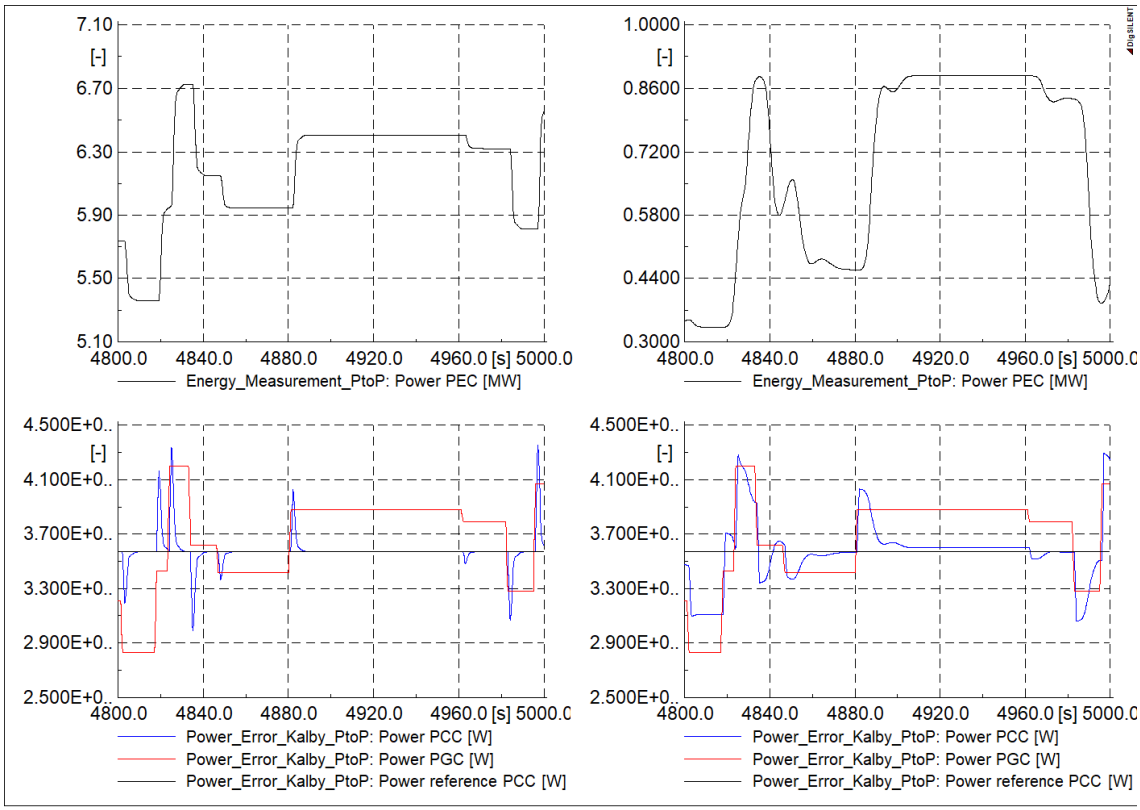

Figure 6.8: Comparison of Power PCC with and without charger saturation limits reached

Table 6.2 contains the same parameters previously defined. However, the data related to the whole day are reported in parenthesis, while the data obtained just when the EVs are plugged in (so then excluding the time period 6 *am* – 6 *pm*) are reported out of parenthesis. Regarding *PGC* and *PCC power fluctuations* in *VW*, Figure 6.9 can be used for a more simple understanding. In parenthesis, it is possible to observe how the *PGC power fluctuations* of 15.64 % obtained previously are now reduced to 13.66 % instead to 8.66 % at the PCC, as a consequence of the applied EVs behavior. Indeed, the red and blue bar charts are completely overlapped in between 6 *am* – 6 *pm*, leading to an higher fluctuations' injection. Then, neglected the time period 6 *am* – 6 *pm*, the aforementioned fluctuations counting for 13.13 % at the PGC, become 9.18 % at the PCC. From the suggested figure, it is clearly seen how the turbulence intensity is decreased when the EVs are grid connected. The same considerations can be done for the NW and *W*, which graphs are collected in Appendix D.

Table 6.2: Results of *Power-to-Power controller* under real conditions

	VW	**W**	**NW**
PGC power fluctuations [%]	13.13 (15.64)	14.08 (13.47)	19.00 (19.70)
PCC power fluctuations [%]	9.18 (13.66)	9.53 (11.24)	10.56 (15.47)
PGC energy output [kWh]	24,483 (43,599)	42,820 (89,704)	13,598 (26,470)
PCC energy output [kWh]	24,338 (43,454)	42,746 (89,630)	13,700 (26,572)
PGC energy reference [kWh]	24,483 (43,599)	42,820 (89,704)	13,598 (26,470)
PEC power max / min [kW]	886.8 / 332.6	886.8 / 332.6	886.8 / 332.6
PEC energy gained [kWh]	145	74	-102
PEC energy managed [kWh]	1,275	2,190	1,612
PEC energy consumed [kWh]	710	1,132	755
PEC energy released [kWh]	565	1,058	857

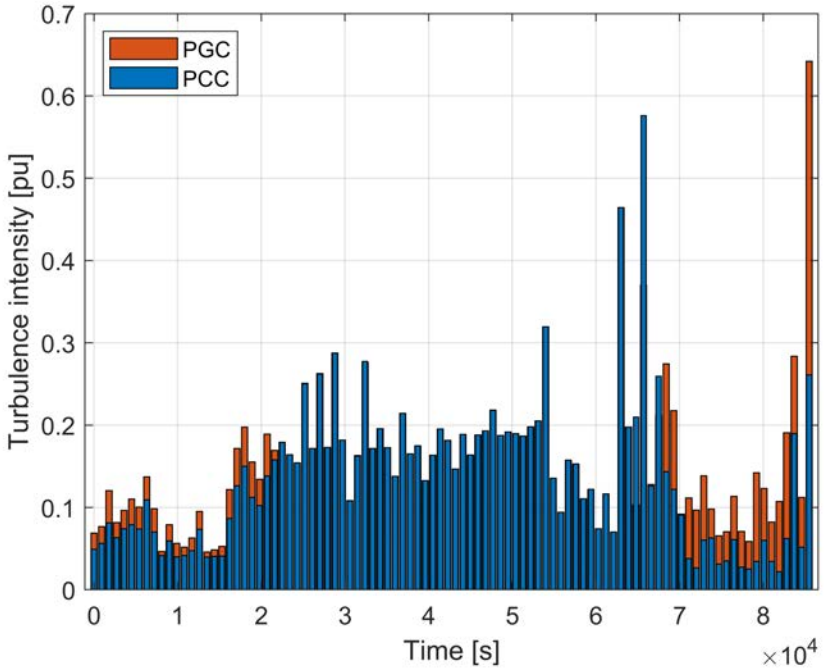

Figure 6.9: Turbulence intensity at PGC and PCC in the *VW*

Moreover, the *PEC energy gained* results in collecting/delivering greater amount of energy in respect to what is observed in Table 6.1, consequence of chargers' saturation levels as well as applied delays and Gaussian distribution effect. Although the final SOC level in each charging window is partially varied, the SOC_{max} level is never reached, the EVs being able to deliver grid services for the whole time they are connected to the power grid. These data can be detected from Table 6.3. The goal of this table is to show how the SOC is evaluated as a function of the stored energy, these values being obtained from the lower plot in Figure 6.7. For each EVs' group in a charging window, the *Initial* and *Final SOC* level is reported, separated by the *Energy gained* from the EVs to increase the SOC. This *Energy gained* differs from *PEC energy gained* because it considers both the *Power PEC* and not only the *Delta Power PEC*, as well as the charger efficiency η. As a consequence, the *Final SOC* is mainly varied in between midnight – 6 *am*, when the chargers' saturation levels are reached mostly, but still without any appreciable variation in

respect to the final forecasted SOC level of 0.963 *pu* with a constant charging set-point current of 11 *A*. The values in parenthesis represent the energy variation in respect to the forecasted energy consumption for each EVs' group in a charging window. This kind of analysis will be more useful in the *Energy-to-Power controller*, when the inaccurate scenario is instead considered and the EVs are required to absorb/release energy to balance the forecast errors.

Table 6.3: SOC analysis in *VW* with *Power-to-Power controller*

	Initial SOC [pu]	**Energy gained [kWh]**	**Final SOC [pu]**
00 am - 02 am	0.62	1,159 (+62)	0.9822
02 am - 04 am	0.62	1,151 (+54)	0.9797
04 am - 06 am	0.62	1,113 (+16)	0.9678
06 am - 06 pm	0	0	0
06 pm - 08 pm	0.62	1,096 (-1)	0.9625
08 pm - 10 pm	0.62	1,098 (+1)	0.9631
10 pm - 12 pm	0.62	1,098 (+1)	0.9631

6.3 Energy-to-Power controller results

This section collects the technical results obtained with the *Energy-to-Power controller* and it follows the same structure as with the *Power-to-Power controller* analysed in the previous section. First, the controller behavior analysis is carried out (Section 6.3.1), observing how the outcomes could result under EVs' ideal conditions. In this case, the energy bands are created using an accurate energy forecast. Then, the EVs' charging influences are considered one by one (Section 6.3.2), later applied to the controller as a whole in two different conditions: under accurate forecast scenario (Section 6.3.3), so when the WF produces exactly the expected energy amount, and under an inaccurate energy forecast (Section 6.3.4), when instead the WF energy production is deviating in respect to the planned one because of wind fluctuations. Since the only $Ch-3ph$ is considered in this section, a selected EVs' group is charged for two hours, being necessary that the EV aggregator will replace the charging EVs when this charging time is over. As already underlined, the *Energy-to-Power controller* is investigated only for the *VW* scenario.

6.3.1 Controller behavior

Firstly, the behavior of the *Energy-to-Power controller* is shown. To exhibit its functioning, each EVs' group under charge is fix to be composed of 800 EVs. Moreover, since the EVs' charging influences are still not considered, the minimum T_{del} of 1 *s* is applied to the EVs aggregation, after which all the EVs could adjust their charging point linearly in between the minimum and maximum allowed charging power.

The energy control logic function is shown in the upper plot of Figure 6.10, in which the 96 energy windows are represented, each of them acting for 15 $'$. The injected energy at the PCC (*Energy PCC*) is controlled to remain inside the created bands thanks to the adjustment of *Power PEC*, parameter that can be seen in Figure 6.11 on the upper plot, where it is clear to see that *Delta Power PEC* is applied to the forecasted and constant EVs' charging power of 6.097 *MW* with 800 EVs. Again, it is worthwhile to remember, although it is defined as *Energy PCC*, this parameter shows how the applied variations at the EVs' offset energy consumption will influence the WF's

energy output (the application of *Delta Energy PEC* to *Energy PGC*), as underlined in Section 5.4.2. Finally, the related EVs' SOC analysis is represented in the lower graph of this latter figure, while the influence of *Power PEC*'s variations at the PCC in power terms is shown in the lower graph of Figure 6.10.

These figures are combined with Table 6.4, which facilitates a better understanding.

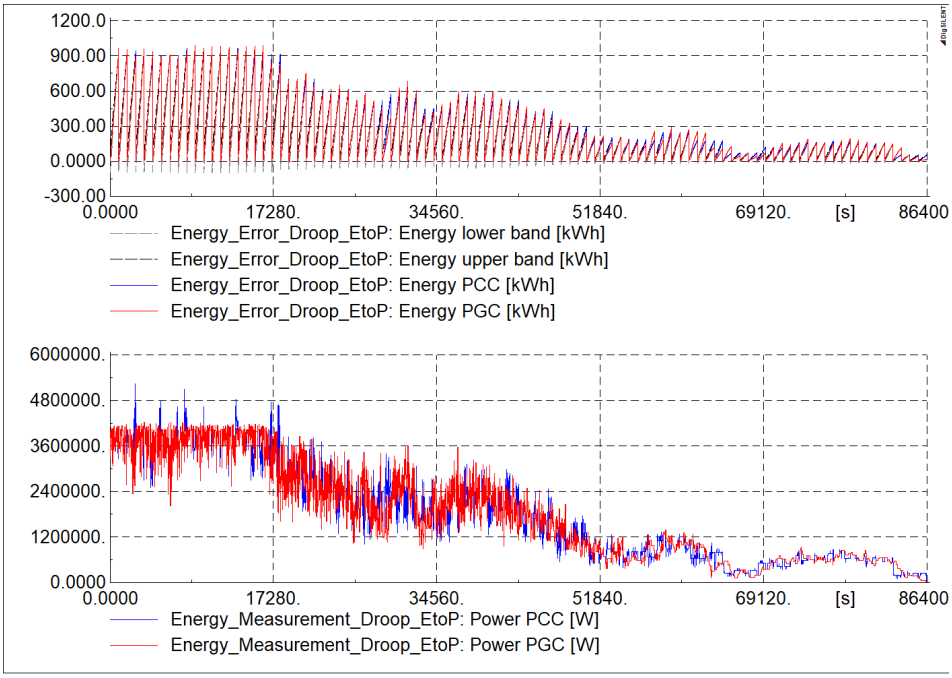

Figure 6.10: Energy bands and power production under ideal conditions

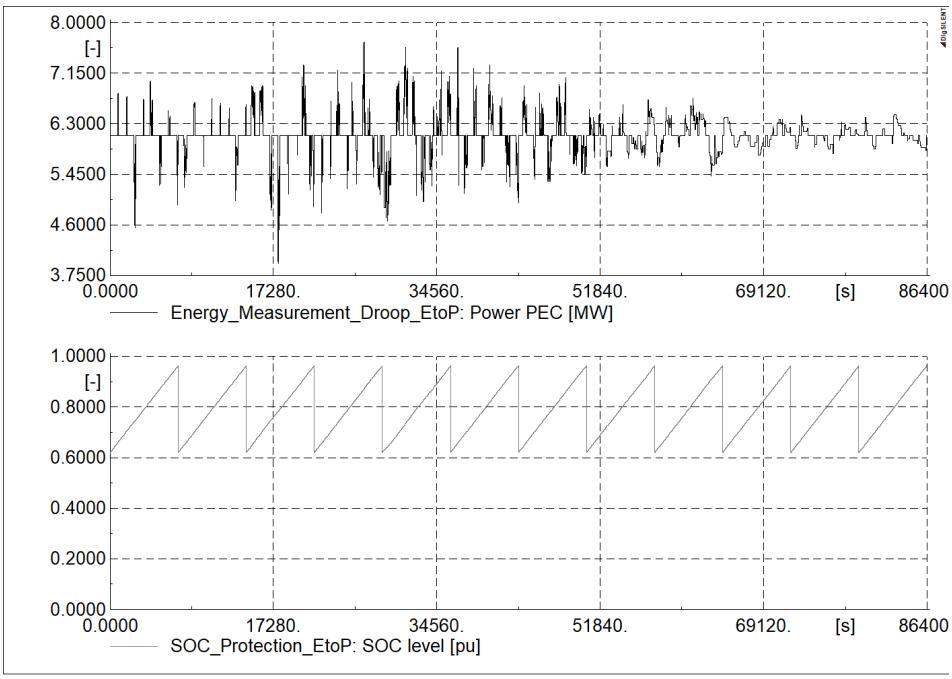

Figure 6.11: Power PEC and SOC level under ideal conditions

Table 6.4: Results of *Energy-to-Power controller* under ideal conditions

	VW
PGC energy output [kWh]	43,599
PCC energy output [kWh]	43,588
PCC energy reference [kWh]	43,599
PEC power max / min [kW]	7,664 / 3,949
PEC energy gained [kWh]	11
PEC energy managed [kWh]	3,165
PEC energy consumed [kWh]	1,588
PEC energy released [kWh]	1,577

As already stated, the aim for the *Energy-to-Power controller* is to control the energy injection at the PCC in order to satisfy the forecasted hourly energy production from the WF. As a consequence, the controller acts on *Power PEC*, varying the overall injected *Power PCC* as seen in the lower graph of Figure 6.10. However, the hourly energy balance being the scope, the power profile at the PCC is not anymore controlled to fulfill a certain reference power as it was with the previous controller, allowing the *Power PCC* to sudden oscillations. Indeed, when *Energy PCC* goes out of the energy control band, the *droop* regulator will change the EVs' power consumption proportionally to the energy error itself, as it will be explained later while discussing about Figure 6.12. In Figure 6.11, it is clearly observable how *Power PEC* shows fluctuations less crammed than with the previous controller, being necessary to modify the EVs' power consumption in the case in which the energy production is not balanced with the forecasted one, then it is not necessary to follow a reference power continuously. Since the control logic function is composed of narrowed bands, the error signals that control the *Power PEC* are more common in the last minutes of each bands, being the part in which the *upper* and *lower energy bands* are closer, thus it is easier that the detected *Energy PCC* goes out of these bands. As a consequence, being not the main goal for this controller, the overall injected fluctuations into the grid are not investigated and the only energy balance is considered, instead.

The chargers' saturation limits are not reached, being of $8,868\ kW$ for the upper level and $3,326\ kW$ for the lower one. In addition, the SOC_{max} level is not reached throughout the whole day as well. Ideally, the *PEC energy gained* should be zero in this scenario, being the energy bands created using an accurate energy forecast. However, the small energy gained in respect to the forecasted one is a consequence of the delays considered (M_{del} and T_{del}), which is not influencing the overall final SOC level, being approximately constant around $0.963\ pu$ at the end of each charging window.

6.3.2 Electric vehicles' charging behavior influence

Step by step, the EVs time delays, their Gaussian distribution response when subject to a change in the control signal as well as the granularity of each EV's power output is introduced. Each variation is set one by one, validating it before to check the influence of another attribute.

EVs' delay effect

First, the mean T_{del} is shifted from being 1 *s* to 5.5 *s*, which latter value is the mean delay of the Gaussian distribution applied in the following step. Figure 6.12 shows the last 300 *s* of the fifth energy band, meaning in between 1 *am* – 1 : 15 *am*.

The graphs on the left of Figure 6.12 are just a simple zoom of the previously plotted figures under ideal conditions, which can be used to better understand the *Energy-to-Power controller* work. Basically, when the *Energy PCC* is going over the *Energy upper band*, it means that the injected energy in the grid should be reduced. As a consequence, *Power PEC* increases to absorb part of the generated energy from the WF, bringing *Energy PCC* back into the energy bands (always remember the difference in the applied convention). Since the controller acts, the two curve *Energy PGC* and *Energy PCC* are not coincident anymore. The *Energy PGC* is plotted to see which would be the energy injected if the controller were not acting, even though the *Energy PCC* is the energy that must be adjusted and maintained into the admitted values. It could be pointed out that *Power PEC* is not at the offset EVs' power consumption in the last seconds of this energy band, meaning the *Energy PCC* is slightly outside the *Energy upper band*. This problem is clearly function of the two defined time delays and the continuously evolving WF energy production. A deeper error analysis for each of the considered control bands will be later carried out, when the EVs behavior will be applied under real conditions, thus greater errors could come out.

Applying the new mean T_{del} of 5.5 *s*, the *Power PEC*'s response is shown on the right of Figure 6.3. The new applied delay results in greater elongations of the EVs' power consumption. However, the energy target achievement is not undermined when all the EVs act together after 5.5 *s*.

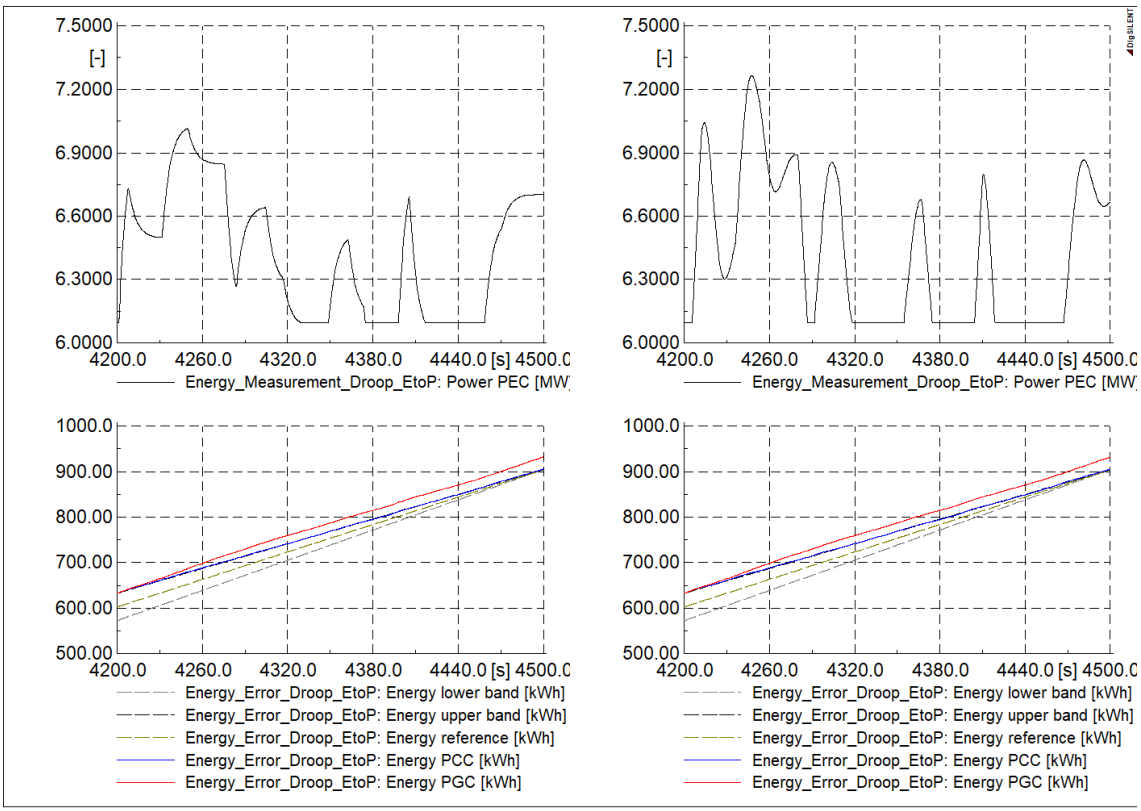

Figure 6.12: Comparison between T_{del} of 1 *s* and 5.5 *s* with *Energy-to-Power controller*

Gaussian distribution effect

Second, considering the new mean T_{del} of 5.5 s, the EVs' response represented with a Gaussian distribution is analysed in Figure 6.13. The description of the Gaussian distribution implementation can be found in both Section 5.5.2 and 6.2.2.

In Figure 6.13, the consequence of applying the Gaussian distribution with the same mean T_{del} is shown on the right. The softener *Power PEC* variations can be detected thanks to a more gradual EVs' response than in the graph on the left when all the EVs act together at the defined T_{del} of 5.5 s. Indeed, because of some EVs change their charging power before the mean T_{del}, it can be detected how *Power PEC* will deviate from the offset EVs' power consumption more gradually (as seen on the upper-right graph) than with a strict angle (as seen on the upper-left graph). The same consideration can be done with the EVs acting with greater T_{del} than the mean one. Moreover, since some EVs start to apply the energy management before the mean T_{del}, the energy exchanged being equal the power elongations are slightly reduced. As a conclusion, this new applied effect does not influence the overall energy target achievement.

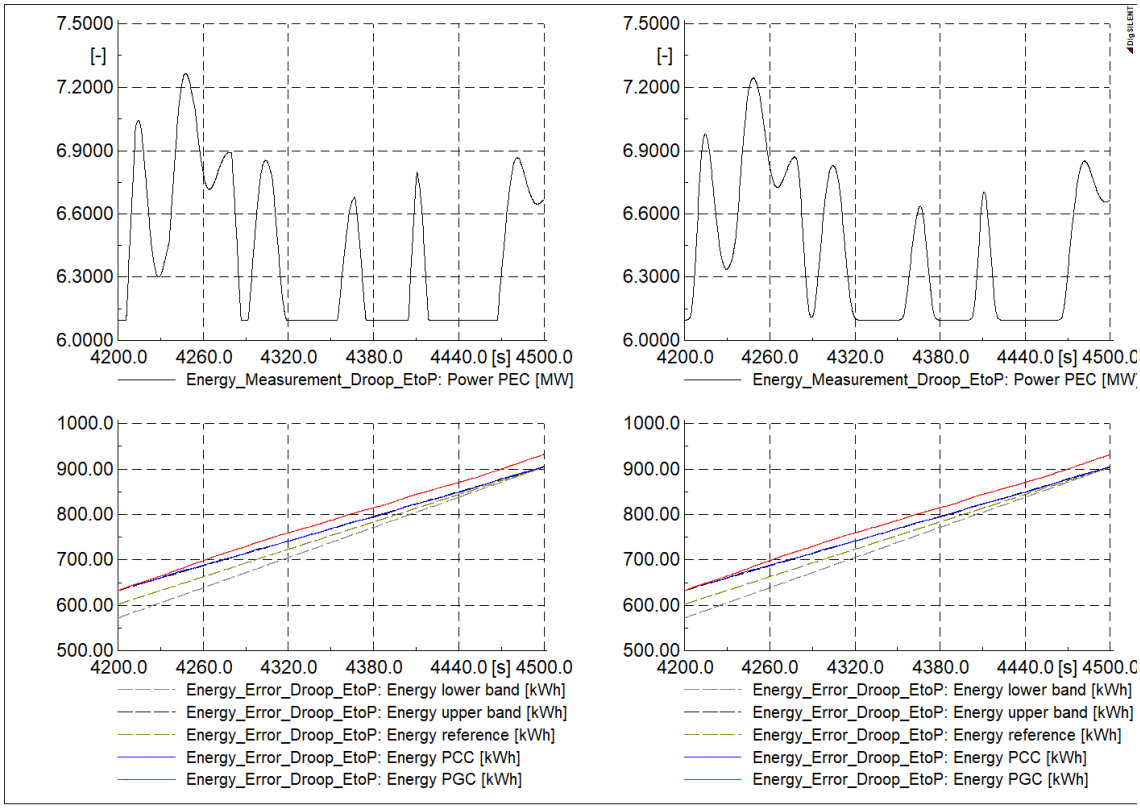

Figure 6.13: Comparison without and with Gaussian distribution effect with *Energy-to-Power controller*

Granularity effect: possible with the *Energy-to-Power controller*

After that the granularity effect has been disregarded in the *Power-to-Power controller*, it is very interesting to observe how the *Energy-to-Power controller* is influenced, instead. In Figure 6.14 (upper-right plot), it is possible to see how the *Power PEC* can reach just discrete offset powers, not all the power values as in the upper-left plot. However, the aim of this controller being the energy balance, so then the subtended area to the curve, the *Power PEC* profile is not considered in power terms but rather in energy terms (*Energy PEC*, or better *Delta Energy PEC* as highlighted in Figure 5.11). As a consequence, the granularity effect of each EV's power output could be applied for this controller, being not undermined the overall energy target achievement.

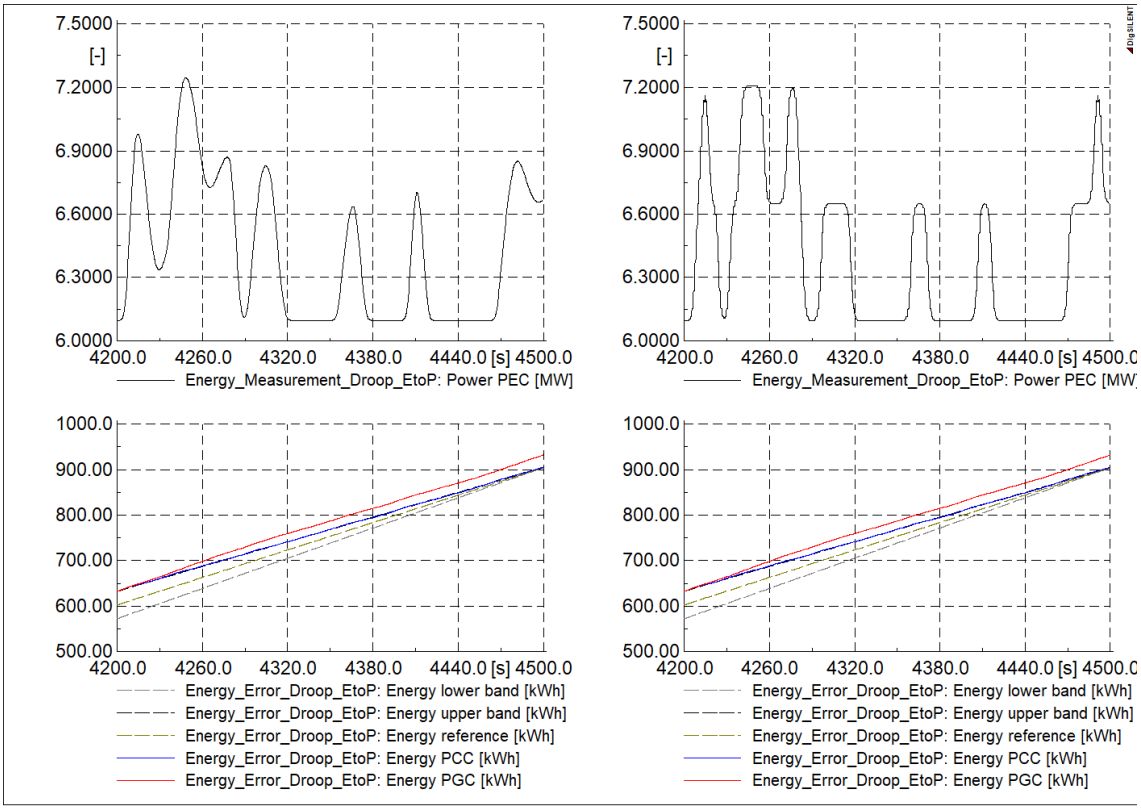

Figure 6.14: Comparison without and with granularity effect with *Energy-to-Power controller*

6.3.3 Electric vehicles behavior in Åkirkeby: accurate forecast

Considering all the aforementioned EVs attributes, the *Energy-to-Power controller* is applied to the investigated EVs population in Åkirkeby. In order to define the EVs behavior, in addition to the delays and the Gaussian distribution effect, each group of EVs is considered to be composed of 80 EVs and the availability for grid services is just in between midnight – 6 *am* as well as 6 *pm* – midnight. The following results are obtained in the case in which an accurate energy forecast scenario is applied, as applied under ideal conditions in Section 6.3.1.

Figure 6.15 and 6.16 represent the previously considered parameters in this real scenario, figures that can be connected to Table 6.5.

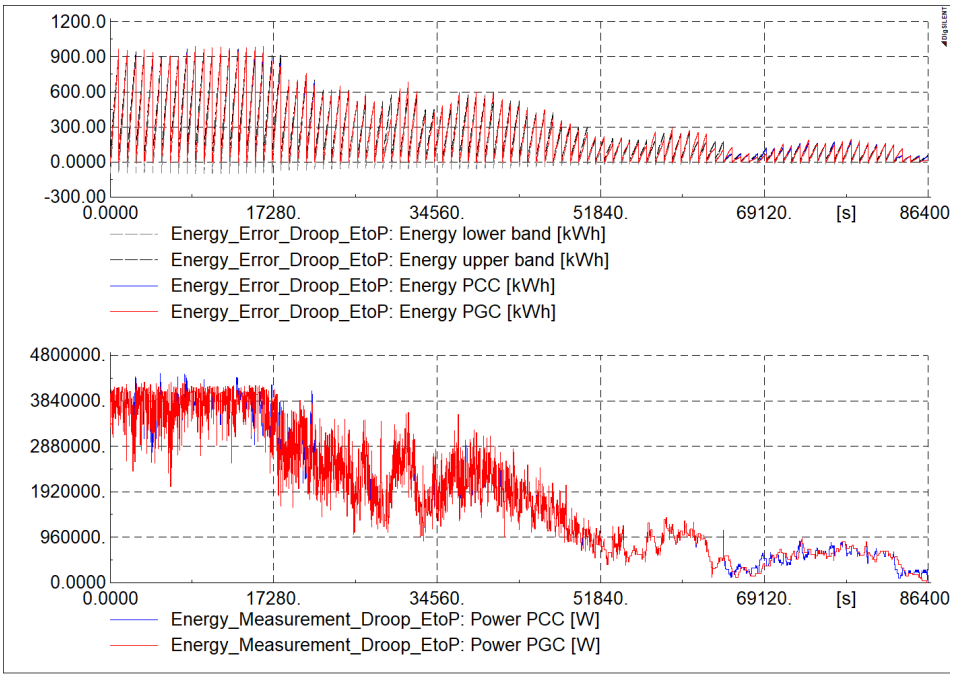

Figure 6.15: Energy bands and power production under real conditions and accurate forecast

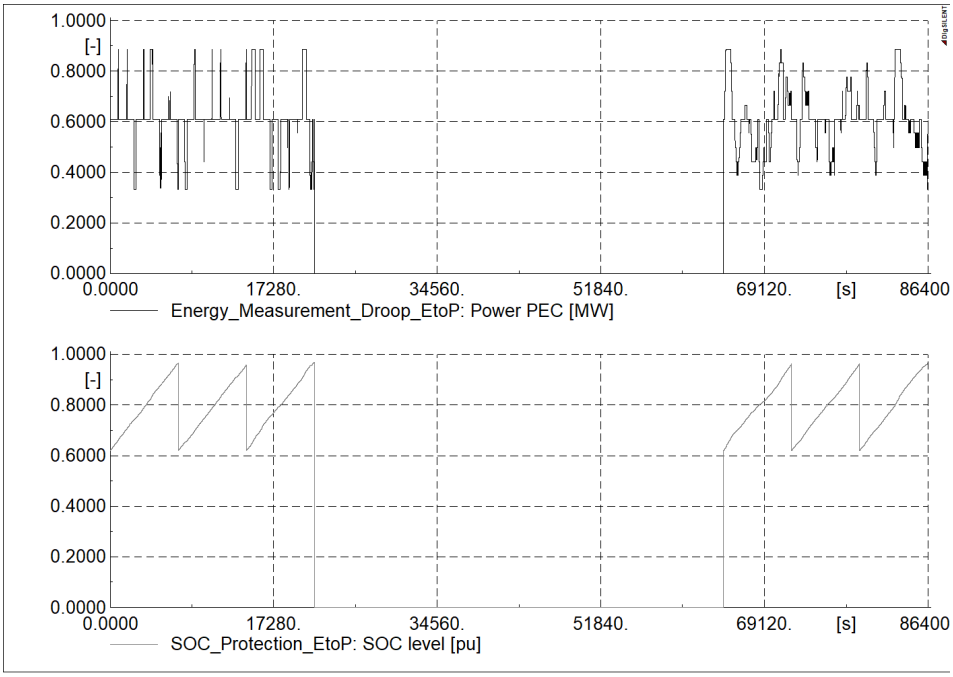

Figure 6.16: Power PEC and SOC level under real conditions and accurate forecast

At first blush, it is clear how the EVs are not grid connected in between 6 *am* – 6 *pm*, thus *Power PEC* and the related *SOC level* are stable at zero. From the grid's perspective, it means that *Energy PGC* and *Energy PCC* (as well as the related power) are coincident in that time period, since no energy management is carried out. Instead, considering instead when the EVs are plugged in, it is detected how the upper and lower chargers' saturation levels are reached, especially in

between midnight – 6 *am*. Indeed, decreasing the amount of available EVs, the power flexibility that EVs can give for grid services is reduced too. Being now the EVs' offset power consumption of 609.7 kW with 80 EVs, the upper and lower chargers' saturation levels are 886.8 kW and 332.6 kW, respectively, ten times smaller than the previous ideal condition with 800 EVs. As a consequence, the EVs are forced to work at their maximum/minimum charging power in order to absorb as more/less energy as possible if required by the regulator. Indeed, thanks to the defined K_{droop} and the applied granularity, the EVs will be charged at max/min power if the energy error is 4.5 kWh over/under the energy bands (consideration deducted from Section 5.4.2). Since the reduced number of EVs in respect to the ideal scenario, the required time to absorb/release a certain amount of energy is well longer. As an example in order to have "a bit of tact" of the required time, one needs only to consider that 800 EVs linked with this *droop* regulator, M_{del} of 1 s and a unique T_{del} of 1 s, they will absorb 1 kWh in approx. 8.5 s, while 80 EVs will required 67 s. As a consequence, the energy error cannot be erased quickly, rather it will continue to rise if the WF energy production is greater than the EVs' energy consumption, forcing the EVs' chargers to work at their saturation levels.

Thanks to the accurate energy forecast, the WF produces exactly the foreseen hourly energy. As a consequence, it is expected the *Energy-to-Power controller* to not influence the energy production. Unfortunately, from Table 6.5 it can be seen how the daily *PEC energy gained* counts for 20 kWh. For a better understanding, the measured energy errors throughout the day are collected in Figure 6.17. The red bars show the energy errors between the WF energy production (*PGC energy output*) and the forecasted WF energy production (*PCC energy reference*), meaning the energy errors that would be injected if the controller were out of order. The blue bars are instead related to the energy errors in between the effectively injected energy into the grid (*PCC energy output*) and *PCC energy reference*, showing the controller's influence. In particular, Figure 6.17a and 6.17b report the hourly energy errors, which are the sum of the energy errors detected for each of the four energy bands per hour that govern the *Energy-to-Power controller* itself, which are shown in Figure 6.17c and 6.17d, instead. The graphs on the left collect absolute errors, while on the right the relative ones in respect to the forecasted energy production, positive/negative if more/less energy is injected in respect to the forecasted energy production. The time period 6 *am* – 6 *pm* is simply omitted. Starting from the graphs on the bottom, it can be appreciated how the EVs can reduce the energy error in each of the defined energy band. The hourly energy prediction is simply divided into four equally split values to define the energy that must be injected into the grid for each 15 $'$. However, although the accurate energy prediction, the WF could produce more in one quarter-hour than in the remaining ones, but the defined controller cannot predict this possible working condition. As a consequence, even though the hourly energy error would not require any adjustment from the controller (PGC bars are constantly at zero in the upper plots), the controller's action influences the injected energy (PCC bars). At high wind power production (midnight – 6 *am* in the *VW*), the maximum error is of -21.5 kWh, so -0.6 %, while it is of -5 kWh, equivalent to -2.1 %, at low wind power production (6 *am* – midnight).

Table 6.5: Results of *Energy-to-Power controller* under real conditions and accurate forecast

	VW
PGC energy output [kWh]	24,483 (43,599)
PCC energy output [kWh]	24,463 (43,579)
PCC energy reference [kWh]	24,483 (43,599)
PEC power max / min [kW]	886.8 / 332.6
PEC energy gained [kWh]	20
PEC energy managed [kWh]	748
PEC energy consumed [kWh]	384
PEC energy released [kWh]	364

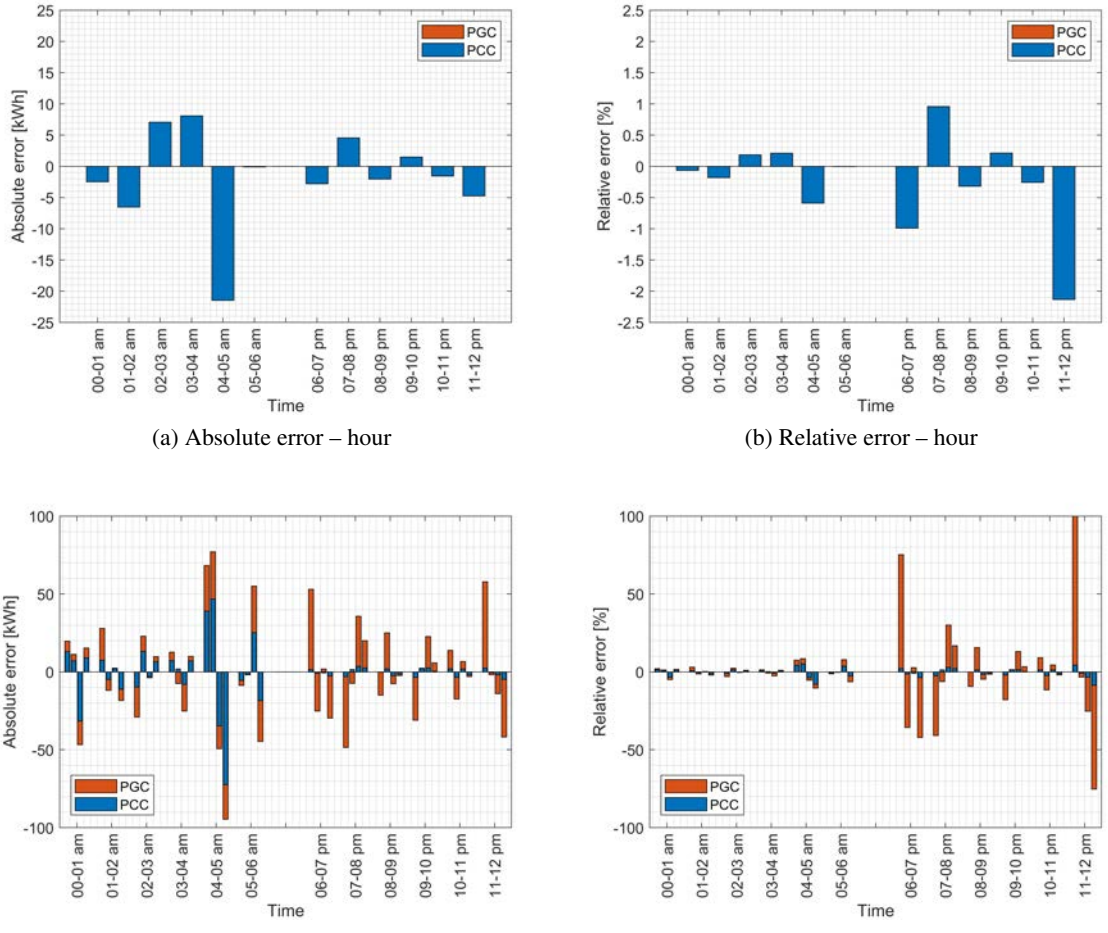

(a) Absolute error – hour

(b) Relative error – hour

(c) Absolute error – quarter-hour

(d) Relative error – quarter-hour

Figure 6.17: Energy errors analysis with accurate forecast

Finally, the SOC analysis is shown in Table 6.6. The *Final SOC* is mainly varied in between midnight – 6 *am*, when the chargers' saturation levels are reached mostly, but still without any appreciable variation in respect to the final forecasted SOC level of 0.963 *pu* with a constant charging set-point current of 11 *A*. The values in parenthesis represent the energy variation in respect to the forecasted energy consumption in a charging window, not being zero even though the accurate forecast energy prevision, because of all the aforementioned justifications.

Table 6.6: SOC analysis with *Energy-to-Power controller* with accurate forecast

	Initial SOC [pu]	**Energy gained [kWh]**	**Final SOC [pu]**
00 am - 02 am	0.62	1,105 (+8)	0.9652
02 am - 04 am	0.62	1,084 (-13)	0.9586
04 am - 06 am	0.62	1,117 (+20)	0.969
06 am - 06 pm	0	0	0
06 pm - 08 pm	0.62	1,096 (-1)	0.9625
08 pm - 10 pm	0.62	1,098 (+1)	0.9631
10 pm - 12 pm	0.62	1,103 (+6)	0.9648

6.3.4 Electric vehicles behavior in Åkirkeby: inaccurate forecast

Finally, the defined EVs population in Åkirkeby is tested if an inaccurate energy forecast is considered. This inaccurate prevision, manually obtained from the accurate curve as shown in Figure 6.18, is created in such way to force the EVs to absorb/release a consistent amount of energy in addition to their offset power consumption, thus the *Final SOC* could result stressed and limitations due to EVs behavior in Åkirkeby come out. The inaccurate forecast shows a -10 % prediction in between midnight – 2 *am* as well as in between 6 *pm* – 8 *pm* in respect to the accurate forecast. Then, a $+10$ % is fixed in the time frame 2 *am* – 4 *am* as well as 8 *pm* – 10 *pm*. Finally, a -10 % is set between 4 *am* – 5 *am* as well as 10 *pm* – 11 *pm*, whereas the remain hours (5 *am* – 6 *am* as well as 11 *pm* – 12 *pm*) have a forecasted energy production of $+10$ %. The biased forecasted is done considering the $Ch-3ph$ connected to the EVs aggregation. Indeed, the EVs will be forced to absorb/release energy in the same direction (consuming more/less power in respect to offset set-point power) for the whole charging window (2 *h*). The time period in between 6 *am* – 6 *pm* are not considered since no EVs are under charge and available for grid services.

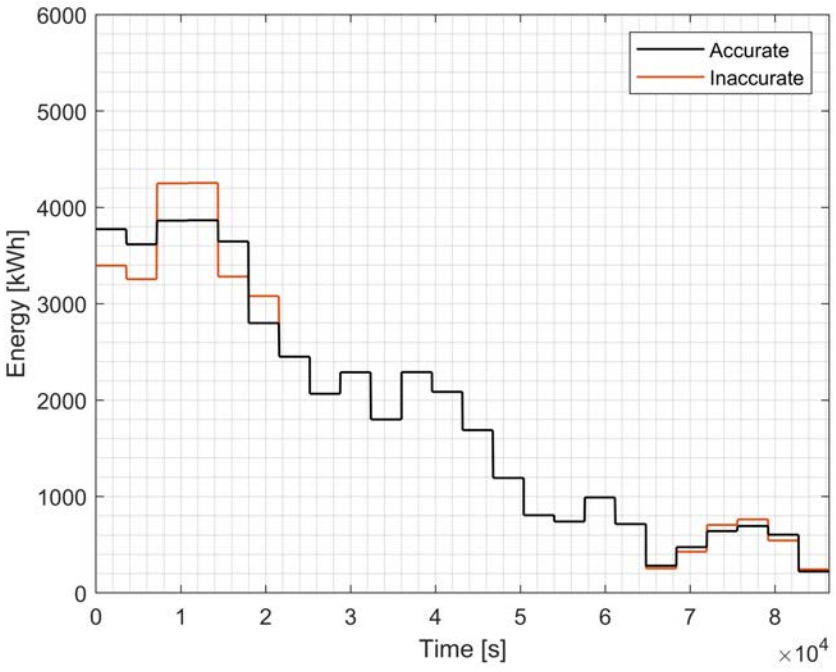

Figure 6.18: Accurate and inaccurate PCC hourly energy forecasts comparison

Figure 6.19 and 6.20 represent the previously considered parameters in this real scenario, figures that can be connected to Table 6.7. It can be seen how the energy bands differ from the previously implemented with the accurate forecast, in fact being function of the hourly energy forecast itself.

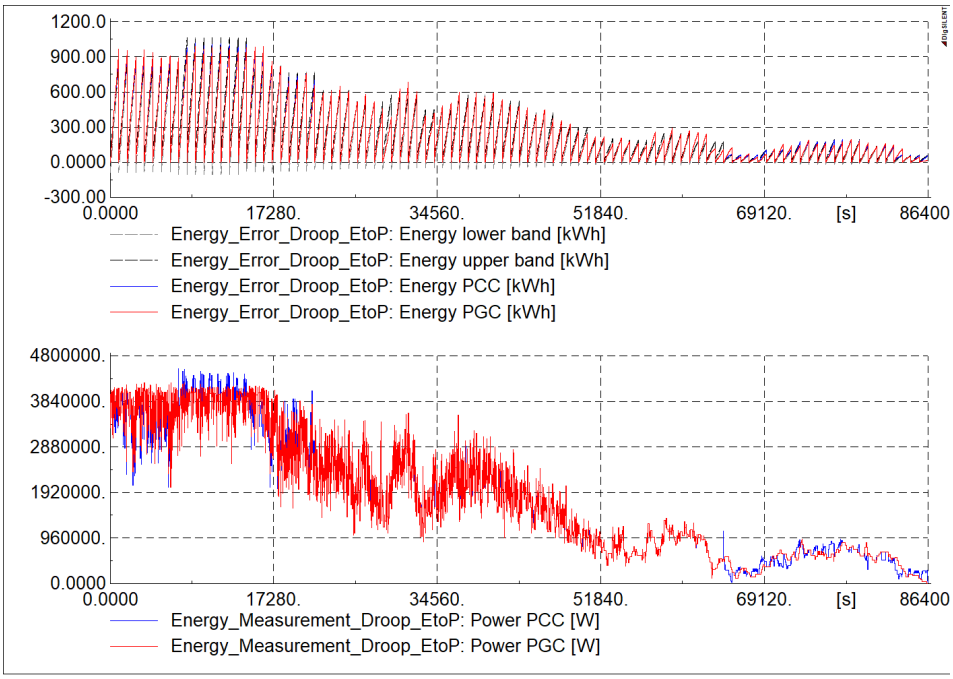

Figure 6.19: Energy bands and power production under real conditions and inaccurate forecast

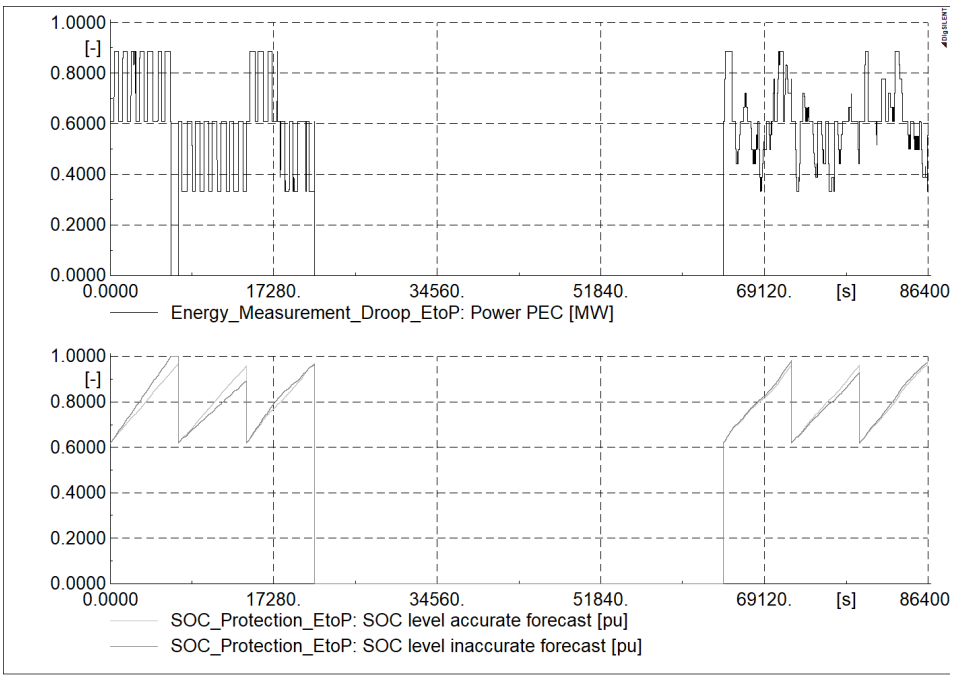

Figure 6.20: Power PEC and SOC level under real conditions and inaccurate forecast

Table 6.7: Results of *Energy-to-Power controller* under real conditions and inaccurate forecast

	VW
PGC energy output [kWh]	24,483 (43,599)
PCC energy output [kWh]	24,485 (43,601)
PCC energy reference [kWh]	24,452 (43,566)
PEC power max / min [kW]	886.8 / 0
PEC energy gained [kWh]	-2
PEC energy managed [kWh]	1,306
PEC energy consumed [kWh]	652
PEC energy released [kWh]	654

The influence of the inaccurate energy forecast can be seen evidently in the *Power PEC* graph, in which the EVs are forced to increase/decrease their charging power always in the same direction is a charging window, mainly in between midnight – 6 *am*. The direct consequence is detected from the SOC analysis of Table 6.8. The lower plot of Figure 6.20 reports the SOC evolution of Figure 6.16 with the accurate forecast in light grey, which is used as comparison term for the new SOC level with the inaccurate forecast in dark grey. In this latter case, because of the WF's overproduction, the EVs absorb more energy than the offset one, reaching the SOC_{max} in the first charging window, then unplugged and no grid services are carried for the remaining time of this charging window. Contrarily, when a new EVs' group will be considered in the second charging window, the WF's underproduction results in a decremented EVs' charging power since the EVs should try to absorb as less energy as possible. Thus, the EVs are able to provide the grid service for the whole charging window, with the drawback of the *Final SOC* well lower than the forecasted value of 0.963 *pu*. Similar considerations can be carried out for the time frame 6 *pm* – 8 *pm* as well as 8 *pm* – 10 *pm*. However, it is important to point out how an inaccuracy of ± 10 % with a low WF power production results in a more restrained SOC variation in respect to the same error applied to a high WF power production, being obviously different the amount of energy the EVs have to manage to erase the forecast's inaccuracy.

Table 6.8: SOC analysis with *Energy-to-Power controller* with inaccurate forecast

	Initial SOC [pu]	**Energy gained [kWh]**	**SOC final [pu]**
00 am - 02 am	0.62	1,216 (+237)	1
02 am - 04 am	0.62	868 (-229)	0.8911
04 am - 06 am	0.62	1,103 (+6)	0.9647
06 am - 06 pm	0	0	0
06 pm - 08 pm	0.62	1,155 (+58)	0.9810
08 pm - 10 pm	0.62	991 (-106)	0.9297
10 pm - 12 pm	0.62	1,133 (+36)	0.9741

The energy errors analysis can make clearer the latter introduced concept. Figure 6.21 is created with the same structure as the analysis carried in Section 6.3.3. It is well satisfactory to observe how the *Energy-to-Power controller* applied to the EVs behavior in Åkirkeby helps evidently the WF to reduce the error in the energy forecast. The chosen ± 10 % energy error in the time period midnight – 6 *am* gives rise to well greater absolute energy error in respect to the one in the time period 6 *pm* – midnight, as evinced from Figure 6.21a. Although the amount of energy managed is greater in between midnight – 6 *am*, in relative terms the result seems to be more satisfying in

the last hours of the day. To be thorough, it can be detected how the EVs do not apply any energy management in the eighth energy band in Figure 6.21c and 6.21d, since the SOC_{max} was reached.

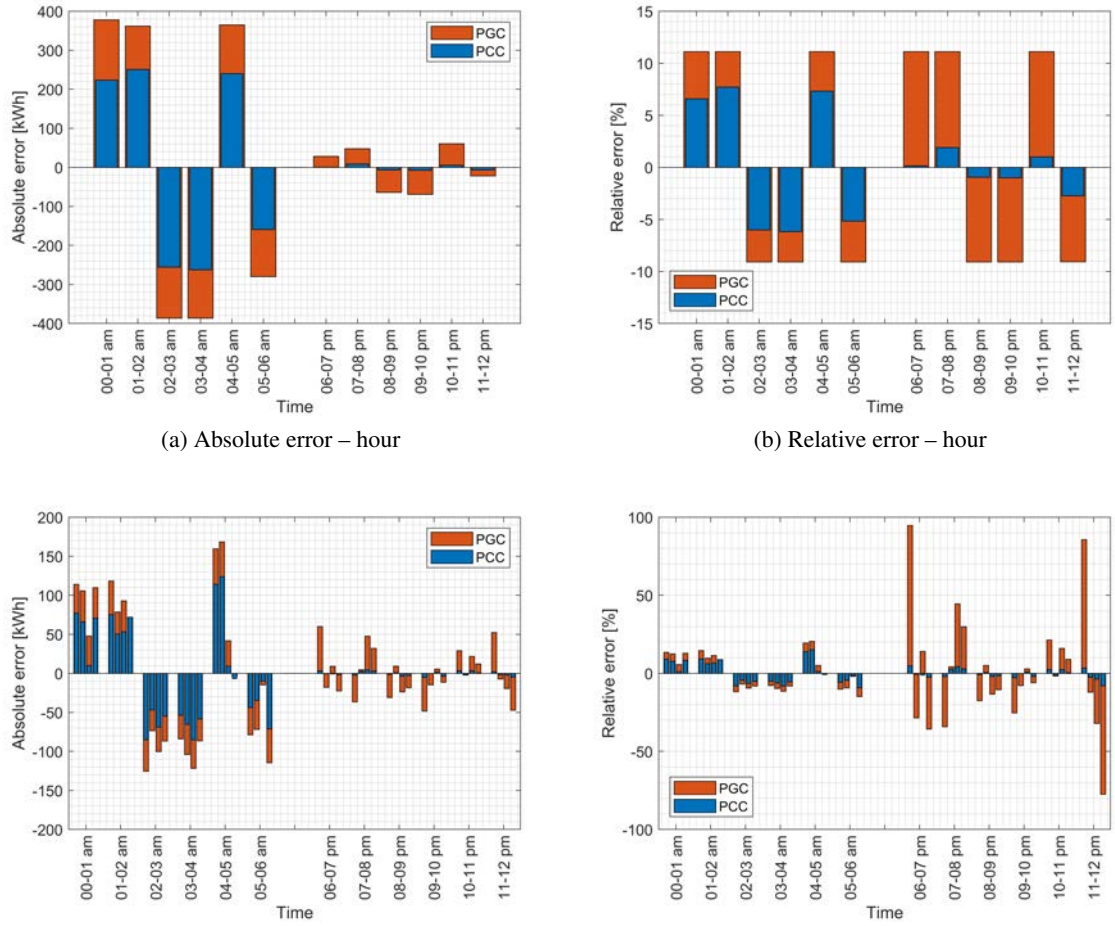

(a) Absolute error – hour

(b) Relative error – hour

(c) Absolute error – quarter-hour

(d) Relative error – quarter-hour

Figure 6.21: Energy errors analysis with inaccurate forecast

6.4 Comparison between three and single phase chargers

The last section of the results' chapter is based on the chargers' comparison. Basically, the results show the influence if the $Ch-1ph$ is applied, instead to the previously considered $Ch-3ph$. The investigations are carried under real conditions, meaning after applying all the EVs' attributes and the EVs behavior in Åkirkeby, first with the *Power-to-Power controller*, then with the *Energy-to-Power controller*. As a consequence of the different chargers, the EVs require to be charged for 6 h, being then possible to increase the number of EVs in a charging window from 80 EVs to 240 EVs.

6.4.1 *Power-to-power controller* combined with single phase chargers

Figure 6.22 shows the power comparison at the PCC if the *Power-to-Power controller* is applied to EVs charged via $Ch-1ph$, results obtained with the installed PI regulator tuned with K_p of 5 and K_i of 1.2. The *Power PEC* comparison is shown in Figure 6.23, in which it can be clearly

seen that the two curves show the same profile. Even though the $Ch-1ph$ has a charging power three times lower than the $Ch-3ph$, the longer requested charging time from the EVs admits to an higher amount of EVs that can participate in the charging window, making possible to triplicate the EVs available considering the EVs population in Åkirkeby. As a direct consequence, the power flexibility that EVs can give for grid services will remain the same, then showing the same power variations since the applied tuning remained unvaried. The tabulated results are in Table 6.2.

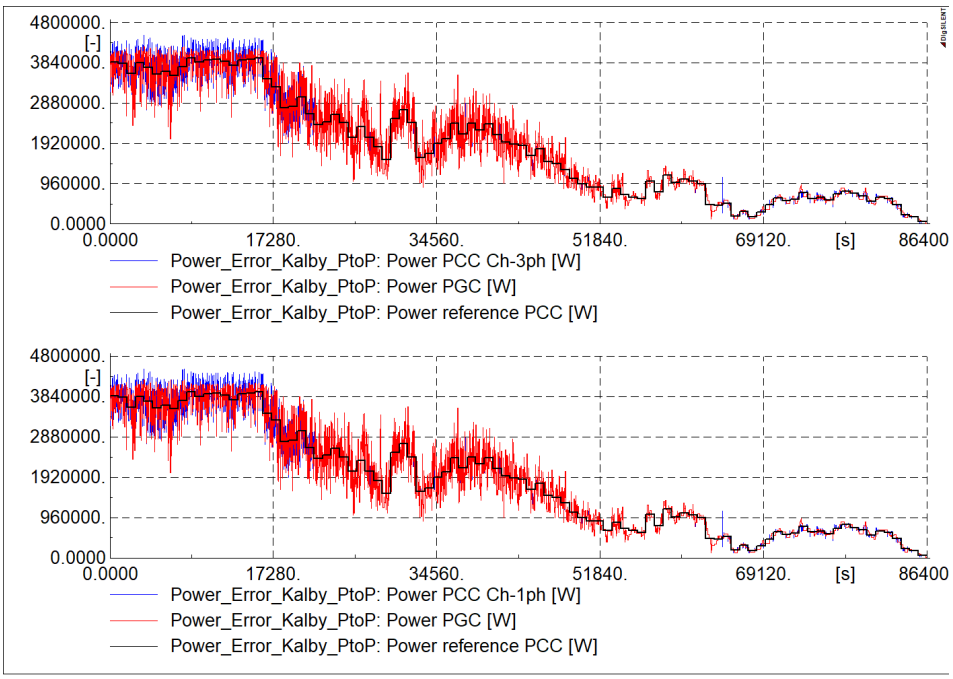

Figure 6.22: PGC, PCC and reference power comparison with *Power-to-Power controller*

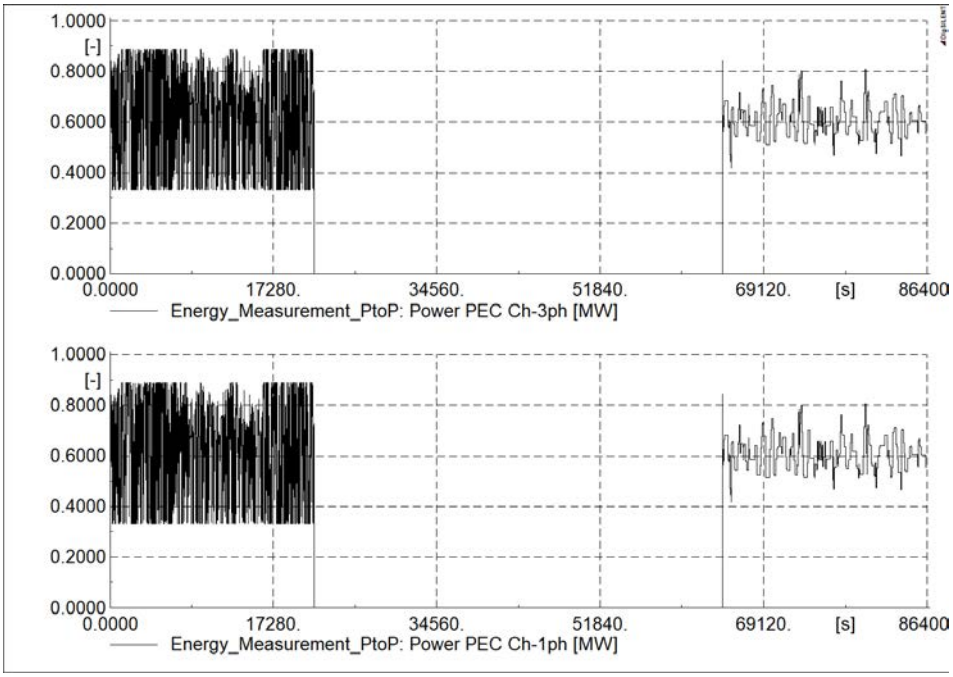

Figure 6.23: Power PEC comparison with *Power-to-Power controller*

The only difference that can be detected is in the SOC analysis, as plotted in Figure 6.24 and reported in Table 6.9. Since the three times lower charging power through $Ch-1ph$ in respect to the $Ch-3ph$, as much longer time is requested from the $Ch-1ph$ and it is well visible in this figure. However, the total energy gained in respect to the offset EVs' charging energy is unvaried, as can be easily detected comparing the values in parenthesis with the ones written in Table 6.3.

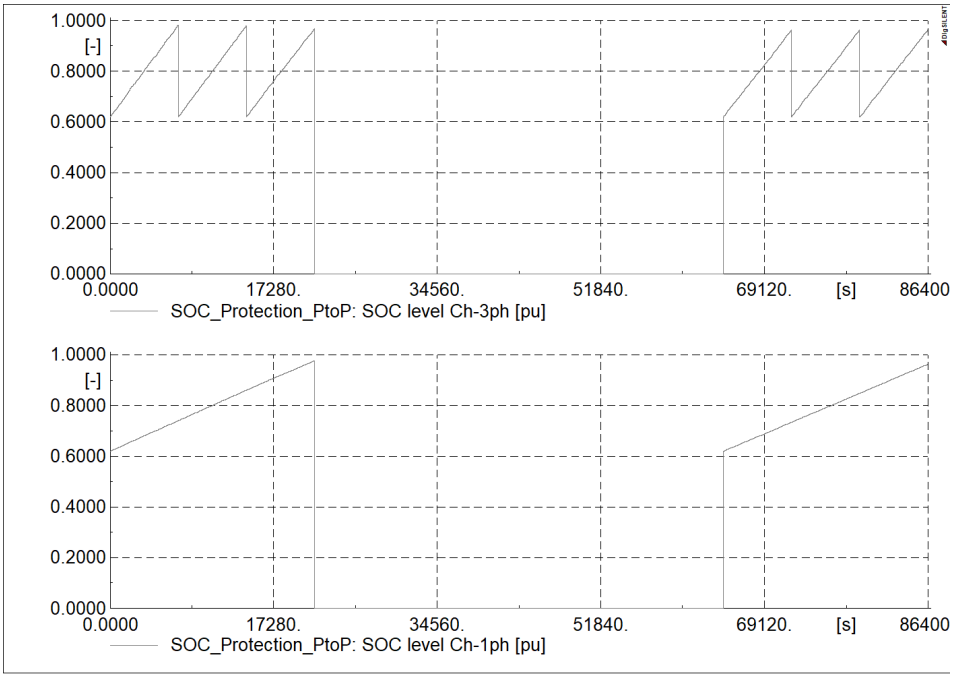

Figure 6.24: SOC level comparison with *Power-to-Power controller*

Table 6.9: SOC analysis with *Power-to-Power controller* and $Ch-1ph$

	Initial SOC [pu]	**Energy gained [kWh]**	**Final SOC [pu]**
00 am - 06 am	0.62	3,423 (+132)	0.9766
06 am - 06 pm	0	0	0
06 pm - 12 pm	0.62	3,292 (+1)	0.9629

6.4.2 Energy-to-Power controller combined with single phase chargers

When discussed about the *Energy-to-Power controller*, the controller was analysed with an accurate and inaccurate energy forecasts. From the evaluation made in the previous section for the *Power-to-Power controller*, it is not surprising to detect how the *Energy-to-Power controller* applied to $Ch-1ph$ in the accurate energy forecast scenario does not show any deviation in respect to what found previously with the $Ch-3ph$. The power comparison can be found in Figure D.11 and D.12, collected in Appendix D, while the overall tabulated results can be found in Table 6.5.

Nevertheless, considering the same inaccurate energy forecast shown in Figure 6.18, a difference in between the $Ch-3ph$ and the $Ch-1ph$ can be found. As a consequence, the related comparison is here reported. Although the control logic function is based in the energy bands, in Figure 6.25 the power comparison in between *PGC* and *PCC* is reported. The observed fluctuations at the *PCC* are the natural consequence of the adjustment in *Power PEC*, profile shows in Figure 6.26. Thanks

to the $Ch-1ph$, it is detected how the EVs are not grid disconnected due to the accomplishment of SOC_{max}, being unplugged only in between 6 *am* – 6 *pm*, since the EVs behavior. Consequently, the overall tabulated results are collected in Table 6.10 because of this varied charging condition. In respect to Table 6.7, a slightly greater *PEC energy managed* can be noticed, which leads to a *PCC energy output* closer to the *PCC energy reference*. The energy errors analysis is neglected, being altered in the eighth energy band only, since SOC_{max} is not reached with $Ch-1ph$.

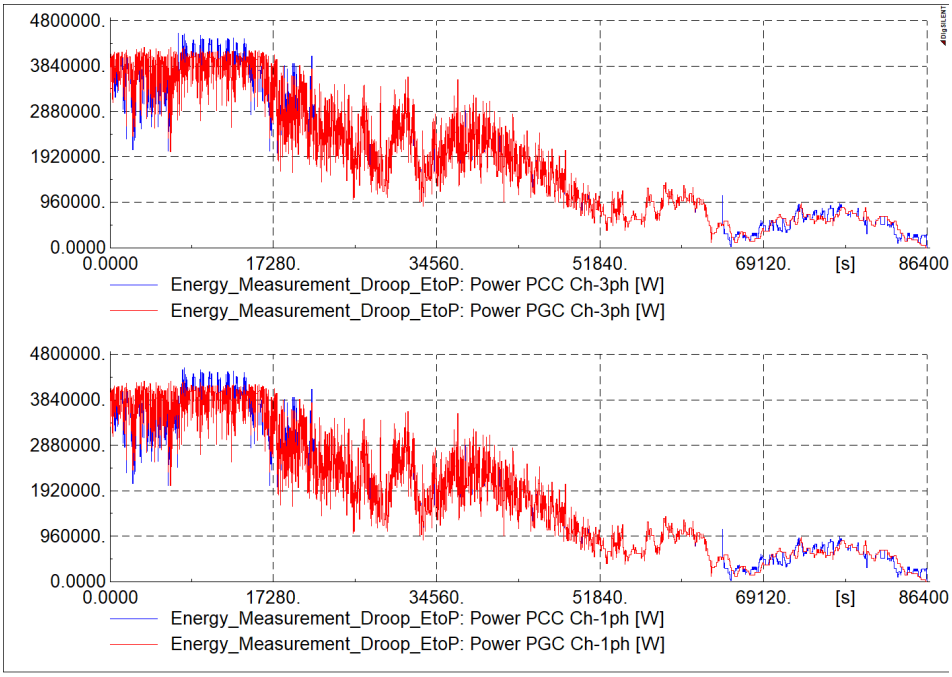

Figure 6.25: PGC and PCC comparison with *Energy-to-Power controller* with inaccurate forecast

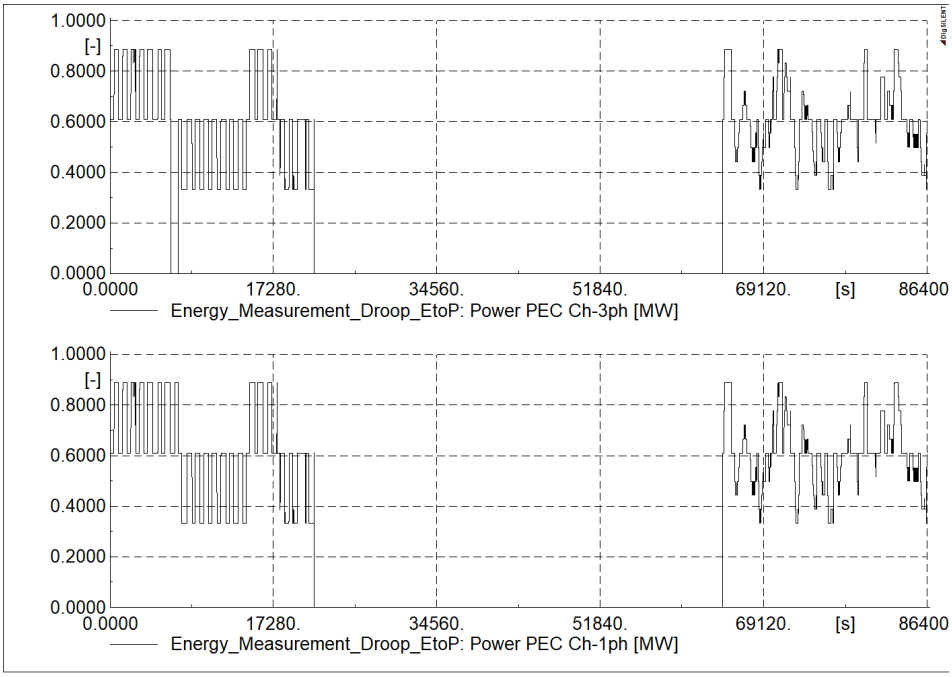

Figure 6.26: Power PEC comparison with *Energy-to-Power controller* with inaccurate forecast

Table 6.10: Results of *Energy-to-Power controller* with inaccurate forecast and $Ch-1ph$

	VW
PGC energy output [kWh]	24,483 (43,599)
PCC energy output [kWh]	24,458 (43,574)
PCC energy reference [kWh]	24,452 (43,566)
PEC power max / min [kW]	886.8 / 332.6
PEC energy gained [kWh]	25
PEC energy managed [kWh]	1,333
PEC energy consumed [kWh]	679
PEC energy released [kWh]	654

The SOC analysis is plotted in Figure 6.27 and reported in Table 6.11. Since the three times lower charging power through $Ch-1ph$ in respect to the $Ch-3ph$, as much longer time is requested from the $Ch-1ph$ and it is well visible in this figure. The consequence of an higher/lower charging power, which well affects the $Ch-3ph$, is instead relaxed via a $Ch-1ph$. This occurrence is just a effect of the manually defined inaccurate energy forecast. Indeed, if a new inaccurate energy forecast were designed with ± 10 % error applied for 6 h consecutively, instead of just 2 h, the same outcomes would have gathered with the $Ch-1ph$ as detected with the $Ch-3ph$.

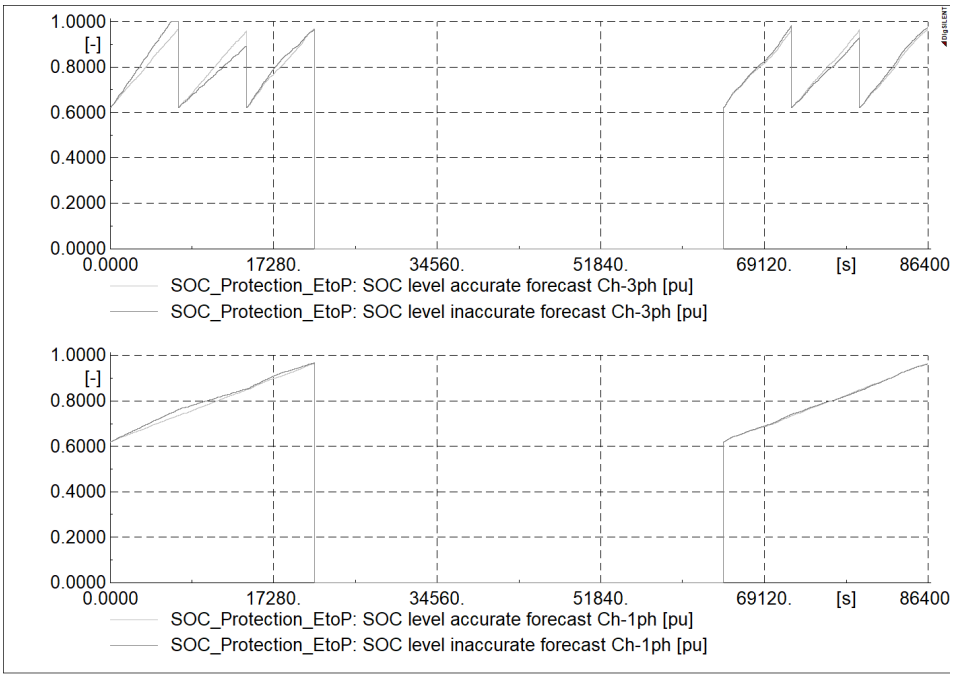

Figure 6.27: SOC level comparison with *Energy-to-Power controller*

Table 6.11: SOC analysis with *Energy-to-Power controller* and $Ch-1ph$

	Accurate			*Inaccurate*		
	Initial SOC [pu]	**Energy gained [kWh]**	**Final SOC [pu]**	**Initial SOC [pu]**	**Energy gained [kWh]**	**Final SOC [pu]**
00 am - 06 am	0.62	3,306 (+14)	0.9644	0.62	3,328 (+37)	0.9667
06 am - 06 pm	0	0	0	0	0	0
06 pm - 12 pm	0.62	3,297 (+4)	0.9634	0.62	3,279 (-12)	0.9616

6.5 Summary

The technical results have been displayed with the objective to compare the two implemented controllers as well as the influence of EVs' constraints while under charge and delivering grid services.

The designed *Power-to-Power controller* is defined with a very rigid control logic. Indeed, the EVs' power consumption is adjusted assiduously to force the injected power in the grid to follow a defined reference power. As a consequence, if EVs are characterized with delayed time response, the required transient time to reach the reference power will increase, increasing the injected fluctuations and deteriorate into instability if the delays are too long. Moreover, the applied EVs population in Åkirkeby results in a limited EVs' power flexibility, thus the chargers' saturation levels could be reached more frequently, increasing the injected power fluctuations as well. Finally, it has been show how the granularity effect cannot fit with the proposed controller, without succeeding to adapt and maintain stable the EVs' power consumption at the desired reference power.

A second controller has been investigated in order to mitigate the EVs' influence. Thus, the *Energy-to-Power controller* shows a more relaxed control logic function. Indeed, the goal is to verify the energy production in a defined time window here fixed of $15\,'$, then not anymore instantaneously as with the previous controller. As a consequence, the influence of the delayed EVs' time response is alleviated as well as the granularity of each EV's charging power can be applied. The limited amount of EVs has a double disadvantage. First, the restricted power flexibility increases the overall required time to absorb more/less energy, in order to balance the injected energy following the energy forecasted. Second, the total storage capacity is reduced, meaning the EVs and their SOC are more influenced. Indeed, if it is required to store more energy in respect to the forecasted amount in a charging window, the EVs will reach more easily the SOC_{max}, being not able to provide the grid service for the remaining time. Contrarily, if the requirement is to decrease the EVs' charging power because it is necessary to increase the injected energy in the grid, the final SOC level could be highly conditioned, reaching a SOC level well far from the forecasted one.

Finally, thanks to the comparison in between $Ch-3ph$ and $Ch-1ph$ applied to the same EVs population, it has been proven how a proper EVs' partition into charging groups can make the $Ch-1ph$ capable to fulfill the same operational conditions as with the $Ch-3ph$.

To be thorough, the substation's loading was always lower than the maximum admitted level in the chosen days. As a consequence, the EVs had never to stop their charging session because of an overloaded condition.

7 Conclusion

This thesis focused on assessing the potential of power regulation in an HPP composed of a wind farm and an aggregation of EVs. Particularly, the main goal was to investigate **how the EVs could be coupled with the HPP to mitigate the injection of wind power fluctuations into the power grid**. The project is based on the substation of Åkirkeby, where the wind farm and the EVs population are connected at the 10.6 kV voltage level. First, an existing PF model of Åkirkeby substation was verified and improved. Then, two controllers have been designed, which detect the injected wind power production to control the EVs power consumption. Finally, the EVs aggregation connected via unidirectional chargers has been implemented, wherein the EVs' attributes can be set to analyse how these features could weaken the interaction WF – EVs. The analysis has been carried out assuming an 100 % EVs penetration scenario in Åkirkeby and following the research questions listed in Section 1.4 and concluded in this chapter:

- **How can EVs manage their output in order to satisfy a desired power or energy profile at the PCC?**
  First, a very rigid controller, the *Power-to-Power controller*, has been investigated. Its goal is to adjust the EVs' power consumption as a consequence of the deviation of the injected wind power production in respect to a predefined reference power profile. Thanks to the implemented PI regulator, the sudden active power oscillations due to unpredictable wind speed variations are erased in the shortest possible time. The request to follow the defined power profile so strictly at the PCC forces the EVs to adjust their power consumption continuously, putting the EVs' batteries under stress. Moreover, the granularity of each EV's charging power cannot be applied if this kind of control action is required. Therefore, a more relaxed controller has been designed, considering the wind farm more as an energy source than a power source, shifting from a "Power Smoothing" analysis to an "Energy Management" investigation.
  Indeed, the *Energy-to-Power controller* aims to balance the wind hourly energy production. Every hour, four identical energy windows are defined, one per each quarter-hour, and with the responsibility to send a control signal to the EVs aggregation and manage its power consumption to maintain the energy balance at the PCC. These energy windows are composed of an upper and lower energy band, coincident at the end of the quarter-hour of competence. The control signal is sent if the wind farm's energy production is over/under the upper/lower energy bands. Then, thanks to the implemented *droop* regulator, the energy production is brought back into the defined energy window. The controller results are being less strict than the one previously explained since the EVs' power consumption is not varied continuously but mainly in the last minutes of the considered quarter-hour, avoiding stressful conditions for the EVs' batteries. Furthermore, the granularity of each EV's charging power can be applied in this second controller without any negative effect.
  Finally, despite the fact that the investigated EVs are connected to the power grid via unidirectional chargers, the power output bidirectionality is obtained considering the

EV aggregator's duty, which has the competence of forecasting the overall EVs' power consumption knowing the available EVs and fixing their offset charging set-point current at 11 A. As a consequence, the applied variation at the EVs' charging current in the range 6 A – 16 A modify the power consumption in respect to the forecasted one, obtaining the desired bidirectional effect if WF – EVs are seen as a whole hybrid wind power plant.

- **How much does the EVs' delay influence the HPP's power output controllability?**
  As any physical system, the EVs are characterized by a certain response time to react to a control signal and modify their charging power. This response time is not uniquely defined, thus each EV could react with different delays. As a consequence, the investigation was carried out dividing the EVs population into 10 groups, each of them subject to different delays equally spaced in time between 1 s and 10 s. The EVs related to each group are not equally divided, but they follow a Gaussian distribution, which aims to represent the real response of an EVs aggregation, with the most EVs response around the mean delay in between 5 s – 6 s.
  On the one hand, because of the *Power-to-Power controller* rigidity, the delay influences highly its operation, with longer transient period before the stability at the predefined power reference is reached. As a consequence, an ideal instantaneous time response is well desired to decrease wind power oscillations in the grid, being the controller able to regulate the EVs' charging set-point power as soon as the power is slightly deviating from the reference profile. On the other hand, the *Energy-to-Power controller* results in a less influenced behavior because of this delay. Indeed, the request to balance the energy production in each quarter-hour for the defined energy window makes this controller able to better accept the EVs delay.

- **How can EVs' charging pattern influence the possibility to control the EVs for power regulation?**
  EVs, in respect to battery energy storage systems, are not always grid connected. Indeed, the EVs' charging pattern analysis was necessary to detect when and in which state the EVs can be available for grid services in Åkirkeby. Considering the only domestic charging, it was assumed that EVs are grid-connected during night hours in between 6 pm – 6 am, providing services for just half of the day. Moreover, with an average daily driving behavior of the considered Nissan LEAF 40 kWh in Åkirkeby, each EV could be connected for 2 h via $Ch-3ph$ or 6 h via $Ch-1ph$. Thus, the EVs population is split into 6 groups via $Ch-3ph$ or 2 groups via $Ch-1ph$ and it is of EV aggregator's concern to select the EVs groups that must be charged as well as exploited for grid services. As an overall, the amount of EVs are not sufficient to meet the controllers' requests all night long. On the one hand, a reduced number of EVs linked to the *Power-to-Power controller* brings the charging current at saturation levels more frequently, making impossible to reach the reference power profile and increasing the injected power fluctuations as well. On the other hand, the *Energy-to-Power controller* shows a doubled disadvantage. First, the EVs need more time to cover a requested energy amount to balance the energy production. Second, the total storage capacity is reduced, meaning the EVs aggregation's SOC could be more influenced.

To conclude, a clear potential of using EVs population for mitigating wind power fluctuations into the power grid was shown in the thesis. Even though power and energy errors cannot be completely avoided, the synergies on connecting EVs to a wind farm could enhance the wind production

reliability, making a very interesting hybrid configuration to better regulate wind farm power output. Moreover, RES in the power grid can be significantly increased thanks to this configuration, leading to a further decarbonization of the energy sector.

Further assessments and investigations could be carried out to analyse more deeply the interconnection WF – EVs, which have not been covered in this project:

- Due to the different technical characteristics, it would be interesting to consider the combination of different EV models and battery capacities instead of the only Nissan LEAF 40 kWh. This will give a possibility to estimate possible consequences of substituting a unique aggregated SOC with different SOC levels in terms of energy management.
- The project have been carried out considering the wind power production along the solar day (midnight – midnight), whereas it was assumed that the EVs are connected to the grid only throughout the night (6 *pm* – 6 *am*). As a consequence, it would be interesting to import production profiles on a shifted time period (i.e. midday – midday), so then it is possible to evaluate the EVs aggregation's SOC through a whole night. Thus, since the SOC level of each EVs' group could be highly influenced because of energy management, an additional charging session could be planned in the early morning (i.e. 6 *am* – 7 *am*) to compensate eventual energy missed to reach the full charge.
- The forecasted power and energy production profiles used in the analysis were manually created from the real power measurement profiles at the PCC of the substation. To make the wind model more realistic, it would be great to have wind speed measurements at the three wind turbines' hub in Kalby, from which the power production can be obtained through the power curve of these *V80 - 2.0 MW* wind turbines. At this point, with the wind speed forecast available, the two controllers still react on power or energy errors at the PCC, although these errors can be directly related to wind speed errors coming from the known wind speed forecast.
- As mentioned through the project, the implemented Åkirkeby substation lacks in the 7.5 *MW* Bodelyngsvejen PV park active and reactive power production. The interest on collecting these data arises because these missing profiles could increase the overloading level at the substation, showing possible drawbacks of considering the additional EVs feeder with the existing substation transformers.

References

[1] European Commision, "Energy 2020. A strategy for competitive, sustainable and secure energy ," Tech. Rep., 2010. [Online]. Available: https://www.buildup.eu/sites/default/files/content/com2010_0639en01_0.pdf

[2] H. Ritchie and M. Roser, "Energy - Our World in Data," 2018, [Online]. Available: https://ourworldindata.org/energy, visited on 24.04.2020.

[3] "Climate Change | United Nations," [Online]. Available: https://www.un.org/en/sections/issues-depth/climate-change/, visited on 24.04.2020.

[4] "Climate strategies and targets," [Online]. Available: https://ec.europa.eu/clima/policies/strategies_en, visited on 24.04.2020.

[5] "Environmental Report 2018 | Energinet," [Online]. Available: https://en.energinet.dk/About-our-reports/Reports/Environmental-Report-2018, visited on 24.04.2020.

[6] Prabha Kundur, *Power System Stability And Control*, 1994. [Online]. Available: https://www.academia.edu/29057543/Power_System_Stability_And_Control_by_Prabha_Kundur.pdf

[7] J. Wang, Y. Zong, S. You, and C. Traeholt, "A review of Danish integrated multi-energy system flexibility options for high wind power penetration A review of Danish integrated multi-energy system flexibility options for high wind power penetration," *Clean Energy*, vol. 1, no. 1, pp. 23–35, 2017.

[8] "Security of electricity supply report 2019 | Energinet," Tech. Rep. [Online]. Available: https://en.energinet.dk/About-our-reports/Reports/Security-of-electricity-supply-report-2019

[9] Danish Ministry of Energy, Utilities and Climate, "Energy for a Green Denmark," 2018. [Online]. Available: https://efkm.dk/media/11857/energiudspillet_eng.pdf

[10] Rebel Saffold, "What is Smart Grid Technology - Rebel Saffold - Medium," 2016, [Online]. Available: https://medium.com/@lebertech/what-is-smart-grid-technology-5a70fa56ee9f, visited on 25.04.2020.

[11] "Smart Grid in Denmark 2.0 2011 | Danish Energy Association," Tech. Rep. [Online]. Available: https://www.usef.energy/app/uploads/2016/12/Smart-Grid-in-Denmark-2.0-2.pdf

[12] E. Pasca, G. Petretto, S. Grillo, M. Marinelli, and F. Silvestro, "Characterization of Wind and Solar generation and their influence on distribution network performances," Universities Power Engineering Conference (UPEC), 2009 Proceedings of the 44th International, pp.1-6, Glasgow, 1-4 Sep. 2009.

[13] J. Østergaard and J. E. Nielsen, "THE BORNHOLM POWER SYSTEM An overview," Centre for Electrical Technology, Department of Electrical Engineering, May 2010.

[14] Danish Energy Association, "Bornholm combines biomass, wind and solar," 2017. [Online]. Available: https://stateofgreen.com/en/partners/danish-energy/news/bornholm-combines-biomass-wind-and-solar/

[15] Z. Zarkov, "Hybrid Power Systems with Renewable Energy Sources – Types, Structures, Trends for Research and Development," Eleventh international conference on electrical machines, drivers and power systems ELMA 2005, Sep. 2005, Sofia, Bulgaria.

[16] L. Petersen, B. Hesselbaek, and A. Martinez, "Vestas Power Plant Solutions Integrating Wind, Solar PV and Energy Storage," Tech. Rep., 3rd International Hybrid Power Systems Workshop, May 2018.

[17] T. H. Nguyen and D. Lee, "LVRT and power smoothening of DFIG-based wind turbine systems using energy storage devices," ICCAS 2010, pp. 1070-1074.

[18] Y. Sawle, S. C. Gupta, and A. K. Bohre, "PV-wind hybrid system: A review with case study," *Cogent Engineering*, 2016.

[19] X. Li, D. Hui, and X. Lai, "Battery Energy Storage Station (BESS)-Based Smoothing Control of Photovoltaic (PV) and Wind Power Generation Fluctuations," *IEEE Transactions on Sustainable Energy*, vol. 4, no. 2, Apr 2013.

[20] K. Yoshimoto, N. Toshiya, G. Koshimizu, and Y. Uchida, "New control method for regulating State-of-Charge of a battery in hybrid wind power/battery energy storage system," in *IEEE Power Systems Conference and Exposition, PSCE*, 2006, pp. 1244–1251.

[21] H. Xu, C. Wang, C. Lu, and Z. Lu, "An adaptive wind power smoothing method with energy storage system," in *IEEE Power and Energy Society General Meeting*, no. 29, Oct 2014.

[22] L. Pan, J. Gu, J. Zhu, and T. Qiu, "Integrated control of smoothing power fluctuations and peak shaving in Wind/PV/Energy storage system," in *8th International Conference on Intelligent Human-Machine Systems and Cybernetics, IHMSC*, vol. 2, Dec 2016, pp. 586–591.

[23] F. Sossan and M. Marinelli, "An auto tuning substation peak shaving controller for congestion management using flexible demand," in *Proceedings of the Universities Power Engineering Conference*, 2013.

[24] A. A. Akhil, G. Huff, A. B. Currier, B. C. Kaun, D. M. Rastler, S. B. Chen, A. L. Cotter, D. T. Bradshaw, and W. D. Gauntlett, *SANDIA REPORT DOE/EPRI Electricity Storage Handbook in Collaboration with NRECA*, 2015.

[25] G. C. Tarnowski, P. C. Kjær, R. Lærke, and F. Iov, "Power system stabilising features from wind power plants augmented with energy storage," vol. 2, pp. 1093–1100, 2014.

[26] D. Rastler, *EPRI Project Manager Electricity Energy Storage Technology Options*, 2010.

[27] M. Marinelli, F. Sossan, G. T. Costanzo, and H. W. Bindner, "Testing of a predictive control strategy for balancing renewable sources in a microgrid," *IEEE Transactions on Sustainable Energy*, vol. 5, no. 4, pp. 1426–1433, Oct 2014.

[28] T. Gabderakhmanova, J. Engelhardt, J. M. Zepter, T. Meier Sørensen, K. Boesgaard, H. H. Ipsen, and M. Marinelli, "Demonstrations of DC Microgrid and Virtual Power Plant Technologies on the Danish Island of Bornholm," Universities Power Engineering Conference (UPEC), 2020 Proceedings of the 55th International, pp. 1-6, Torino, 1-4 Sep. 2020. (in press).

[29] "Insulae h2020," [Online]. Available: http://insulae-h2020.eu/, visited on 28.05.2020.

[30] G. Cheimonas, "Design of an electric vehicle fleet model for service provision in Bornholm power system," MSc in Sustainable Energy, DTU, July 2019.

[31] J. M. Zepter, T. Gabderakhmanova, K. Maribo Andreasen, K. Boesgaard, and M. Marinelli, "Biogas Plant Modelling for Flexibility Provision in the Power System of Bornholm Island," Universities Power Engineering Conference (UPEC), 2020 Proceedings of the 55th International, pp. 1-6, Torino, 1-4 Sep. 2020. (in press).

[32] Y. Chen, Z. Xu, and J. Østergaard, "Frequency Analysis for Planned Islanding Operation in the Danish Distribution System-Bornholm," 43rd International Universities Power Engineering Conference, Padova, 2008, pp. 1-5.

[33] J. E. Nielsen, "The Danish demonstration site BORNHOLM." [Online]. Available: https://docplayer.net/8507032-Dtu-technical-university-of-denmark-the-danish-demonstration-site-bornholm-john-eli-nielsen.html

[34] P.S.R. Murty, *Symmetrical Component*, 2017. [Online]. Available: https://www.sciencedirect.com/topics/engineering/symmetrical-component

[35] F. Blaabjerg and K. Ma, "Wind Energy Systems," *IEEE*, 2017.

[36] M. Marinelli, S. Massucco (supervisor), and F. Silvestro (supervisor), "Wind Turbine and Electrochemical Based Storage Modeling and Integrated Control Strategies to Improve Renewable Energy Integration in the Grid," Ph.D. dissertation, University of Genova, 2011.

[37] "Wind Turbine Control Methods - National Instruments," [Online]. Available: https://www.ni.com/da-dk/innovations/white-papers/08/wind-turbine-control-methods.html, visited on 12.06.2020.

[38] Vestas, "2 MW Vestas Technology," Tech. Rep., 2011. [Online]. Available: https://www.ledsjovind.se/tolvmanstegen/VestasV90-2MW.pdf

[39] "Weather Archive," [Online]. Available: https://www.dmi.dk/vejrarkiv/, visited on 29.05.2020.

[40] "IEA webstore. Nordic EV Outlook 2018," Tech. Rep., 2019. [Online]. Available: https://webstore.iea.org/nordic-ev-outlook-2018

[41] "Electric Vehicles | ACEA - European Automobile Manufacturers' Association," [Online]. Available: https://www.acea.be/industry-topics/tag/category/electric-vehicles, visited on 11.05.2020.

[42] G. Berckmans, "Cost Projection of State of the Art Lithium-Ion Batteries for Electric Vehicles Up to 2030," *Energies*, 2017. [Online]. Available: http://www.mdpi.com/1996-1073/10/9/1314

[43] "Cheaper Batteries, More Chargers for Electric Car Buyers in 2020 - Bloomberg," [Online]. Available: https://www.bloomberg.com/news/articles/2020-01-13/cheaper-batteries-more-chargers-for-electric-car-buyers-in-2020, visited on 11.05.2020.

[44] S. Martinenas, M. Træholt, C.;and Marinelli, and P. Andersen, "Enabling Technologies for Smart Grid Integration and Interoperability of Electric Vehicles," Ph.D. dissertation, Technical University of Denmark, 2017.

[45] "IEC 61851 - Electric vehicle conductive charging system – Electric vehicles requirements for conductive connection of an a.c./d.c. power supply | IEC Webstore," [Online]. Available: https://webstore.iec.ch/publication/31282, visited on 12.05.2020.

[46] K. Jacobsen, N. Juul, and R. Bergamini, "Danish household load profiles and the effect of savings for appliance categories," Tech. Rep., Bergen Economics of Energy and Environment Research Conference 2015, Bergen, Norway. [Online]. Available: http://www.elforbrugspanel.dk/Pages/Rapportering.aspx,

[47] L. Calearo, A. Thingvad, K. Suzuki, and M. Marinelli, "Grid Loading due to EV Charging Profiles Based on Pseudo-Real Driving Pattern and User Behaviour," Sept 2019, Transportation Electrification, IEEE Transactions on, Vol. 5.

[48] "History | Nord Pool," [Online]. Available: https://www.nordpoolgroup.com/About-us/History/, visited on 03.05.2020.

[49] "Renewables in Electricity Markets – Pierre Pinson," [Online]. Available: http://pierrepinson.com/index.php/teaching/, visited on 04.05.2020.

[50] A. Zecchino, A. Thingvad, P. B. Andersen, and M. Marinelli, "Test and modelling of commercial V2G CHAdeMO chargers to assess the suitability for grid services," World Electr. Veh. J., 2019, Vol. 10.

[51] W. Kempton and J. Tomić, "Vehicle-to-grid power implementation: From stabilizing the grid to supporting large-scale renewable energy," *Journal of Power Sources*, vol. 144, no. 1, pp. 280–294, Jun 2005.

[52] "Regulations for grid connection | Energinet," 2019. [Online]. Available: https://en.energinet.dk/Electricity/Rules-and-Regulations/Regulations-for-grid-connection

[53] "IEC 61000-3:2020 SER | IEC Webstore," [Online]. Available: https://webstore.iec.ch/publication/62426, visited on 12.05.2020.

[54] K. Knezovic, C. Træholt (supervisor), M. Marinelli (supervisor), and P. Andersen (supervisor), "Active integration of electric vehicles in the distribution network-theory, modelling and practice," Ph.D. dissertation, Technical University of Denmark, 2017.

[55] "The Danish National Travel Survey - Center for Transport Analytics," [Online]. Available: https://www.cta.man.dtu.dk/english/national-travel-survey, visited on 13.05.2020.

[56] European Commission, “Analysis of National Travel Statistics in Europe,” 2013. [Online]. Available: https://publications.jrc.ec.europa.eu/repository/bitstream/JRC83304/tch-d2.1_final.pdf

[57] “The Norwegian National Travel survey 2013/14 - Transportøkonomisk institutt,” 2014. [Online]. Available: https://www.toi.no/travel-behaviour/the-norwegian-national-travel-survey-2013-14-article32991-836.html

[58] “Bornholm (Denmark) - Population Statistics, Charts, Map and Location,” [Online]. Available: https://www.citypopulation.de/en/denmark/hovedstaden/400__bornholm/, visited on 30.05.2020.

[59] A. Kieldsen, A. Thingvad, S. Martinenas, and T. M. Sørensen, “Efficiency Test Method for Electric Vehicle Chargers,” EVS29 - International Battery, Hybrid and Fuel Cell Electric Vehicle Symposium, 2016.

[60] V. T. Samundsson, M. Rezkalla, A. Zecchino, and M. Marinelli, “Aggregation of Single-phase Electric Vehicles for Frequency Control Provision Based on Unidirectional Charging,” Universities Power Engineering Conference (UPEC), 2017 Proceedings of the 52nd International, pp. 1-6, Heraklion, 29 Aug. – 1 Sep. 2017.

[61] A. Junior, “DIG SILENT - Power Factory 15 - manual.”

[62] “Thorlabs.com - Tutorials,” [Online]. Available: https://www.thorlabs.com/tutorials.cfm?tabID=5DFCA308-D07E-46C9-BAA0-4DEFC5C40C3E, visited on 04.05.2020.

A Danish wind atlas

In this illustrative appendix, few additional data related to the chosen wind scenarios are collected. All the data have been downloaded from the Danish Meteorological Institute [39]. The three days have been defined as follows:

- *Windy day*: with an average wind speed of 8.9 m/s, substantially constant high wind speed through the whole day with gusts up to 20.1 m/s, the 3^{rd} January 2020 is identified as a windy day, from now on marked with *W*, displayed in Figure A.1a.
- *Not windy day*: with an average wind speed of 5.5 m/s, substantially constant low wind speed through the whole day with gusts up to 12.8 m/s, the 27^{th} January 2020 is identified as a not windy day, from now on marked with *NW*, displayed in Figure A.1b.
- *Variable windy day*: although with an average wind speed of 6.4 m/s, the 22^{nd} January 2020 was characterized by a constant decrease in the wind speed intensity, passing from an average wind speed of 10.6 m/s between midnight and 6 am to an average wind speed of 3.2 m/s between 6 pm and the following midnight. For this reason, this day is identified as variable windy day, from now on marked with *VW*, displayed in Figure A.1c.

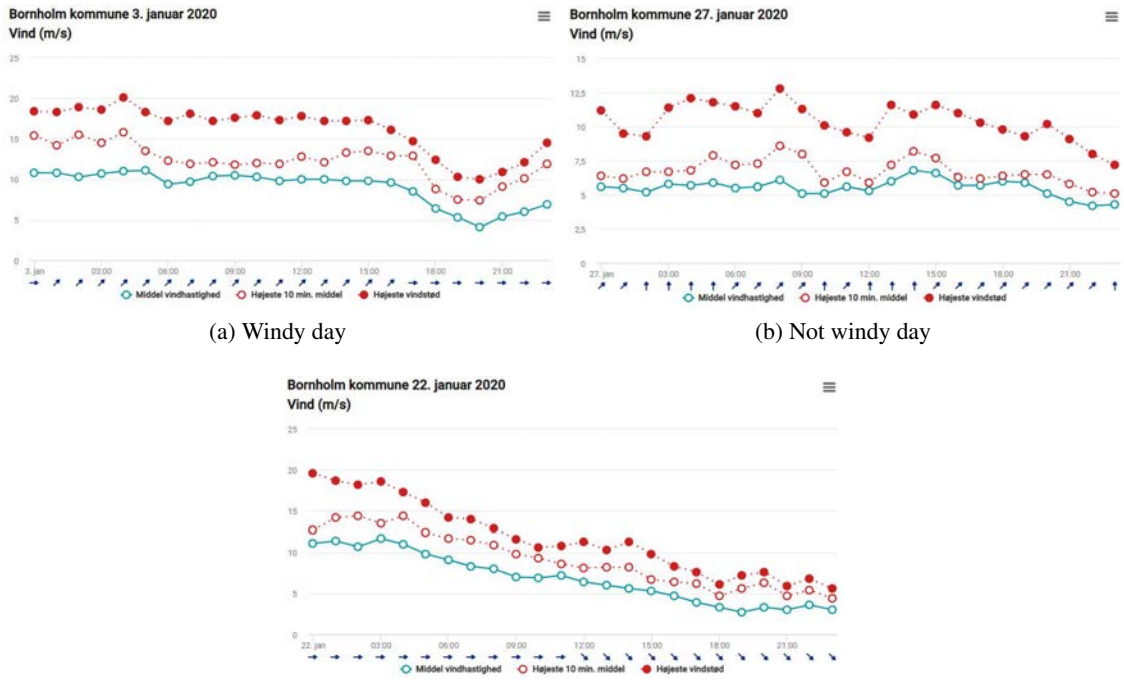

(a) Windy day

(b) Not windy day

(c) Variable windy day

Figure A.1: Hourly wind speed in Bornholm [39]

In Figure A.1, three segmented lines are reported for each scenario:

- Blue line with empty circles, which represents the hourly average wind speed in Bornholm used to evaluate the daily average wind speed previously reported;
- Red dashed line with full circle, which represents the maximum wind gust detected for each hour in Bornholm;
- Red dashed line with empty circles, which represents the maximum 10 minutes average wind speed in Bornholm.

In Figure A.2 the average wind speed and wind direction have been collected, considering this time the whole Denmark to show a big picture about these selected scenarios. On the left side, the average wind speed is shown, while on the right side the average wind direction from which the wind blew in the selected days.

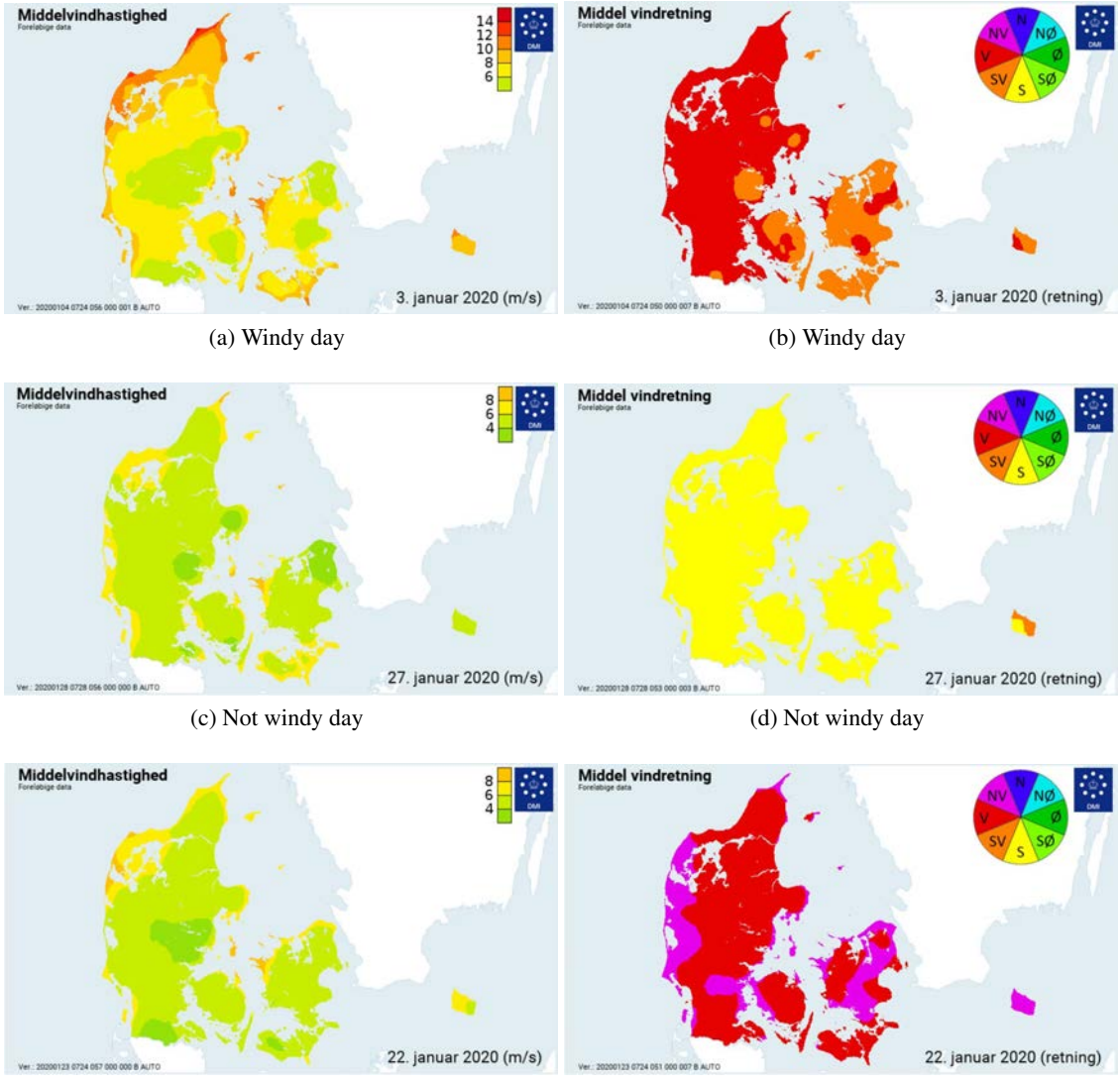

(a) Windy day (b) Windy day

(c) Not windy day (d) Not windy day

(e) Variable windy day (f) Variable windy day

Figure A.2: Average wind speed and wind direction in Denmark [39]

B Power profiles for Åkirkeby substation feeders

In Section 3.3, the active power injection at the 10.6 *kV* line from Kalby wind farm is described, underlying how the power production coming from this unpredictable source is highly fluctuating. Moreover, for each production and consumption feeder previously described and shown in Figure 2.2, the data related to active and reactive power consumption at the 10.6 *kV* bus have been collected. These data are reported in this appendix.

Although the investigated controllers are applied directly at the feeder related to Kalby wind farm, it is necessary to import all the shown profiles in the PF model to analyse the loading level of the main transformers of the Åkirkeby substation. Indeed, it is required to know both active and reactive power consumption for each of these feeder to evaluate the overall power flow through the two transformers connected in parallel. However, power production coming from the installed PV power plant in Åkirkeby is neglected due to the inability to represent and gather the measurement data for this plant from the SCADA.

Industriområde

The active power consumption profile of Industriområde feeder (Figure B.1) shows a typical daily load profile with a certain correlation among the three analysed days. Although the feeder is always consuming active power through each of the considered days, the reactive power consumption shows a reversal in sign. Summarily, at high active power consumption, the reactive power is delivered by the substation itself, from the 10.6 *kV* line to the feeder. In the opposite situation, observed mainly through the night, thanks to the beneficial reactive power compensation effect coming from the installed underground cables, connecting Industriområde to the 10.6 *kV* bus, the required reactive power is delivered to Industriområde itself, injecting additional reactive power in the 10.6 *kV* line.

Boværk

The active and reactive power consumption of Boværk feeder (Figure B.2) shows an increase in between 7 *am* – 3 *pm* approximately, in conjunction with the typical Danish working hours.

Biogas

Characterized with a negative active power consumption, meaning an injection of active power into the 10.6 *kV* line, the Biogas power plant feeder (Figure B.3) shows a fairly constant active and reactive power consumption. The observable active power spikes are not analysed being not of main interest for the project.

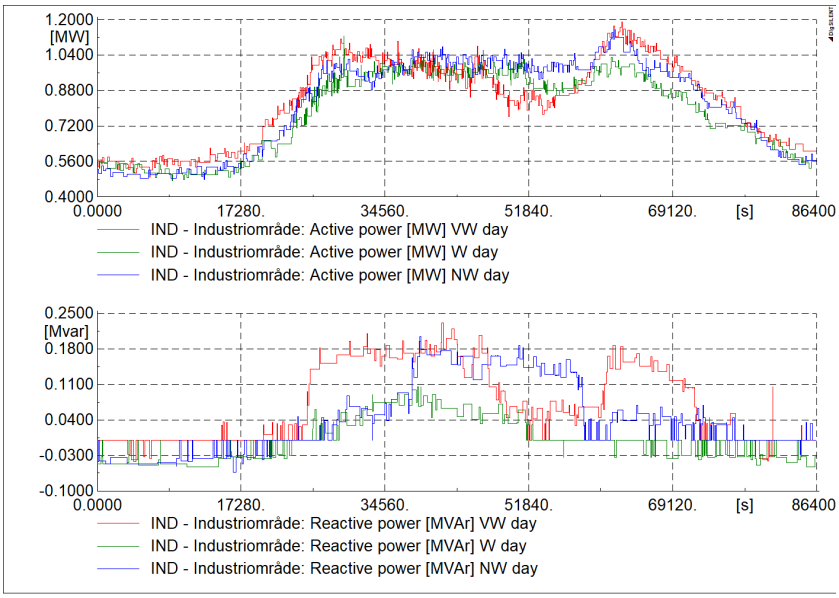

Figure B.1: Active and reactive power consumption for Industriområde feeder

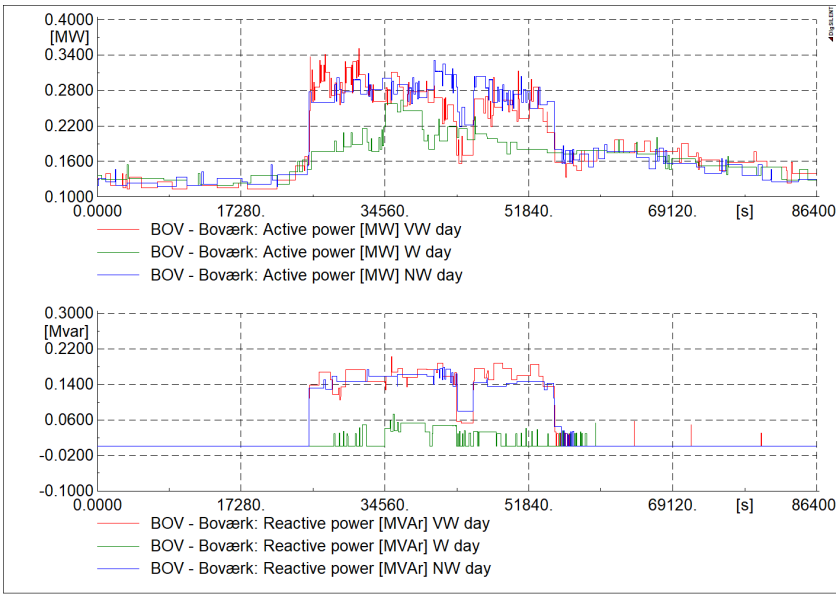

Figure B.2: Active and reactive power consumption for Boværk feeder

Kalby wind farm

The active power injection from Kalby wind farm feeder (Figure B.4) is reported one more time together with the reactive power consumption. It can be clearly noticed how the reactive power consumption is practically proportional to the active power injection, as the wind farm is composed of three WTGs Type C, each equipped with an asynchronous machine.

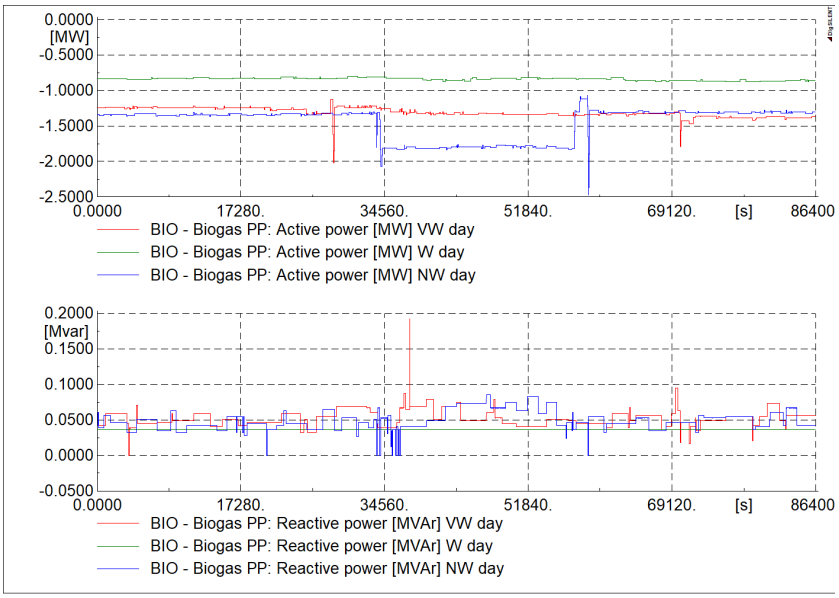

Figure B.3: Active and reactive power consumption for Biogas feeder

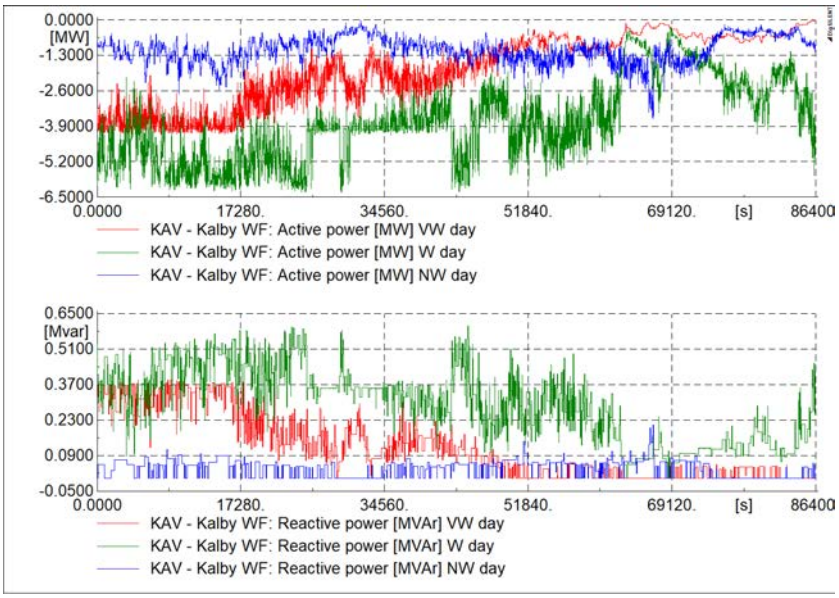

Figure B.4: Active and reactive power consumption for Kalby wind farm feeder

Sose wind farm

The active power injection of Sose wind farm feeder (Figure B.5) is reported, additionally to the reactive power consumption. As Kalby wind farm, Sose wind farm has a highly variable power profile that will influence the overall power in Åkirkeby substation. As a conclusion, it can be clearly noticed how the reactive power consumption is practically proportional to the active power injection, being the wind farm composed of five WTGs Type A, each of them equipped with an asynchronous machine.

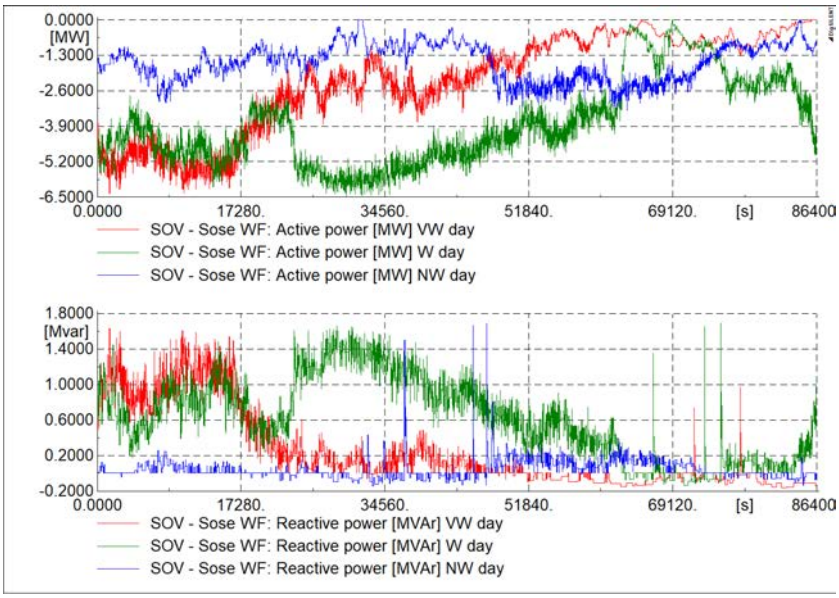

Figure B.5: Active and reactive power consumption for Sose wind farm feeder

Kastelbakken

The active power consumption profile of Kastelbakken feeder (Figure B.6) is a typical daily load profile with a certain correlation among the three analysed days, having similarities with profiles of the Industriområde feeder (Figure B.1). Although the feeder is always consuming active power through each of the considered days, the reactive power consumption shows always a negative sign. Thanks to the beneficial reactive power compensation effect coming from the installed underground cables, connecting Kastelbakken to the 10.6 kV, the required reactive power is delivered to Kastelbakken itself, injecting additional reactive power in the 10.6 kV line.

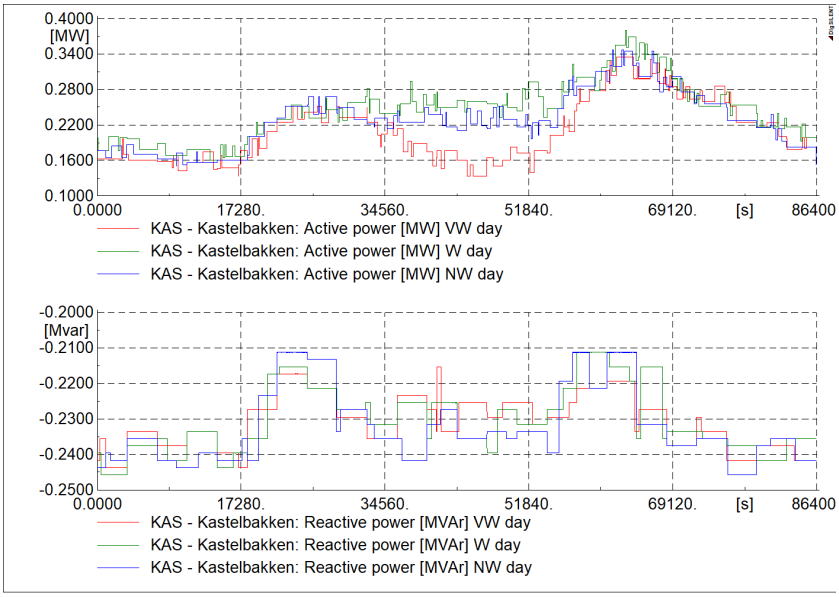

Figure B.6: Active and reactive power consumption for Kastelbakken feeder

Rytterknægten

The active power consumption profile of Rytterknægten feeder (Figure B.7) is a typical daily load profile with a certain correlation among the three analysed days, as previously mentioned load feeders. The consideration regarding the reactive power consumption in Kastelbakken can be applied to this feeder as well.

Åkirkeby

The active power consumption of Åkirkeby feeder (Figure B.8) is a typical daily load profile with a certain correlation among the three analysed days, having similarities with the previously mentioned feeders. However, it has a higher peak consumption between 5 *pm* – 8 *pm*, that corresponds to the typical Danish dinner hours. For to the reactive power consumption, small but constant magnitude variations can be noticed through the whole day, without any specific appreciable trend.

Sydlinien

The active power consumption of Sydlinien feeder (Figure B.9) is the typical daily load profile with a certain correlation among the three analysed days, having similarities with previously mentioned feeders. The consideration regarding the reactive power consumption in Kastelbakken can be applied to this feeder as well.

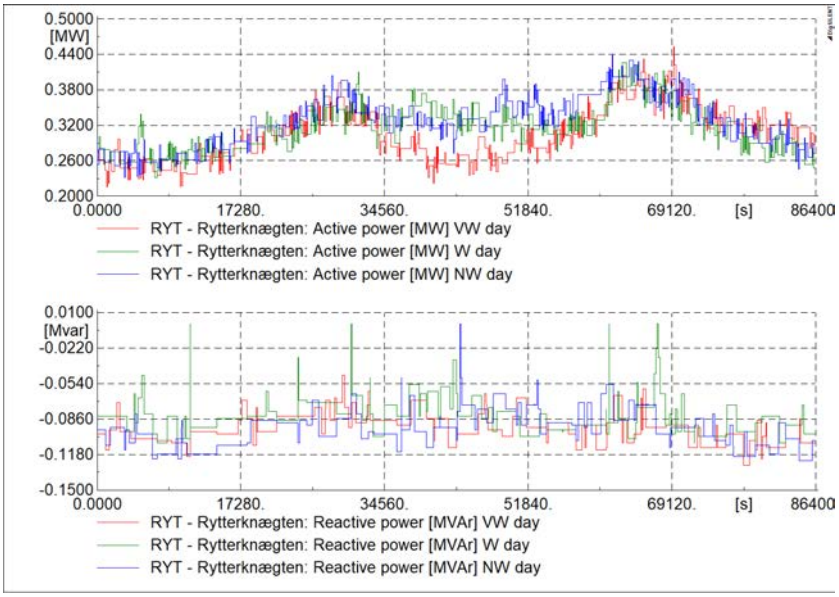

Figure B.7: Active and reactive power consumption for Rytterknægten feeder

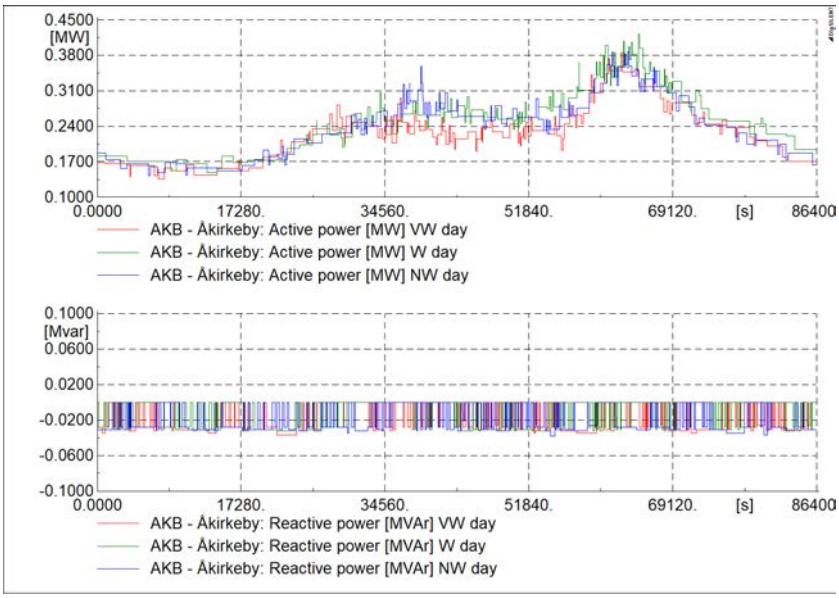

Figure B.8: Active and reactive power consumption for Åkirkeby feeder

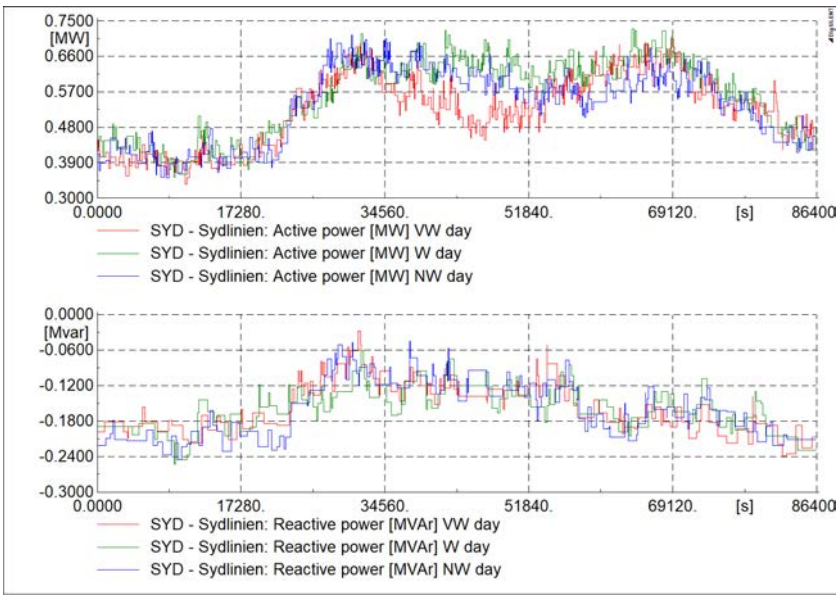

Figure B.9: Active and reactive power consumption for Sydlinien feeder

Sose

The active power consumption of Sose feeder (Figure B.10) is the typical daily load profile with a certain correlation among the three analysed days, having similarities with previously mentioned feeders. The consideration regarding the reactive power consumption in Kastelbakken can be applied to this feeder as well.

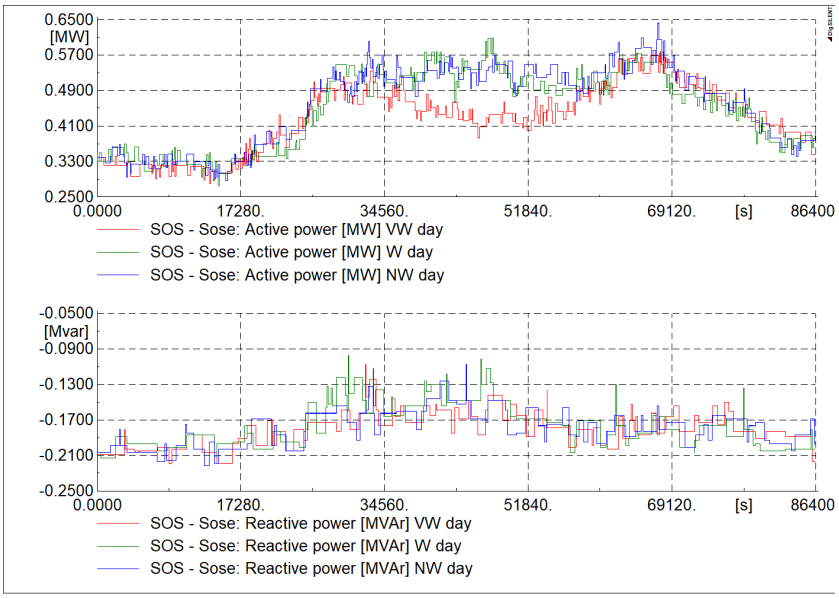

Figure B.10: Active and reactive power consumption for Sose feeder

C Integral reset

Throughout the implementation of the hybrid power plant controllers investigated in Chapter 5, integral blocks have been required in PF. Moreover, it has been found necessary to reset some integrals' output under determined circumstances. Particularly, the reset were always linked to the simulation time, the integrals' output being necessary to be reset after fixed period of time function of the required task. For example, the integrals designed in the composite block definition *Energy Error* (Figure 5.11) need to be reset every 15 $'$. Again, the integrals installed in the composite block definition *SOC protection* (Figure 5.16) have to be reset each 2 h or 6 h, depending at which chargers is connected to.

Unfortunately, the PF version 15.2 considered for this project lacks of the possibility to set when the integral output must be reset. As a consequence, the 'Integral reset' function was implemented manually, the reset time being known.

The "trick" provides the definition of several state variables, each of them applied to a specific time period (15 $'$, 2 h or 6 h). In Figure C.1, it is reported the example for the integral connected to the $Ch-1ph$, which requires 4 different state variables.

```
! Integral with reset every 6 h to evaluate SOC for Ch-1ph

! STATE VARIABLES initialization
inc(x_03)=0; ! State variable integral
inc(x_02)=0; ! State variable integral
inc(x_01)=0; ! State variable integral
inc(x_00)=0; ! State variable integral
inc(yo)=0;

! FORMULAS
x_00.=select(time()>=0,select(time()<21600,yi,0),0);
y_00=select(time()>=0,select(time()<21600,x_00,0),0);
x_01.=select(time()>=21600,select(time()<43200,yi,0),0);
y_01=select(time()>=21600,select(time()<43200,x_01,0),0);
x_02.=select(time()>=43200,select(time()<64800,yi,0),0);
y_02=select(time()>=43200,select(time()<64800,x_02,0),0);
x_03.=select(time()>=64800,select(time()<86400,yi,0),0);
y_03=select(time()>=64800,select(time()<86400,x_03,0),0);

yo=y_00+y_01+y_02+y_03;
```

Figure C.1: "Integral reset" function

As observable, through the simulation time, the input *yi* is assigned to the derivative of one of the state variable as a function of the actual simulation time. Indeed, the first state variable x_00 is considered in between midnight – 6 *am*, the second x_01 in between 6 *am* – 12 *am*, the third x_02 in between 12 *am* – 6 *pm* and the fourth x_03 in between 6 *pm* – midnight. With this approach,

each derivative is then integrated to obtain y_00, y_01, y_02, y_03, while being each of them zero outside the competency time. As a consequence, the overall output *yo* is obtained as a sum of the just mentioned variable.

With the described strategy, all the required integrals have been designed, defining 96, 12 and 4 state variables when it is required to reset the integral every 15 $'$, 2 h or 6 h, respectively.

D Additional technical results

In this appendix, additional technical results are collected. In Section D.1, the graphs connected to the *Power-to-Power controller* in the *W* scenario are gathered. Then, in Section D.2, the *Power-to-Power controller* is applied in the *NW* scenario. Finally, in Section D.3, the additional graphs not included in Section 6.4.2 when discussing about the comparison $Ch-3ph$ and $Ch-1ph$ are shown.

D.1 *Power-to-Power controller* applied to the windy day

Figure D.1 and D.2 collect the results when the *Power-to-Power controller* is applied under ideal condition in the *W*. Then, in Figure D.3 and D.4 the controller is instead investigated when the EVs behavior in Åkirkeby is applied, with the additional Figure D.5 to show how the turbulence intensity is observed throughout the day. The main considerations behind these graphs are collected and exposed in Section 6.2.

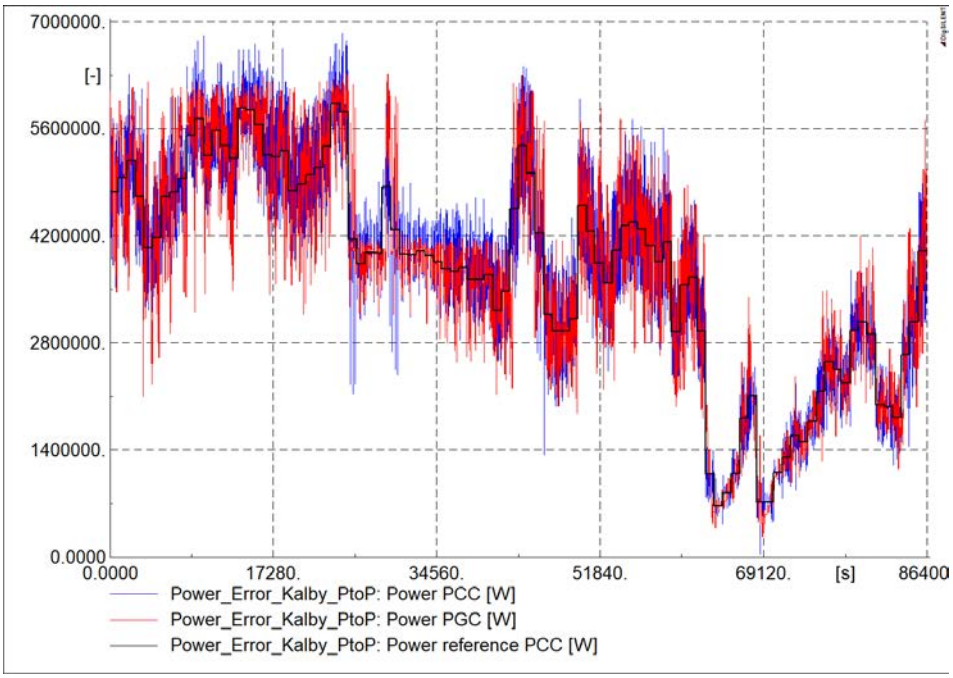

Figure D.1: PGC, PCC and reference power in *W* under ideal conditions

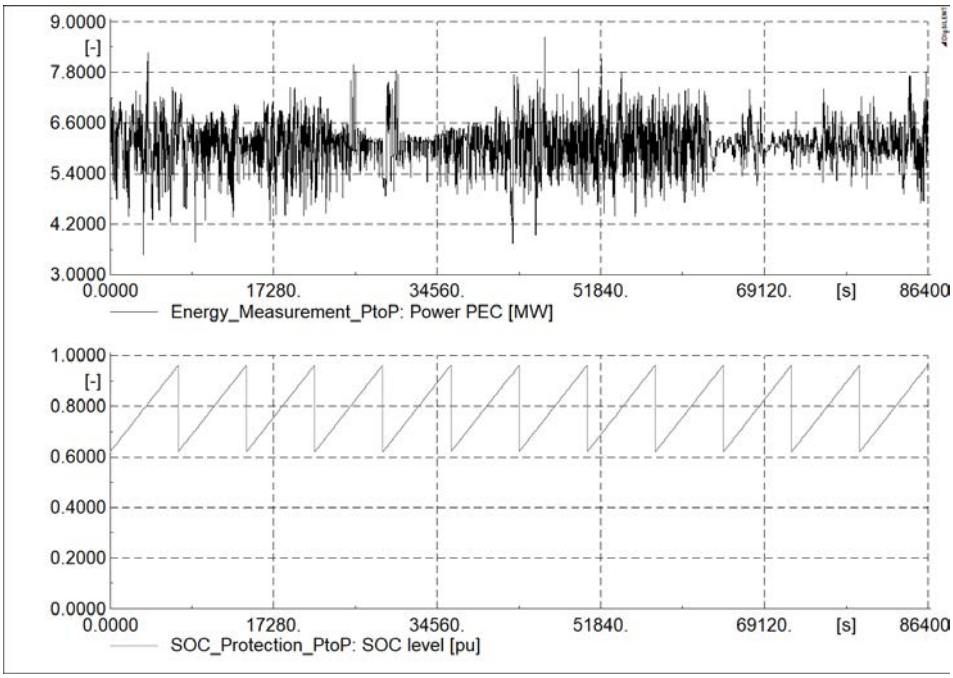

Figure D.2: PEC power output and SOC level in *W* under ideal conditions

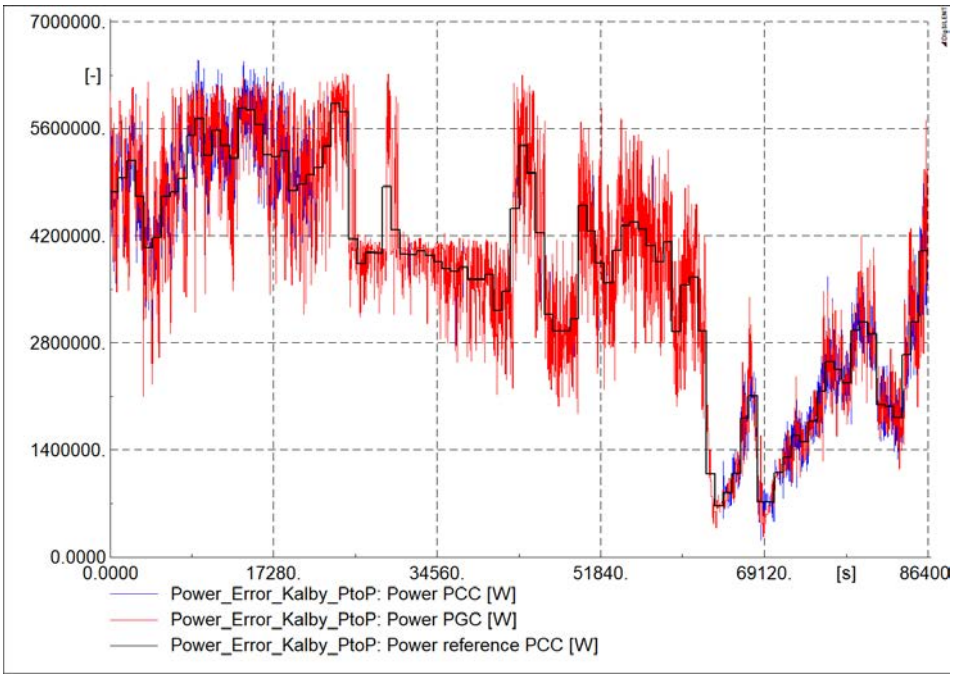

Figure D.3: PGC, PCC and reference power in *W* under real conditions

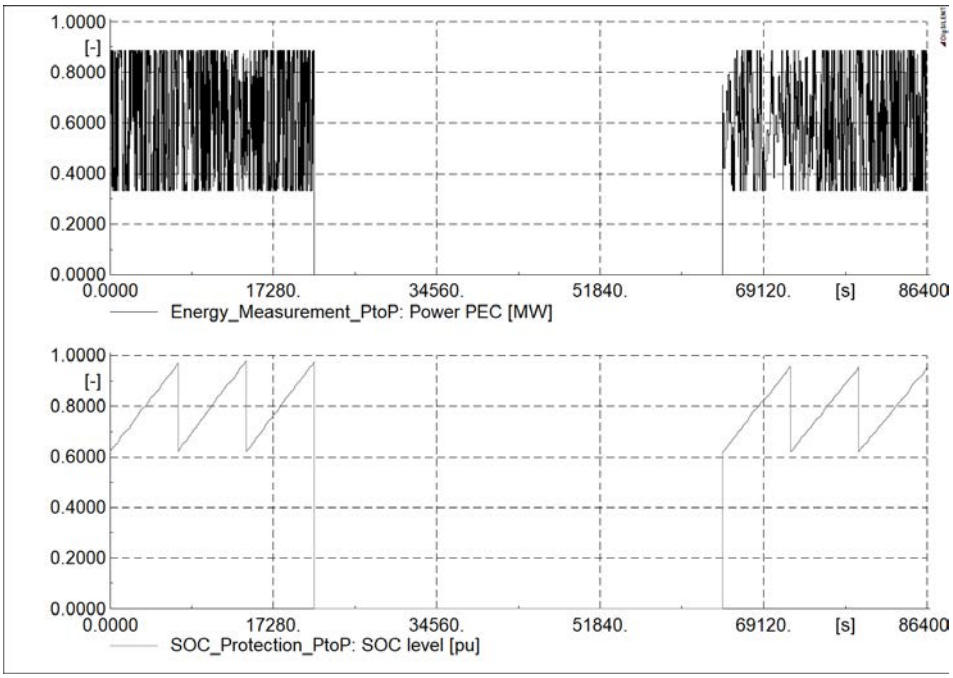

Figure D.4: PEC power output and SOC level in *W* under real conditions

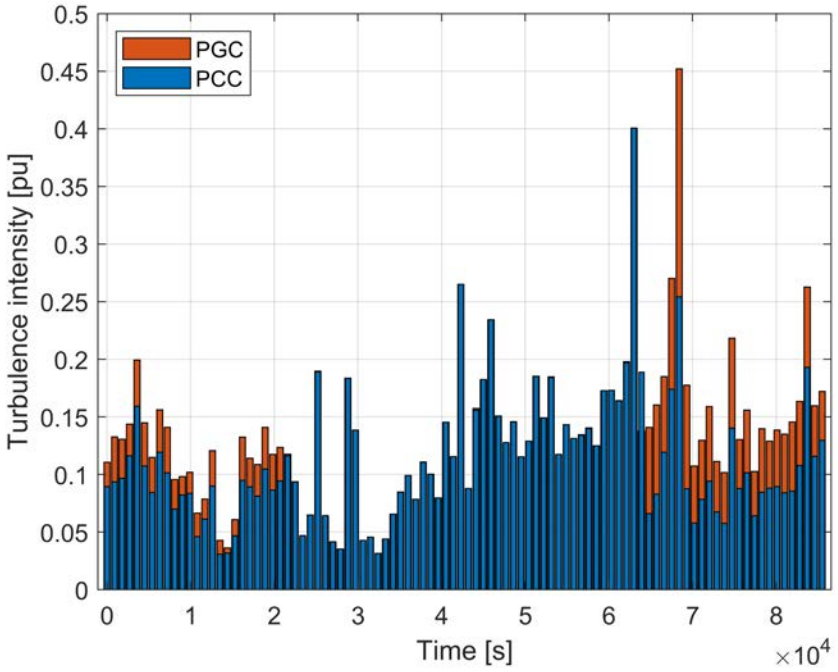

Figure D.5: Turbulence intensity at PGC and PCC in *W*

D.2 *Power-to-Power controller* applied to the not windy day

Figure D.6 and D.7 collect the results when the *Power-to-Power controller* is applied under ideal condition in the *NW*. Then, in Figure D.8 and D.9 the controller is instead investigated when the EVs behavior in Åkirkeby is applied, with the additional Figure D.10 to show how the turbulence intensity is observed throughout the day. The main considerations behind these graphs are collected and exposed in Section 6.2.

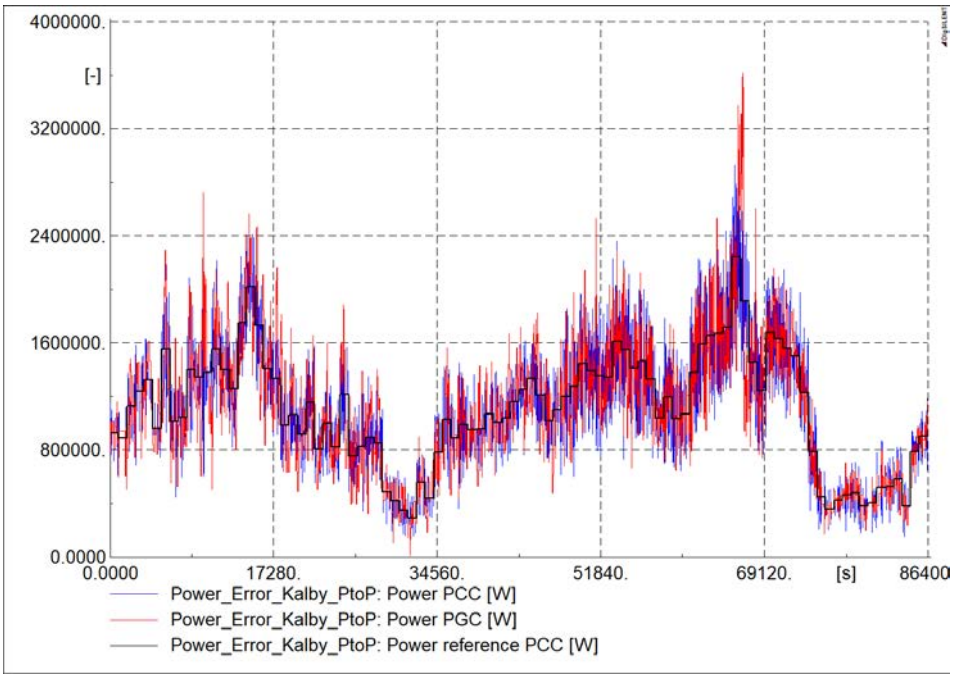

Figure D.6: PGC, PCC and reference power in *NW* under ideal conditions

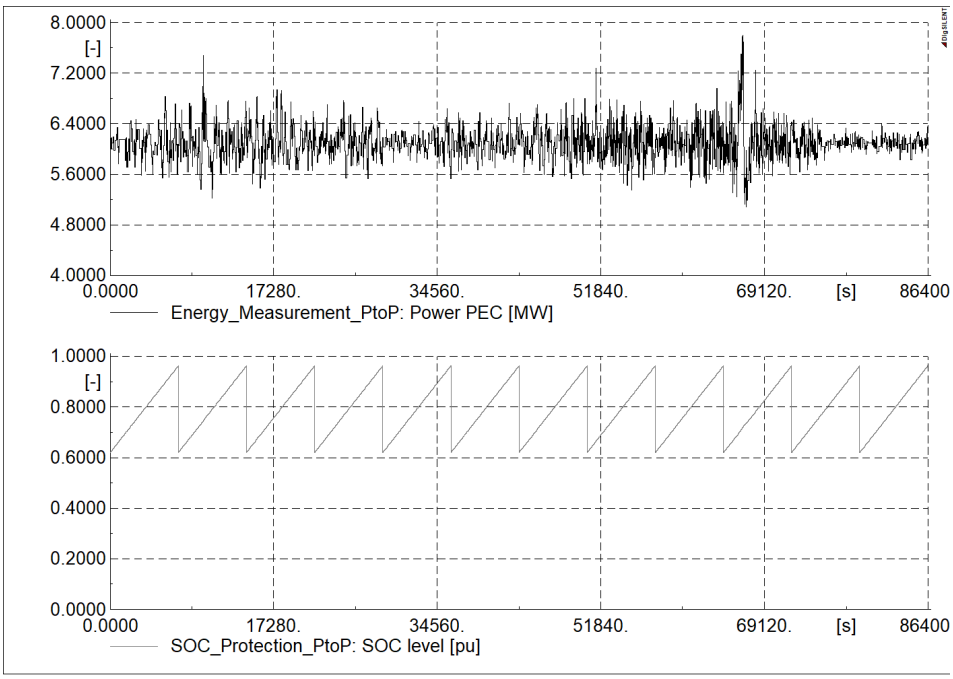

Figure D.7: PEC power output and SOC level in *NW* under ideal conditions

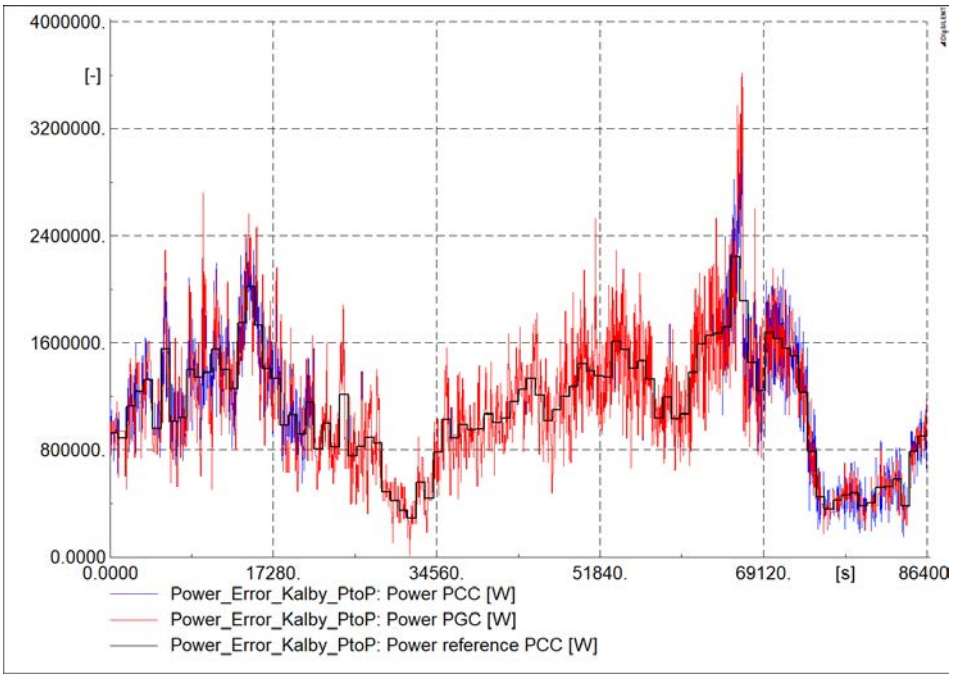

Figure D.8: PGC, PCC and reference power in *NW* under real conditions

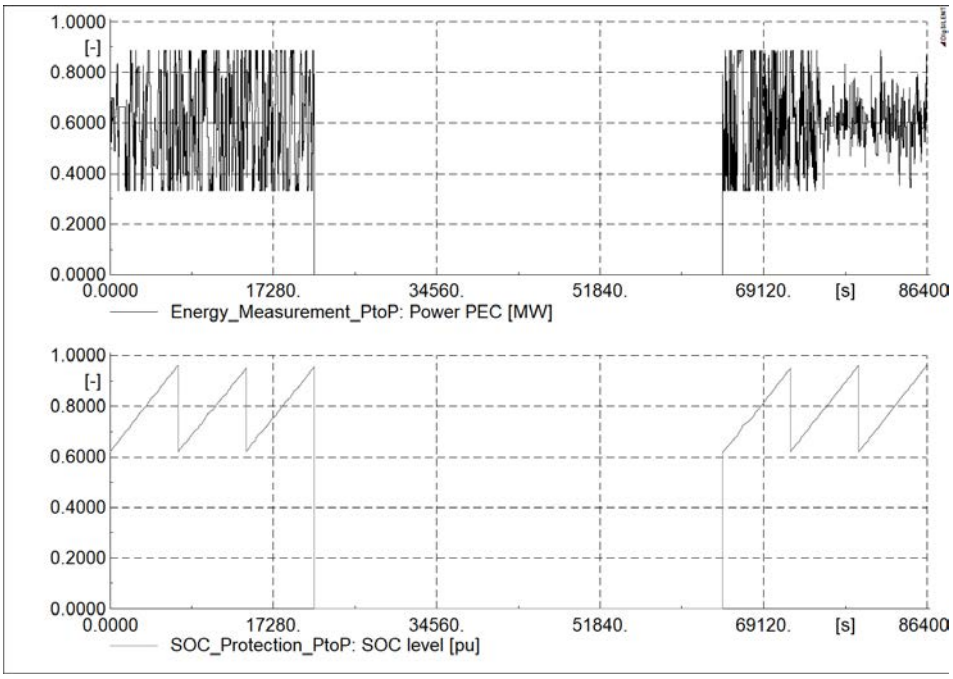

Figure D.9: PEC power output and SOC level in *NW* under real conditions

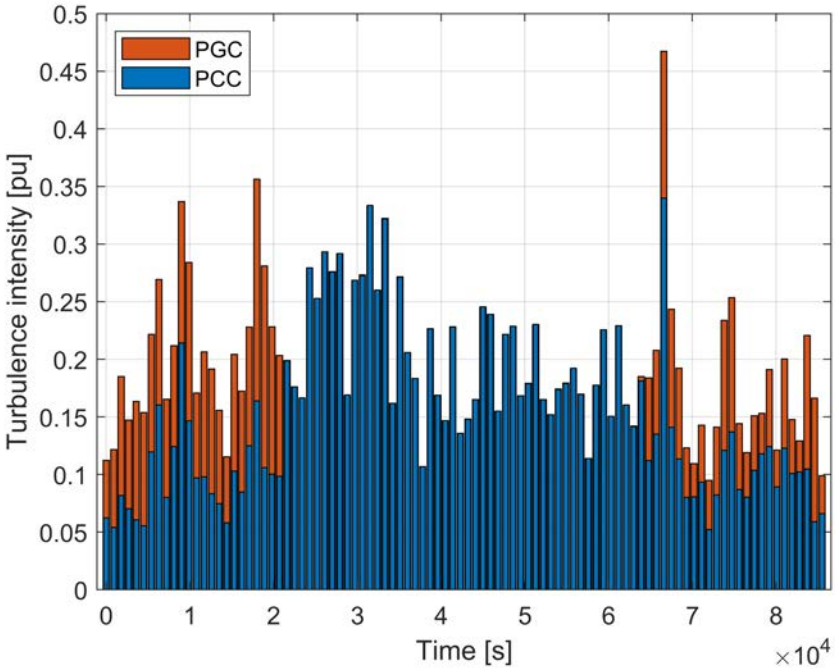

Figure D.10: Turbulence intensity at PGC and PCC in *NW*

D.3 *Energy-to-Power controller*, single phase charger and accurate forecast

In this section, the obtained results with the *Energy-to-Power controller*, when investigating the accurate forecast scenario with $Ch-1ph$ are collected. Figure D.11 show the comparison between $Ch-3ph$ and $Ch-1ph$ in terms of power injection at the PCC, fluctuations obtained as a consequence of the adjusted *Power PEC* shown in Figure D.12. The profiles do not show any variations in between $Ch-3ph$ and $Ch-1ph$, which is motivated in the related Section 6.4.2.

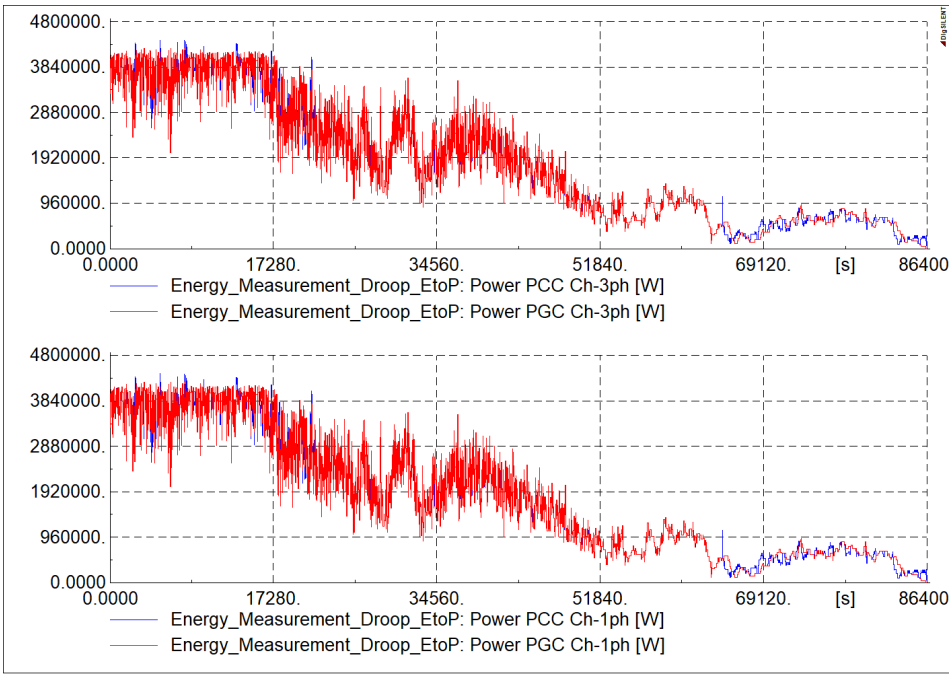

Figure D.11: PGC and PCC comparison with *Energy-to-Power controller* with accurate forecast

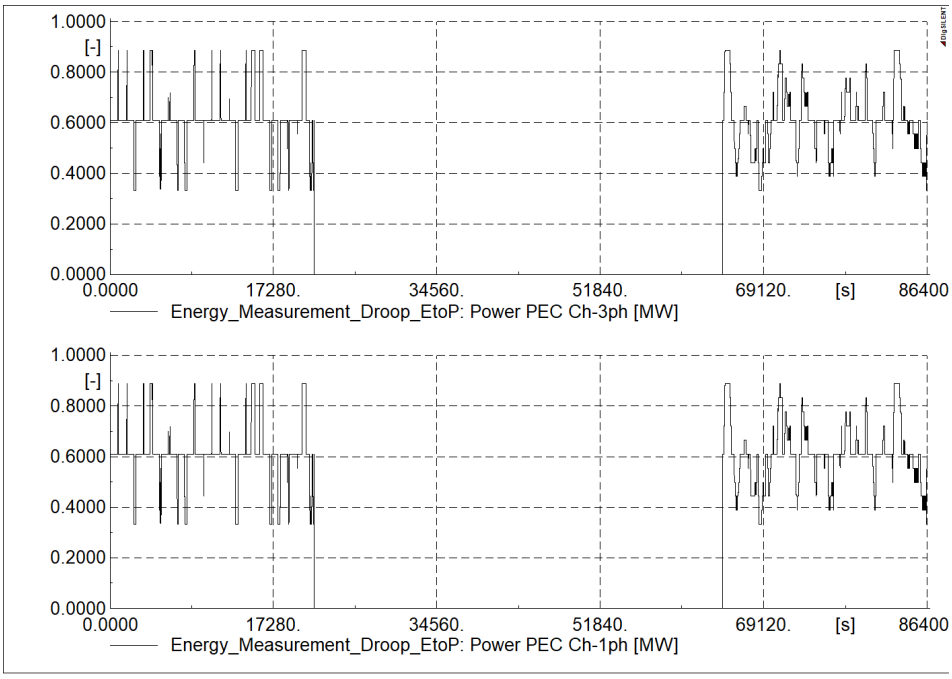

Figure D.12: Power PEC comparison with *Energy-to-Power controller* with accurate forecast

Department of Electrical Engineering
Centre for Electric Power and Energy (CEE)
Technical University of Denmark
Elektrovej, Building 325
DK-2800 Kgs. Lyngby
Denmark

www.elektro.dtu.dk/cee
Tel: (+45) 45 25 35 00
Fax: (+45) 45 88 61 11
E-mail: cee@elektro.dtu.dk